Impact of DCF properties on system design

René-Jean Essiambre[1], Peter J. Winzer[2] and Diego F. Grosz[3]

[1] Lightwave Systems Dept., Bell Labs, Lucent Technologies, Holmdel, NJ 07733
E-mail: rjessiam@lucent.com,
[2] Photonic Networks Dept., Bell Labs, Lucent Technologies, Holmdel, NJ 07733
[3] Instituto Tecnológico de Buenos Aires (ITBA), Eduardo Madero 399, C1106AD Buenos Aires, Argentina

Abstract. The dispersion-compensating fiber is an important optical element of current and future optical networks. In this paper, we review the impact that various properties of dispersion-compensating fibers has on the performance of optical communication systems.

1. Introduction

Dispersion compensating fibers (DCFs) have become an important building block making up today's high-capacity optical transport networks. To appreciate the importance of DCF for high-capacity lightwave systems, we briefly look at the historic evolution of optical fiber transmission [1,2].

The first single-mode optical fibers to be fabricated with low loss were step-index silica fibers [3], now referred to as standard single-mode fibers (SSMFs) and specified in the International Telecommunication Union (ITU) standard G.652. In the late 1970s and early 1980s, transmission over such fibers was performed in the spectral window around 1300 nm, where this fiber's chromatic dispersion (hereafter just referred to as "dispersion") is lowest, and permitted loss-limited transmission over about 100 km at about 1 Gb/s using Fabry-Perot lasers. However, the minimum intrinsic loss of SSMFs at 1300 nm is still $\sim$0.4 dB/km, twice the minimum value of $\sim$0.2 dB/km found in the wavelength band around 1550 nm. But even at such low loss, and with the use of both distributed feedback (DFB) lasers and highly sensitive coherent detection, transmission distances were attenuation-limited to about 200 km at 1-Gb/s data rates.

With the development of erbium-doped optical amplifiers (EDFAs) operating in the 1550 nm window, the limitation from fiber loss was circumvented, and transmission over distances of thousands of kilometers became possible. However, since dispersion of SSMFs in the 1550-nm window amounts to around 17 ps/(nm km), it was now the accumulated dispersion that limited transmission distances to a few hundred kilometers at 2.5 Gb/s. To overcome this dispersion limit, new optical fibers with a dispersion zero shifted from 1300 to the 1550-nm region were designed and fabricated (ITU standard G.653). Using such dispersion-shifted fibers (DSFs), the dispersion limit was pushed out to a few thousand kilometers without the need for DCFs. However, with the advent of wavelength-division multiplexing (WDM), it was discovered [4] that the effects of Kerr fiber nonlinearities over fibers having low-dispersion values [$\lesssim 2$ ps/(nm km)], such as DSFs, leads to signal distortions from four-wave mixing (FWM) [4] and nonlinear mixing of signal and noise [5], which strongly limits transmission distance. As a result, non-zero dispersion-shifted fibers (NZDFs) were developed to provide a sufficient value of dispersion [$\gtrsim 2$ ps/(nm km)] in the 1550-nm window to prevent FWM (ITU standard G.655). The presence of NZDFs and SSMFs in optical networks along with the increase in signal speed and growth in the bandwidth of optical amplifiers all contributed in making dispersion compensation needed in current and future optical networks.

The need for dispersion compensation in the low-loss amplification window has been identified as early as 1980 [6] to extend the dispersion-limited transmission distance. Among the early technologies used to demonstrate dispersion compensation were chirped fiber Bragg gratings [7], all-pass filters [8] and micro strip delay equalizers in combination with coherent detection [9]. The first use of negative-dispersion optical fibers as dispersion compensators in system experiments has been demonstrated starting in 1993 [10] where eight wavelength-division multiplexed (WDM) channels operating at 10 Gb/s were transmitted over 280 km of NZDFs. Many experimental demonstrations followed [11–14] in terrestrial applications as well as in submarine systems [14–16]. The capacity of WDM transport then increased dramatically as dispersion compensated transmission lines became efficient (see [17] for an early review).

The beginning of the deployment of 10-Gb/s-based WDM communication systems near the end of the 1990s fostered the incorporation of dispersion compensation in various optical transmission systems. By the beginning of the 3rd millennium, deployment of 10-Gb/s technologies had become widespread in backbone terrestrial networks, making dispersion compensation omnipresent in the fabric of the worldwide fiber-optic communication infrastructure. The types of backbone terrestrial networks requiring dispersion compensation includes ultra long-haul (ULH, > 3000 km), long-haul (LH, 1000–3000 km) and regional (300–1000 km). A few years after its apparition in backbone networks, dispersion compensation also started to appear in regional and metropolitan optical networks (< 300 km) as they started to adopt 10-Gb/s technologies.

The increased demand in transport capacity, first in backbone and later in metropolitan networks, and the cost reduction of 10-Gb/s transponders is what allowed the large-scale deployment of dispersion compensation to take place. Nowadays, fiber-optic communication systems are, de facto, designed with dispersion compensation built in, so as to accommodate transport at any bit rate from 2.5 to 40 Gb/s.

This paper focuses on the basic properties of DCFs and how they impact systems. The chapter is organized as follows. The Introduction section presents the basic prop-

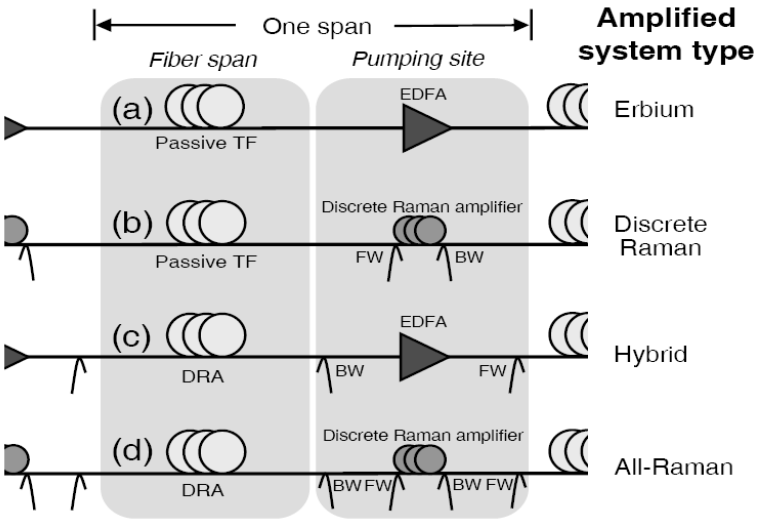

Fig. 1. Classification of transmission line types according to amplification technologies and amplifiers locations: a) EDFA; b) Discrete Raman; c) Hybrid (EDFA and Raman) and d) All-Raman. (FW/BW: Forward/Backward Raman pumping, TF: transmission fiber, DRA: Distributed Raman amplifier, EDFA: erbium-doped fiber amplifier)

erties of DCFs and the way DCFs are used in systems. Section 2 describes the tools used to quantify the effects of noise and fiber properties on transmission. The analysis of the impact of DCFs in various system configurations is presented in Sec. 3 which focuses on providing physical understanding of the impact of DCFs' properties on basic dispersion compensation schemes. Finally, the last section discusses the system impacts of using non-DCF-based dispersion compensation technologies.

1.1. System Layouts and Classification

Optical transmission lines can differ from one another in various ways. The most common features that are used to differentiate transmission lines are *amplification technologies*, *fiber types* and *dispersion compensation schemes*. Owing to the overwhelming importance of optical amplification in overcoming the attenuation limit, it has become customary to classify transmission lines according to the amplification scheme used in the line.

In terrestrial systems, one generally distinguishes four types of amplification schemes, as represented in Fig. 1. In the first two transmission line types (Fig. 1a and 1b), the fiber spans are made of passive transmission fibers, separated by *discrete optical amplifiers*. Depending on whether the discrete amplification scheme is based on EDFAs [1] or on discrete Raman amplifiers [18], we distinguish between *'EDFA'* and *'discrete Raman'* systems. Discrete amplification is also known as *lumped* amplification. In the situation where in addition to lumped amplification, the transmission

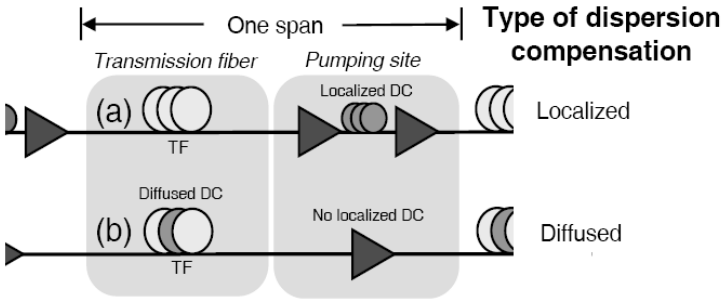

Fig. 2. Dispersion compensation placed at a specific physical location within the transmission line (a), and dispersion compensation diffused within the transmission fiber (b). In a) the DCF does not contribute to extend the transmission distance while in b) the full length of the DCF is used to bridge distance. (TF: Transmission fiber, DC: dispersion compensation)

fiber is transformed into a distributed optical amplifier using Raman pumping, one either refers to a *'hybrid'* transmission line (if EDFAs are used as discrete amplifiers) or an *'all-Raman'* system (if *all* amplifiers in the system are based on Raman pumping). Discrete Raman amplification is generally implemented by Raman pumping the DCF [19] even though other fibers could be used as well [20]. Raman amplifiers, like EDFAs, can use both forward and backward pumping. However, unlike most EDFAs[4], Raman amplification can be used on very long fibers [22–24] that can exceed 100 km in length. Typically, the Raman gain remains large for not more than a few tens of kilometers inside the fiber, after which the Raman pumps are too attenuated to provide appreciable gain. Because of the long fiber lengths involved, one often refers to such Raman amplifiers as *distributed Raman amplifiers* (DRAs). Whether or not a Raman amplifier can be considered as a DRA also depends on the importance of other fiber properties (such as Rayleigh backscattering and fiber Kerr nonlinearity) occurring within the fiber. Rayleigh backscattering and fiber nonlinearity are treated in Secs. 2.2 and 2.3, respectively. Note that the most commonly used amplification schemes described in Fig. 2 are, in order of prevalence, discrete EDFA, hybrid, all-Raman and discrete Raman. The discrete Raman amplification scheme is generally used only to access amplification bands that lie outside the amplification window of EDFAs and other rare-earth doped fiber amplifiers [24]. Note that even though the strongest natural gain of EDFAs is the 1530–1565 nm range (C-band), the amplification window has been extended at wavelength as short as 1500 nm [25] (S-band) and as long as 1610 nm (L-band).

A second way to classify systems is according to their dispersion compensation scheme. One generally uses two broad dispersion compensation categories: *localized* and *diffused* dispersion compensation (see Fig. 2). Localized dispersion compensation applies to systems where DCFs are localized at the amplification or Raman pumping sites between transmission spans, but are not used to bridge distance. In commercially deployed systems, localized dispersion compensation is implemented by inserting reels

[4] A noticeable exception is a 68-km long EDFA developed to become a transmission fiber [21].

of DCFs in huts, periodically located along a transmission line. In contrast, diffused dispersion compensation is generally implemented by using advanced transmission fibers that are composed of fiber segments with opposite-sign dispersion [26–37]. Such fibers are referred to as dispersion-managed fibers (DMFs) and cables containing such fibers are called dispersion-managed cables (DMCs). Note that, even though the DCF is shown near the center of the fiber span in Fig. 2b, it could be placed anywhere within the fiber span. From a practical standpoint, the favored locations are the center of the fiber span (symmetric configuration) or the end of a fiber span, to minimize the number of fiber segments and fiber nonlinearity.

An important difference between the two types of dispersion compensation schemes mentioned above is that in localized dispersion compensation, the DCF is *not* used to bridge transmission distance; therefore, the actual propagation distance (i.e., the total fiber length) can significantly exceed the transmission distance (the physical path length connecting two locations). Typically, the amount of negative dispersion provided by a DCF per unit length is about 5 to 25 times higher than that of a transmission fiber. Using localized dispersion compensation, the propagation length thus exceeds the transmission distance by 4 to 20%. This excess propagation length can have several negative impacts, including potentially larger fiber cost from the additional fiber length required to bridge a given distance, additional amplification needed to compensate for the larger total loss that the signal experiences during propagation, and extra transit time in a network. However, there are also benefits to localized dispersion compensation, including the ability to easily deploy new dispersion compensation technologies as they become available, as well as more flexibility in changing the dispersion map when upgrading a system, as discussed in the next section.

1.2. Dispersion Maps

In the absence of fiber Kerr nonlinearity during propagation in optical fiber, the *total cumulative dispersion* or the *net residual dispersion* at the end of the line uniquely determine the signal distortion from dispersion (see Sec. 2.3). However, in order to maximize the optical signal-to-noise ratio (OSNR) delivered to the receiver (see Sec. 2.2), it is generally desirable to operate a system at the highest possible signal launch power into the fiber spans. The maximum power is dictated by the onset of severe signal distortions through fiber nonlinearity (see Sec. 2.3). In the presence of fiber nonlinearity, transmission is no longer linear, and hence the precise location and value of dispersion compensation becomes critical in determining the overall signal distortion after propagation. The technique of managing dispersion in a transmission line in order to minimize the effects of fiber nonlinearity is referred to as *dispersion mapping*. The evolution of the cumulative dispersion along the transmission line is referred to as the *dispersion map*.

Dispersion maps are commonly represented in two different ways (Fig. 3). In the first representation (Fig. 3a), the cumulative dispersion is plotted as a function of the *physical fiber length*, while the fiber length is replaced by the *transmission distance* in the second representation (Fig. 3b). The largest difference between fiber length and transmission distance occurs in transmission lines having localized dispersion compensation where DCFs are not used to bridge distance.

With both the amount and the location of dispersion compensation as free parameters, a large number of dispersion maps can be envisioned. Figure 4 shows a few

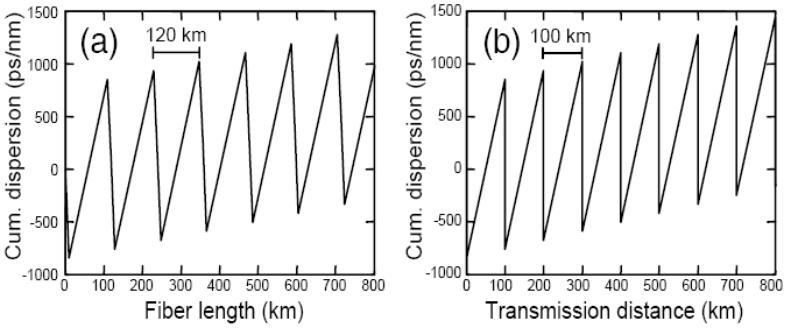

Fig. 3. Representations of dispersion maps for localized dispersion compensation. In a) the dispersion map is plotted as a function of fiber length, while in b) it is plotted as a function of the transmission distance. The dispersions of the TF and DCF are 17 and -85 ps/(nm km), respectively.

possible dispersion maps with relevance to optical networking. In Fig. 4a, no dispersion compensation is present. Dispersion maps like this are used in short-range ($\sim$100 km) and/or low data rate ($<$10 Gb/s) systems, where neither accumulated dispersion nor fiber nonlinearity are of major concern. More recently, this type of dispersion map has also gained some attention for regional and long-haul systems in the context of electronic pre-distortion [38–41]. In Fig. 4b, equal amounts of dispersion compensation are applied periodically along the transmission line, leaving the same amount of residual dispersion per span. Such dispersion map is referred to as *singly-periodic dispersion map* (SPDM). In the dispersion map of Fig. 4c, additional dispersion is inserted or removed every few transmission spans. As a result, a second period of dispersion compensation appears, which gives this *doubly-periodic dispersion map* (DPDM) its name; DPDMs are considered for optically-routed networks [42–44], where it is important to bring the dispersion to reasonably low values at optical add-drop multiplexer (OADM) sites. Finally, if no periodic pattern is visible in dispersion compensation (Fig. 4d), the dispersion map is referred to as an *aperiodic dispersion map*. Aperiodic dispersion maps can arise for instance in SPDM when dispersion accuracy (either of the transmission fibers or the DCFs) is insufficient to accurately achieve the target RDPS. Although even a larger variety of dispersion maps can be envisioned, a dispersion map that leads to simple and robust engineering rules for system deployment is highly desirable. For that purpose, the SPDM of Fig. 4b is attractive, because each span is compensated in the same manner so that only knowledge of one span is necessary to implement dispersion compensation. For this reason, SPDM is the most widely used dispersion map today.

Note that, regardless of the employed dispersion map, inaccuracies in the dispersion values of transmission fibers and dispersion compensators, the dependence of dispersion with wavelength, and the granularity in dispersion compensation may result in significant deviations from the original dispersion map design as discussed in

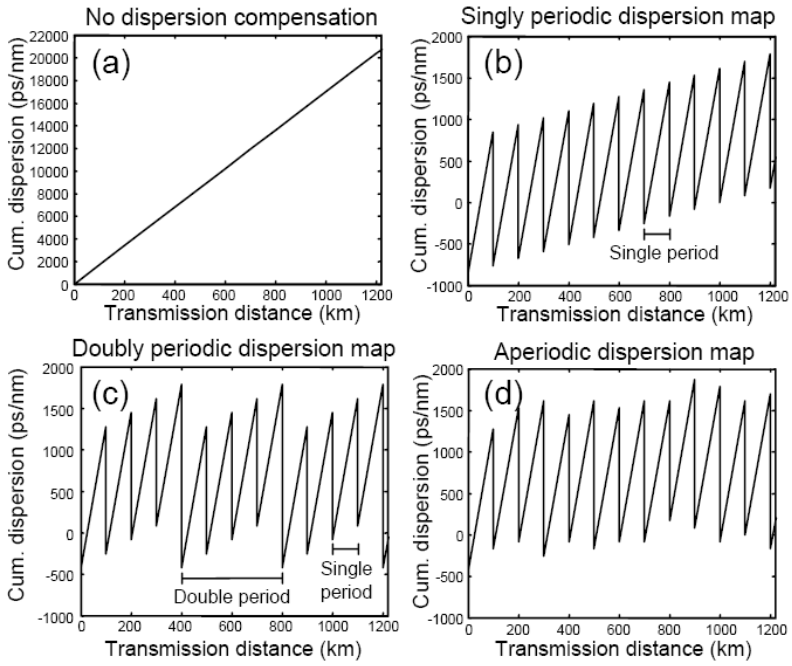

Fig. 4. Examples of dispersion maps: a) No dispersion compensation; b) Singly periodic dispersion map (SPDM); c) Doubly periodic dispersion map (DPDM); d) Aperiodic dispersion map. Fiber dispersion values are the same as in Fig. 3.

Sec. 3.2. The impact of such deviations have to be evaluated for each system individually.

1.3. Properties of Dispersion Compensators

Even though the primary role of dispersion compensation is to reduce the accumulated dispersion, the system impact of inserting dispersion compensating elements into the transmission line is manyfold. The properties of dispersion compensating modules (DCMs) that impact transmission and system design include the following:

– The *insertion loss* of the DCM affects the delivered OSNR at the receiver (Sec. 3.1).

– The DCM bandwidth impacts the accuracy of the dispersion map (see Fig. 5) and the number of WDM channels supported.

– If a DCM is channelized, it limits the per-channel data rates and the WDM channel spacings supported by the system as opposed to a non-channelized DCM (see subsection ‘Channelized and tunable dispersion’ in Sec. 3.2).

– Polarization-Mode Dispersion (PMD) within the DCM adds to the total PMD of a system, which may impact systems operating at high bit rates (Sec. 3.2).

– Polarization-Dependent Loss (PDL) that adds to the system PDL and increases polarization-dependent signal power variations.

– Fiber nonlinearity (for fiber-based dispersion compensation) that increases signal distortions (Sec. 3.2).

– Multi-Path Interference (MPI), including Double-Rayleigh Backscattering (DRB), that acts like an additional source of signal degradation (Sec. 3.1).

– Group delay fluctuations with wavelength (for interferometric devices) that generates additional signal distortions.

The presence and the importance of each property listed above in a system implementation strongly depend on the dispersion compensation technology. In this chapter, we focus mainly on the system impact of DCF technologies, even though some of the analysis may be applied to other dispersion compensation technologies as well. A perspective on alternative technologies to DCFs is presented in Sec. 4, where the impact on system performance and the benefits trade-offs between different technologies are discussed.

1.4. Dispersion-Compensating Fibers

The DCF is, by far, the most commonly used dispersion compensation technology in optical networks. The main advantages of DCFs over other technologies include low (splice) loss ($\lesssim 0.5$ dB) to transmission fibers, low insertion loss, non-channelized compensation allowing arbitrary per-channel bit rates and WDM channel spacings as well as the concatenation of a large number of DCFs, broadband compensation, low PMD, and low PDL. On the other hand, drawbacks of DCF technologies include, long fiber lengths resulting in bulky DCMs, no tunability in dispersion or dispersion slope, and the presence of Kerr nonlinearity in the DCF.

In an effort to capture the impact of various different DCF designs on system performance, certain fiber properties have been combined to form a single parameter characterizing the DCFs [45–47]. An example of such parameter combination is the (linear[5]) *figure of merit* (FOM), defined as [46]

$$\mathrm{FOM} = \frac{|D|}{\alpha}, \tag{1}$$

where D is the local dispersion [ps/(nm km)] of the fiber and α is the fiber loss parameter [dB/km]. Clearly, a high FOM indicates that large dispersion compensation can be accomplished with low loss, helping to lower the impact of inserting a DCF in a line on the OSNR degradation (Sec. 3.1).

Another parameter used to characterize DCFs is the relative dispersion slope (RDS), defined as

[5] An extension of this figure of merit to include fiber nonlinearity [45,46] will be given in Sec. 3.3.

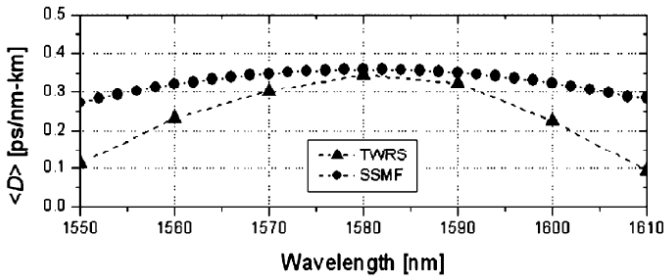

Fig. 5. Example of accuracy of broadband dispersion compensation. Average dispersion, $\langle \mathrm{D} \rangle$, as a function of wavelength for two fiber types. TWRS: Truewave® reduced slope and SSMF: standard single-mode fiber.

$$\mathrm{RDS} = \frac{S}{D}, \tag{2}$$

where S is the dispersion slope, i.e., the first-order derivative of dispersion with wavelength, $\mathrm{d}D/\mathrm{d}\lambda$. A DCF that has an RDS that matches the RDS of a transmission fiber can achieve broadband dispersion compensation, a desired feature for WDM systems. However, the slope S itself often varies considerably across the signal band and, with state-of-the-art DCFs, dispersion slope can only be compensated on *average* across the signal band, leaving residual uncompensated dispersion. For broadband dispersion compensators, a better measure of the quality of the dispersion compensation is the maximum deviation of the cumulative dispersion across the signal band or, alternatively, the maximum deviation of the average dispersion across the signal band. Figure 5 shows an example of how the average dispersion varies across a wavelength band after dispersion compensation for Truewave® Reduced Slope (TWRS), a commercial fiber belonging the NZDF family, and SSMF fibers. Note that the residual dispersion per span is simply given by $\langle \mathrm{D} \rangle$ L, where is L the transmission fiber length.

With the development of new types of transmission fibers, a large number of DCFs have become available. Most DCFs are designed to target compensation of a transmission fiber type. The properties of DCFs can vary greatly depending on the fiber type they compensate. Table 1 shows the range of parameters of the main DCF properties for commercially available DCFs. The choice of DCF for a particular optical network is guided by many factors, such as the transmission fiber type, the transmission distance, the signal bandwidth, the average span loss and the bit rate of the signal.

$\mathrm{A_{eff}}$	FOM	RDS	PMD	PDL
$\mu\mathrm{m}^2$	ps/(nm dB)	nm^{-1}	ps/$\sqrt{km}$	dB
14-21	160-240	0.0036-0.017	< 0.1	< 0.1

Table 1. Range of parameters of commercially available DCFs. $\mathrm{A_{eff}}$: fiber effective area, DGD: Differential group delay, and PDL: Polarization-Dependent Loss.

2. General Design Principles of Transmission Lines

Designing an optical transmission system with optical in-line amplifiers, dispersion management, as well as elements for optically adding, dropping, or routing wavelength channels requires a skillful balance between various sources of *noise* and *signal distortion*. The distinction between noise and distortion depends on which quantities are considered *deterministic* and which quantities are considered *random* in the context of a particular system.

In a typical long-haul transmission system, the most important sources of noise and random impairments are

– *Amplified Spontaneous Emission* (ASE), generated by in-line optical amplification.

– *Multi-Path Interference* (MPI), either due to imperfect extinction properties of OADMs and optical cross-connects (OXCs), or due to DRB. The latter becomes particularly important in Raman-pumped fiber amplifiers.

– *Coherent Crosstalk* between WDM channels in ultra-dense WDM systems.

The most important sources of signal distortion are

– *Net residual dispersion* (NRD) at the end of a transmission line, caused by deviations from the prescribed dispersion map.

– *Kerr nonlinearity*-induced signal distortions of various types, including self-phase modulation (SPM), inter and intra-channel cross-phase modulation (XPM or IXPM), and inter and intra-channel four-wave mixing (FWM or IFWM); these effects are exacerbated if the dispersion map does not follow its prescribed optimum.

– *Polarization-mode dispersion* (PMD), which can severely impair systems operating on older transmission fiber and at bit rates exceeding 10 Gb/s.

– *Narrow-band optical filtering*, which occurs in the presence of multiple OADMs or OXCs along optically-routed transmission paths.

In this section, we will study those sources of noise and distortion that determine system performance. A more detailed discussion of the trade-offs involved in system design due to the presence of DCF in a transmission line is presented in Sec. 3.

2.1. Noise Characterization of Optical Receivers

In order to understand the impact of noise and distortion on the design of lightwave systems, it is crucial to understand the process of signal detection and receiver performance quantification. Both topics will be treated in this section.

Figure 6 shows the basic structure of a direct-detection WDM receiver. The optical field of all WDM signal channels passes through a WDM demultiplexer along with the random optical field of ASE generated from optical amplification along with the random field due to DRB. The latter is especially important in Raman-pumped systems. The demultiplexer spectrally separates the WDM channels and suppresses out-of-band

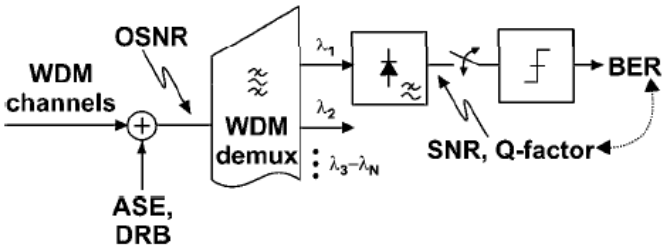

Fig. 6. Basic structure of a direct-detection WDM receiver. The WDM channels, impaired by ASE and DRB, are demultiplexed, and each wavelength is detected using a photodiode. Sampling and decision circuits extract a digital data stream from the (analog) detected signal waveform with some bit error ratio (BER).

ASE. A photodiode followed by a band-limiting electronic circuitry converts the optical power at the detector into an electrical signal, which is then sampled at the bit rate. In today's state-of-the art receivers, the transmitted digital information is restored using simple threshold detection[6]. Detection errors are quantified using the *bit error ratio* (BER).

Performance Measures: BER, SNR, and Q

Bit Error Ratio (BER)

The BER is the ultimate performance measure of optical communication systems. It is *statistically* defined as the time-averaged fraction of wrong bits contained in a bit stream. For long averaging times, the BER can also be considered as the *probability* of having a detection error for an individual bit,

$$\mathrm{BER} = \left\{ \frac{\text{bits in error}}{\text{total number of bits}} \right\}_{\text{time average}} \xrightarrow{\text{long averaging time}} P[\text{bit error}] \; . \quad (3)$$

The BER target that has to be met by a system depends on the system application. Typical values for target BERs are 10^{-12} or 10^{-15} for carrier-class optical transport systems without error-correcting coding, and 6×10^{-5} or 2×10^{-3} for systems employing forward error correction (FEC). In order to measure statistically meaningful values of BER, the average number of detected errors per measurement interval should be at least 10 but preferably 100. If one restricts the BER measurement time to a few minutes, typical for laboratory experiments, the lowest BER that can be accurately measured is $\sim 10^{-9}$ to 10^{-10} at current bit rates used in the Synchronous Optical NETwork (SONET) hierarchy (2.5 Gb/s to 40 Gb/s)[7]. As a consequence, comparisons of system performance in research laboratory experiments have traditionally been done

[6] More advanced receiver structures will be discussed in Sec. 2.3.

[7] Long-term error measurements, i.e. counting errors over days, weeks or even months, becomes necessary for systems with BER specification well below 10^{-10}. Such tests are generally performed in the course of product development and system procurement.

at BER=10^{-9}, the lowest BER that can be reliably measured in a few minutes time period. Additional comments on the impact of target BER specification on the design of systems with FEC can be found at the end of Sec. 2.3.

The Q-Factor

The *Q-factor* is an important parameter that is widely used in optical communications to describe system performance. It appears in several different contexts, with different underlying assumptions. Understanding these assumptions is crucial to making proper use of the Q-factor.

In one of its uses, most frequently employed by experimentalists, the Q-factor is just a different and more convenient way of expressing BER. The strict fundamental equivalence between the Q-factor and the BER is given by

$$\mathrm{BER} = 0.5\ \mathrm{erfc}[Q/\sqrt{2}]\ , \tag{4}$$

where $\mathrm{erfc}[x] = (2/\sqrt{\pi})\int_x^\infty \exp(-\xi^2)\mathrm{d}\xi$ denotes the complementary error function. Note that Eq. (4) is a *mere definition* that as such does *not* rely on any assumptions regarding noise or signal distortion. Typically, the Q-factor is specified in dB, using $Q_{[\mathrm{dB}]} = 20\log(Q_{[\mathrm{lin}]})$. Note that this conversion of the Q-factor to a dB-scale, using $20\log(\cdot)$ rather than $10\log(\cdot)$, is convenient, given the relation between the Q-factor and the signal to noise ratios defined below. Table 2 gives the correspondence between Q and BER for several frequently used BER values.

BER	10^{-2}	$2\cdot10^{-3}$	10^{-3}	$6\cdot10^{-5}$	10^{-6}
Q-factor	7.3 dB	9.2 dB	9.8 dB	11.7 dB	13.5 dB
BER	10^{-9}	10^{-10}	10^{-12}	10^{-15}	10^{-16}
Q-factor	15.6 dB	16.1 dB	16.9 dB	18.0 dB	18.3 dB

Table 2. Correspondence between Q-factor and BER.

Another use of the Q-factor is the experimental extrapolation of system performance to BER values that are too small to be measured directly [48]: Here, the BER is measured as a function of the receiver's decision threshold, which gives a V-shaped curve. If the minimum BER escapes direct measurement, the two legs of the V-curve are extrapolated towards the center. The intersection then yields the estimated BER at the optimum decision threshold. Obviously, this method relies on proper knowledge of the extrapolation function, which is most often taken to be the complementary error function, reflecting Gaussian detection statistics.

Yet another important use of the Q-factor is the *prediction* of system performance, based on the observation of mean and standard deviation of the electrical signal at the receiver's decision gate. In fact, this is the way the Q-factor was first introduced by Personick in 1973 [49]. Leaving detailed derivations to more comprehensive texts [50–52], we restrict ourselves to the key predictive equation,

$$Q = \frac{|s_1 - s_0|}{\sigma_1 + \sigma_0}\ , \tag{5}$$

where $s_{0,1}$ are the noise-free electrical signal amplitudes for a logical '0' and '1' at the decision gate, and $\sigma_{0,1}$ are the associated noise standard deviations. Inserting Eq. (5) in Eq. (4) yields a rough approximation of the BER to be expected in a system.

Note that although Eq. (5) allows for valuable interpretations of system performance trends, and gives reasonable 'first-guess' estimates of the BER, it is based on a series of key assumptions. If violated, the resulting system performance estimate may be severely off its true value. In particular, critical assumptions are

– **Absence of inter-symbol interference (ISI) and pattern effects**
If ISI or other pattern effects are present in a system due to signal distortions or timing jitter from the transmitter, from propagation, or from receiver elements, there is typically no single value for s_1 and s_0 or for σ_1 and σ_0, but each bit has its individual signal mean level and an associated variance. In this case, the eye diagram exhibits several different traces for '1'-bits and '0'-bits, and $s_{0,1}$ is typically taken from the *worst-case* traces forming the inner rim of the eye.

– **Gaussian noise approximation and single-ended detection**
The entire theory around the Q-factor is built upon Gaussian statistics of the electrical signal at the decision gate. It turns out that this assumption is very well met for the important case of ASE-induced beat-noise limited reception of on/off keyed (OOK) modulation [53], but completely fails for, e.g., balanced detection of phase-shift keyed (PSK) transmission [54]. Furthermore, other sources of optical noise, such as in-band crosstalk arising from a limited number of interferers, may lead to non-Gaussian detection statistics, and may therefore not be accurately captured by the Q-factor.

– **Optimized decision threshold**
Both the Gaussian approximation and the Q-factor only work well if the receiver is assumed to operate with optimized decision threshold. Although most modern optical receivers have threshold adaptation built in, caution has to be exerted when studying the impact of temporally varying distortions, which are faster than the threshold adaptation control loop.

As a final remark, we want to emphasize that, in optical communications, the noise variances can be different for each bit, reflected explicitly by the appearance of σ_1 and σ_0 in Eq. (5): as we will see below, many important noise terms are *signal-dependent*, i.e., the noise variance is a function of the optical signal power. For purely *signal-independent* noise ($\sigma_1 = \sigma_0 = \sigma$), Eqs. (5) and (4) reduce to BER$= 0.5\ \mathrm{erfc}[|s_1 - s_0|/(2\sqrt{2}\sigma)]$, a well known expression in classical communication theory [55].

Electrical Signal-to-Noise Ratio (SNR)

While the Q-factor accounts for different noise variances of '1'-bits and '0'-bits, and approximately relates to system performance via Eq. (4), the *electrical signal-to-noise ratio* (SNR) at the receiver's decision gate (cf. Fig. 6) only accounts for the '1'-bit; the SNR is defined as the ratio of the electrical peak power of a '1'-bit (s_1^2) to the associated noise variance (σ_1^2),

$$\mathrm{SNR} = \frac{s_1^2}{\sigma_1^2}\ . \tag{6}$$

Since the SNR only accounts for the statistics of the '1'-bits, analyses based on SNRs generally lead to simpler analytic expressions than using the Q-factor, which also includes '0'-bit statistics. Nevertheless, SNR-based analyses are often sufficient for

crude system performance estimates, even for beat-noise limited reception: Under the frequently met assumptions of a good signal extinction ratio ($s_1 \gg s_0$) and dominance of the '1'-bit noise over the '0'-bit noise ($\sigma_1 \gg \sigma_0$), we use Eqs. (5) and (6) to find the useful relation

$$Q = \sqrt{\text{SNR}}\ . \tag{7}$$

Beat Noise, Shot Noise, and Electronics Noise

Since photodetection converts the *power* of the total optical field incident to the photodiode to an electrical signal $s(t)$, we observe beating effects between the signal field $E_{\text{sig}}(t)$ and the noise fields $E_{\text{noise}}(t)$,

$$s(t) = S|E_{\text{sig}}(t)+E_{\text{noise}}(t)|^2 = S|E_{\text{sig}}(t)|^2+2S\text{Re}\{E_{\text{sig}}(t)E^*_{\text{noise}}(t)\}+S|E_{\text{noise}}(t)|^2, \tag{8}$$

where * is the complex conjugate, and S [A/W] is the photodiode's responsivity, given by

$$S = \eta e/h\nu\ , \tag{9}$$

with $\eta < 1$ being the detector's quantum efficiency, and $e = 1.602 \times 10^{-19}$ A·s denoting the elementary charge.

The first term on the right-hand side of Eq. (8) represents the desired signal information. The second term represents the beating of the signal field with the optical noise field. Since the optical noise field varies randomly in time, this beat term is also random, and therefore acts as noise on the detected electrical signal $s(t)$. Thus, this term is called *signal-ASE beat noise* or *signal-DRB beat noise*, depending on the optical noise field under consideration. The third term on the right-hand side of Eq. (8) represents the instantaneous power of the noise field, which also fluctuates randomly, and thus acts as noise on $s(t)$. Since this term can be viewed as the beating between different frequency components of the optical noise, it is called *ASE-ASE beat noise*, or *DRB-DRB beat noise*, depending on the optical noise field under consideration.

Leaving more complex expressions for the beat noise terms to specialized texts (e.g., [56,18,57]), we give here a useful approximation for systems with Gaussian filters and Gaussian optical pulses, under the assumption that the optical filter bandwidth of the receiver significantly exceeds both the bandwidth of the optical signal and the electrical bandwidth of the receiver[8]. In this case, the signal-ASE and signal-DRB beat noise variances read [18,57]

$$\sigma^2_{1,s-\text{ASE}} = \frac{4S^2N_{\text{ASE}}P_sB_e}{[1+B_s^2/(4B_e^2)]^{1/2}}\ , \tag{10}$$

$$\sigma^2_{1,s-\text{DRB}} = \frac{2S^2P^P_{\text{DRB}}P_s}{[1+B_s^2/(2B_e^2)]^{1/2}[1+B_s^2/(4B_e^2)]^{1/2}}\ , \tag{11}$$

where N_{ASE} [W/Hz] is the ASE power spectral density in the same state of polarization as the signal, P_s [W] is the optical power of a '1'-bit incident to the photodetector, B_e [Hz] is the receiver's electrical bandwidth, and B_s [Hz] is the optical signal bandwidth; P^P_{DRB} [W] is the DRB power co-polarized with the signal.

[8] This approximation is reasonably accurate, unless highly spectrally efficient systems are considered. In that case, one has to resort to the more accurate expressions given in [18,57].

Simplifying further, by assuming quasi-CW signaling ($B_s \ll B_e$), we arrive at the frequently used approximations for signal-ASE and signal-DRB beat noise variances [58,59],

$$\sigma^2_{\text{signal-ASE}} \approx 4S^2 N_{\text{ASE}} P_s B_e \ , \tag{12}$$

$$\sigma^2_{\text{signal-DRB}} \approx 2S^2 P^P_{\text{DRB}} P_s \ . \tag{13}$$

The differences in the expressions for the signal-ASE beat noise and the signal-DRB beat noise have their origin in the different spectral distribution of ASE and DRB, as we will see below. The noise-noise beat terms (ASE-ASE, ASE-DRB, and DRB-DRB) are typically small compared to the signal-noise beat terms, and we will neglect these terms in our discussions to follow.

Apart from beat noise, the electrical signal is also corrupted by fundamentally unavoidable *shot noise*, originating in the quantized (photonic) interaction between light and matter. Leaving the exact expressions for shot noise to more detailed literature (e.g., [60]), we state here an approximation based on Gaussian receive filters and Gaussian optical pulses [18]. Assuming again that the optical receive filter bandwidth exceeds the signal bandwidth, we find

$$\sigma^2_{\text{shot}} = \frac{2eSP_sB_e}{[1 + B_s^2/(4B_e^2)]^{1/2}} \ . \tag{14}$$

Assuming further quasi-CW signaling ($B_s \ll B_e$), this expression reduces to the well-known approximation [60]

$$\sigma^2_{\text{shot}} \approx 2eSP_sB_e \ . \tag{15}$$

Like the signal-noise beat terms, signal shot noise is also *signal-dependent*. Shot noise arising from the detection of ASE and DRB is well below signal shot noise, and can be safely neglected in evaluating system performance. Although signal shot noise is typically well below signal-ASE beat noise, it plays an important role as a reference noise source for defining the optical noise figure, as we will see in Sec. 2.2.

Other types of detection noise, generated within the detection electronics and independent of the optical signals incident to the photodetector, are summarized under the term *electronics noise*. Examples are thermal noise, $1/f$-noise, or transistor shot noise. Since all detection noise sources are statistically independent, their variances may be added up, and the overall system performance is determined by the *sum* of the individual noise variances. Taking into account the most important noise terms only, we thus have

$$\sigma^2_{total} \approx \sigma^2_{\text{s-ASE}} + \sigma^2_{\text{s-DRB}} + \sigma^2_{\text{signal-shot}} + \sigma^2_{\text{electronic}} \ . \tag{16}$$

Beat Noise Limit and Required OSNR

The beat noise terms, Eqs. (10) and (11), or Eqs. (12) and (13), are proportional to the optical power of signal and optical noise incident on the photodetector. When detecting the highly attenuated signal directly at the end of a fiber span, the beat noise terms are thus comparatively small compared to electronics noise. In such a scenario, electronics noise would dominate system noise, and almost exclusively determine the system's

BER. In this case, designing a receiver with lower electronics noise would directly improve system performance up to the point at which beat noise would start to limit system noise. However, reducing electronics noise in uncooled, high-speed electronic circuitry is a non-trivial engineering task. Luckily, receiver performance can be improved by other means: optical amplification prior to detection. Optical pre-amplifiers amplifies the optical signal power, together with the optical noise power coming from the line, by some gain G. As a result, the electrical signal amplitude is increased by G, and the beat noise variances are increased by G^2 [cf. Eqs. (12) and (13)]. As long as the beat noise terms are still below the electronics noise floor, increasing the pre-amplifier gain will linearly increase the electrical signal amplitude, and will thus quadratically increase the SNR. Increasing the pre-amplifier gain further, so that the beat noise terms grow above the electronics noise, no further SNR improvement will be seen, since electrical signal power and electrical noise variance both scale with G^2, and the sum of all noise terms, Eq. (16) is then dominated by beat noise. Since the optically pre-amplified receiver is then largely independent of the specific noise properties of the receiver electronics and is limited by beat noise, this mode of receiver operation is referred to as *beat-noise limited*.

If ASE-induced beat-noise limits receiver noise, the receiver's noise performance can be fully characterized by the *optical signal-to-noise ratio* (OSNR), defined as the ratio of average optical signal power to optical noise power. To see this, consider for simplicity[9] a receiver limited by signal-ASE beat noise only. Using Eq. (12), the SNR [which is approximately related to the Q-factor and the BER through Eqs. (4) and (7)] can then be written as

$$\mathrm{SNR} = \frac{S^2 P_s^2}{4S^2 N_{\mathrm{ASE}} P_s B_e} = \mathrm{OSNR}\frac{B_{\mathrm{ref}}}{2B_e} \ . \tag{17}$$

with the definition

$$\mathrm{OSNR} = \frac{P_s}{2N_{\mathrm{ASE}} B_{\mathrm{ref}}} \ . \tag{18}$$

The factor of 2 in the denominator of Eq. (18) accounts for the fact that the total ASE power is made up of *two* ASE polarization states; B_{ref} is a reference optical bandwidth, which is typically taken to be 12.5 GHz, corresponding to a convenient value of 0.1 nm for a standard resolution setting of optical spectrum analyzers.

The minimum OSNR that is needed at the receiver input to guarantee detection with some specified BER is called the *required OSNR*, and quantifies the amount of optical noise a receiver can tolerate to still maintain transmission performance at the target BER. Obviously, successful system design requires that the OSNR that is actually *delivered* to the receiver equals or exceeds the required OSNR. Table 3 lists the OSNR requirements for some important optical modulation formats at 42.7 Gb/s and for a target BER of 10^{-3}, obtained by numeric simulation [61].

Note from Eq. (17) that the data-rate independent choice of B_{ref} lets the required OSNR become *data-rate dependent*: For a given system performance, i.e., for fixed BER, fixed Q-factor, or fixed SNR, an increase in bit rate requires the same increase in OSNR, since B_e linearly increases with data rate.

[9] Including ASE-ASE beat noise does not change the fact that beat-noise limited receiver performance depends on the OSNR only.

Modulation format	required OSNR
NRZ-OOK	16.5 dB
Duobinary	17.4 dB
33% duty cycle RZ-OOK	14.9 dB
67% duty cycle CSRZ	15.1 dB
67% duty cycle RZ-DPSK	11.1 dB
50% duty cycle RZ-DQPSK	12.2 dB

Table 3. Required OSNR for different modulation formats at 42.7 Gb/s and at a target BER of 10^{-3}. NRZ: Non return-to-zero, RZ: Return-to-zero, CSRZ: Carrier-suppressed return-to-zero, DPSK: Differential phase shift keying, DQPSK: Differential quadrature phase shift keying.

2.2. Optical Noise From the Transmission Line

Having considered the impact of optical noise on receiver performance in the preceding section, we discuss in this section the generation and accumulation of optical noise along an optical communication line. This allows us to quantify the OSNR that is actually *delivered* to the receiver in a particular system; a system can only guarantee a specific BER if the delivered OSNR exceeds the required OSNR for that BER.

Amplified Spontaneous Emission

Amplified spontaneous emission (ASE) is caused by spontaneous relaxations of excited energy states in optical amplifiers, and is therefore intimately related to the gain process [1].

For *discrete* optical amplifiers, such as Erbium-doped fiber amplifiers (EDFAs), the ASE power spectral density at the output of the amplifier is given by [1]

$$N_{\mathrm{ASE}} = n_{\mathrm{sp}}(G-1)h\nu \ , \tag{19}$$

where $h\nu$ is the energy of a photon at the wavelength at which ASE is to be evaluated, G is the amplifier gain, and $n_{\mathrm{sp}} > 1$ is the amplifier's spontaneous emission factor. Note that Eq. (19) denotes the ASE power spectral density per *transversal waveguide mode*, which in a single-mode optical fiber corresponds to one *state of polarization*.

For *distributed* optical amplification, such as Raman-pumped transmission fiber or for *discrete* Raman amplifiers such as Raman-pumped DCF, N_{ASE} is given by [62,18]

$$\mathrm{N_{ASE}} = \mathrm{h}\,\nu \int_0^L \mathrm{C_r}(\lambda_\mathrm{s},\lambda_\mathrm{p}) \left[P_b e^{-\alpha_p(L-z)} + P_f e^{-\alpha_p z}\right] G(z,L)dz, \tag{20}$$

where

$$G(z_1,z_2) = T_F(z_1,z_2)\, G_R(z_1,z_2) \tag{21}$$

is the net gain from distance z_1 to z_2, $T_F(z_1,z_2) = \exp[-\alpha_s(z_2-z_1)]$ is the passive fiber transmission at the signal wavelength from z_1 to z_2, and

$$\begin{aligned}\mathrm{G_R}(z_1,z_2) = \exp\Big\{ \tfrac{\mathrm{C_r}(\lambda_\mathrm{s},\lambda_\mathrm{p})}{\alpha_\mathrm{p}} \Big[P_b \left(e^{-\alpha_p(L-z_2)} - e^{-\alpha_p(L-z_1)}\right) \\ + P_f \left(e^{-\alpha_p z_1} - e^{-\alpha_p z_2}\right) \Big] \Big\},\end{aligned} \tag{22}$$

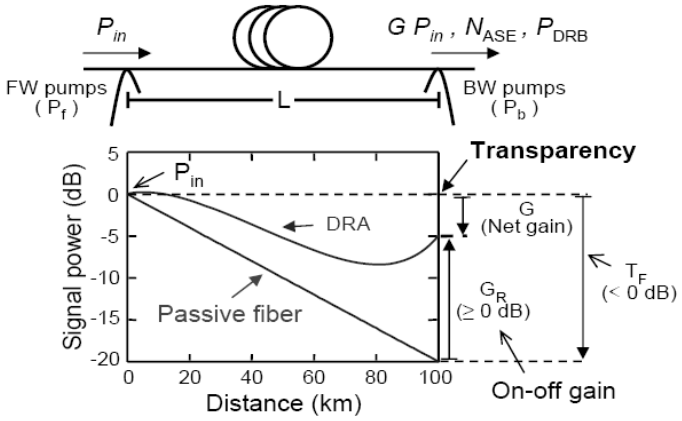

Fig. 7. Definition of parameters for a Raman amplifier.

is the Raman gain, also from z_1 to z_2; $G_R = G_R(0, L)$ is the Raman on-off gain and $T_F = T_F(0, L)$ is the passive fiber transmission (≤ 1) (see Fig. 7). In Eqs. (20) and (22), $C_r(\lambda_s, \lambda_p)$ is the Raman gain efficiency (gain factor per unit of length and power) for signal and pump wavelengths λ_s and λ_p, respectively, α_p and α_s are the loss coefficients at the pump and signal wavelengths, and P_b and P_f are the backward and forward pump powers at the ends of the fiber, respectively. Equations (20) and (22) apply to the general case of a bidirectionally-pumped DRA, and are derived using the undepleted-pump approximation [62]. Under the assumption of perfectly depolarized pumps, the ASE from Raman amplification is randomly polarized.

For both types of amplifiers considered here (EDFA or Raman), the spectral distribution of ASE follows closely the amplifier's gain profile. Since spectral gain variations occur on wavelength scales much larger than the bandwidth of typical communication signals, ASE can be considered white over the signal bandwidth, i.e. the ASE spectral density can be considered constant over the optical signal frequency.

Double-Rayleigh Backscatter

Rayleigh scattering of light is an elastic scattering process caused by small-scale inhomogeneities of the refractive index of the media. The fraction of light that is backscattered depends on the composition of the glass, the waveguide properties of the fiber, and the recapture fraction, which determines the fraction of backscattered optical power that is actually captured in a guided fiber mode. The amount of optical power that is Rayleigh backscattered into a guided fiber mode per unit length is quantified by the Rayleigh backscatter coefficient r. For NZDFs at 1550 nm, with an effective mode area of $A_{\text{eff}} = 53\ \mu\text{m}^2$, we have $r = 9.6 \times 10^{-5}\ \text{km}^{-1}$. For typical DCF, we have $r = 3.7 \times 10^{-4}$ (see Table 5).

Using the Rayleigh backscatter coefficient, the optical power that is Rayleigh backscattered to the fiber input reads

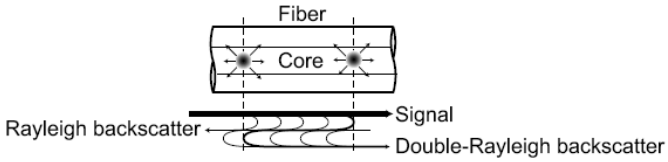

Fig. 8. Generation of Double-Rayleigh Backscatter (DRB) in an optical fiber.

$$\mathrm{P_{RB}} = \mathrm{P_{in}} r \int_0^L G(0,z)^2 dz \tag{23}$$

In an un-pumped (passive) optical fiber, with $G(0,z) = \exp[-\alpha z]$, this expression simplifies to

$$\mathrm{P_{RB}} = \mathrm{P_{in}} \frac{r}{2\alpha}(1 - \exp[-2\alpha L]) \ , \tag{24}$$

which for long fibers and $\alpha = 0.05$ Np/km $= 0.2$ dB/km gives the well-known Rayleigh backscatter ratio of about 30 dB.

Being a linear process, Rayleigh scattering fully preserves the spectral content of the signal, i.e., the power spectral density of the Rayleigh-scattered power matches the magnitude of the launched optical signal spectrum. However, since the scattering process occurs at random locations within the fiber, the spectral frequency components of the backscattered signal are randomly de-phased, and any phase correlation in the backscattered spectrum is lost. This makes the Rayleigh backscattered signal a random process.

If Rayleigh scattering occurs twice within a fiber, such that a doubly-scattered portion of the original signal eventually co-propagates with the original signal, we observe beat noise between the signal and the DRB field at the receiver. The generation of DRB is schematically depicted in Fig. 8.

Under the undepleted pump approximation, the total DRB power, $\mathrm{P_{DRB}}$, is given by [63,18],

$$\mathrm{P_{DRB}} = G\,\mathrm{P_{in}}\, r^2 \int_0^L G(0,z)^{-2} \int_z^L G(0,\zeta)^2 \, d\zeta \, dz, \tag{25}$$

where $\mathrm{P_{in}}$ is the signal input power to the DRA. Oftentimes it is more convenient for system design to specify the amount of DRB in terms of the ratio $\mathrm{P_{DRB}}/\mathrm{P_{out}}$ where $\mathrm{P_{out}} = \mathrm{G\,P_{in}}$ is the signal power at the fiber output. This leads to the definition of the *crosstalk ratio*, $\mathrm{R_c}$, as [18]

$$\mathrm{R_c} \equiv \frac{\mathrm{P_{DRB}}}{\mathrm{G\,P_{in}}} = r^2 \int_0^L G(0,z)^{-2} \int_z^L G(0,\zeta)^2 \, d\zeta \, dz. \tag{26}$$

For a passive fiber, this equation becomes

$$\mathrm{R_c} = \frac{r^2}{4\alpha^2}(\exp[-2\alpha L] - 1 + 2\alpha L) \ , \tag{27}$$

which yields a typical crosstalk ratio of -50 dB. If the transmission fiber is made active through DRA, the crosstalk ratio can reach unacceptably high values, as will be discussed in Sec. 3.1.

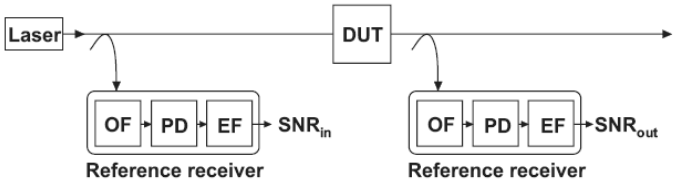

Fig. 9. The definition of noise figure. OF: Optical filter, EF: Electrical filter, PD: Photo detector.

It is worth noting that DRB is *not* completely depolarized, but has a degree of polarization of 5/9, co-polarized with the signal [64], which has to be taken into account in evaluating beat noise, since beating at photodetection only occurs between co-polarized optical fields [cf. Eq. (8)]. Together with the non-white spectral characteristics, this fundamentally distinguishes DRB from ASE, and leads to the different beat noise expressions (12) and (13).

Amplifier Noise Figure

In analogy to microwave amplifiers, optical amplifiers are conveniently characterized by their *noise figure* NF, which quantifies the noise enhancement by the amplifier. The noise figure is generally defined as the signal-to-noise ratio (SNR) at the amplifier input divided by the SNR at the amplifier output,

$$\mathrm{NF} = \frac{\mathrm{SNR_{in}}}{\mathrm{SNR_{out}}}, \tag{28}$$

where $\mathrm{SNR_{in}}$ is given by accounting for a baseline noise reference. In microwave engineering, this baseline noise is typically considered to be thermal noise at room temperature. At optical frequencies it is more convenient to consider the fundamentally unavoidable *signal shot noise* as a noise reference, and consequently to define the noise figure with the help of the *electrical* SNR *after* photodetection. This engineering approach to the definition of noise figure[10] is visualized in Fig. 9, where the *device under test* (DUT) could be an optical amplifier or any other optical component whose noise figure is to be assessed.

Using Eq. (14) for the shot noise variance, we find for the SNR at input of the DUT,

$$\mathrm{SNR_{in}} = \frac{S^2 P_s^2}{\sigma_{\mathrm{shot}}^2} \approx \frac{S P_s}{2eB_e/[1 + B_s^2/(4B_e^2)]^{1/2}} \approx \frac{P_s}{2h\nu B_e}\ , \tag{29}$$

where the last approximation holds for quasi-CW ($B_s \ll B_e$) signaling, and Eq. (9) was substituted for S, assuming a perfect photodiode ($\eta = 1$). The SNR at the output of the DUT, $\mathrm{SNR_{out}}$, is obtained by considering all sources of noise that are present in an ideal receiver (i.e., a receiver with no electronics noise) following the DUT.

In the case of a purely *passive optical element* with transmission $T_F < 1$, we only encounter shot noise, and the output SNR becomes

[10] Related definitions of the noise figure, which are directly based on quantum theory, and are thus more rigorous but less used in an engineering context are discussed in [65,66].

$$\mathrm{SNR}_{\mathrm{out}} = \frac{S^2 T_F^2 P_s^2}{\sigma^2_{\text{shot, out}}} = \frac{S^2 T_F^2 P_s^2}{T_F \sigma^2_{\text{shot, in}}} = T_F \ \mathrm{SNR}_{\mathrm{in}} \ . \tag{30}$$

Therefore, the noise figure of a passive element is equal to its loss ($F = 1/T_F$), in complete analogy to lossy elements in microwave engineering.

If the DUT represents an *optical amplifier* with gain G, the noise within the ideal output reference receiver will contain beat noise in addition to shot noise, and the output SNR becomes

$$\mathrm{SNR}_{\mathrm{out}} = \frac{S^2 G^2 P_s^2}{\sigma^2_{\mathrm{s-ASE}} + \sigma^2_{\mathrm{ASE-ASE}} + \sigma^2_{\mathrm{shot,out}}}. \tag{31}$$

If we neglect the ASE-ASE beat noise term, which can typically be well justified in the context of optical communication systems[11], we find by substituting Eqs. (10) and (14), and taking note of $\sigma^2_{\mathrm{shot,out}} = G\sigma^2_{\mathrm{shot,in}}$,

$$\mathrm{SNR}_{\mathrm{out}} = \frac{S^2 G^2 P_s^2}{4S^2 N_{\mathrm{ASE}} G P_s B_e + 2eSGP_s B_e} [1 + B_s^2/(4B_e^2)]^{1/2} \ . \tag{32}$$

Thus, using Eqs. (29), (32), and (9), the noise figure for an optical amplifier, assuming an ideal ($\eta = 1$) reference photodiode, becomes

$$\mathrm{NF} = \frac{1}{G} \left(\frac{2N_{\mathrm{ASE}}}{h\nu} + 1 \right) \ . \tag{33}$$

Inserting expression (19) for N_{ASE}, we obtain

$$\mathrm{NF} = 2n_{\mathrm{sp}}(1 - 1/G) + 1/G \ . \tag{34}$$

Since n_{sp} is lower-bounded to unity, the theoretically minimum noise figure of a high-gain optical amplifier is 3 dB. EDFAs with noise figures approaching this limit to within a few tenths of a dB have been demonstrated [67]. Typical values of noise figures for system-deployable, wide-band EDFAs are between 5 and 7 dB.

One of the main advantages of introducing noise figures is the possibility of assessing the noise performance of an entire system consisting of a concatenation of various elements with individually known gain (or loss) and noise figure, such as a chain of optical amplifiers inserted between transmission fiber and DCF. It is easy to show that in the case of concatenation of DUT_1 (noise figure NF_1) and DUT_2 (noise figure NF_2), the noise figure NF_{12} of DUT_{12} (= DUT_1 immediately followed by DUT_2) is given by [1,68]

$$\mathrm{NF}_{12} = \mathrm{NF}_1 + \frac{\mathrm{NF}_2 - 1}{G_1}, \tag{35}$$

where G_1 is the net gain (or loss) of DUT_1. The noise figure for concatenation of more than two amplifiers can be obtained by using Eq. (35) recursively.

We next consider the noise figure of an entire transmission span [1], consisting of a lossy transmission fiber (transmission $T_F < 1$, and hence noise figure $\mathrm{NF}_{\mathrm{fiber}} = 1/T_F$) in combination with either lumped or distributed optical amplification (noise figure $\mathrm{NF}_{\mathrm{amp}}$ and amplifier gain $G = 1/T_F$, such that the span loss is fully compensated by

[11] Note that this assumption is crucial to our engineering definition of the noise figure of optical amplifiers. If this assumption breaks down, a more rigorous approach has to be taken, as pointed out by Haus [65].

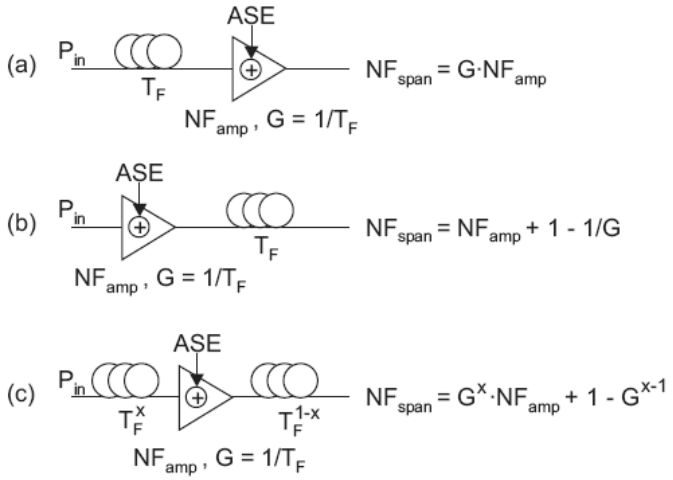

Fig. 10. The benefit of distributed amplification on ASE generation.

the optical amplifier). If, as shown in Fig. 10a, a lumped amplifier (e.g., an EDFA) is placed at the end of the fiber span, we find with the help of Eq. (35),

$$\mathrm{NF}_{\mathrm{span}} = G\mathrm{NF}_{\mathrm{amp}} \qquad [\text{ linear units }], \tag{36}$$

or

$$\mathrm{NF}_{\mathrm{span}} = G + \mathrm{NF}_{\mathrm{amp}} \qquad [\text{ in dB }]. \tag{37}$$

Since typical fiber span losses are on the order of 20 dB, the noise figure of an amplified fiber span is usually dominated by the span loss, and amounts to about 25 to 27 dB. If we were to place the optical amplifier *in front* of the fiber span, and keep the optical power levels as indicated in Fig. 10b, the noise figure of the amplified span would only be $\mathrm{NF}_{\mathrm{span}} = \mathrm{NF}_{\mathrm{amp}} + 1 - 1/G$, significantly less than in the first case, where the amplifier was placed at the end of the span. The general advantage obtained by putting amplification prior to attenuation can be intuitively understood by the fact that any attenuation *after* the injection of noise acts on *signal and noise*, leaving the OSNR constant. On the other hand, any attenuation *prior to* amplification degrades the signal only, while the full amount of noise is injected at the amplifier at the end; this leads to a substantial OSNR degradation. Unfortunately, it is typically not possible to compensate for the full span loss at the fiber input, since the optical signal launch power would be prohibitively high, and would severely degrade the signal due to fiber nonlinearity. Therefore, discrete amplification has to be employed at the end of each transmission span in practice.

A viable compromise between the two extreme cases shown in Figs. 10a and b can be achieved using *distributed amplification*, which we will now illustrate by a simple example, specializing the more general framework found in, e.g., [1]: Turning the transmission fiber into an amplifier across its entire length is conceptually equivalent to pushing a lumped amplifier at the span output inside the transmission fiber, as shown

in Fig. 10c. Doing so, the span loss is divided into a pre-amplifier portion T_F^x and a post-amplifier portion T_F^{1-x}, with $0 < x < 1$; note that the overall fiber span loss is kept constant ($T_F^x T_F^{1-x} = T_F$). Using Eq. (35), we find $\mathrm{NF_{span}} = G^x \mathrm{NF_{amp}} + 1 - G^{x-1}$ for the noise figure of the entire span, which is mainly determined by the first term, representing the amount of attenuation before amplification. We therefore note that pushing amplification inside a span by means of distributed amplification (as emulated by Fig. 10c) results in a better span noise figure without increasing the launch power into the span.

Since the noise figure of an isolated amplifier by itself looses its significance in systems with distributed amplification, it is convenient to benchmark the noise performance of such systems by means of an *effective noise figure*, which is defined as the noise figure of a *hypothetical* discrete amplifier placed at the end of a passive transmission span (according to the setup of Fig. 10a) that would give the *same span noise figure* as the actual transmission span, which uses distributed amplification (e.g., as modeled by the setup of Fig. 10c). To give an example, we calculate the effective noise figure of the system of Fig. 10c: To this end, we equate the noise figure $G\mathrm{NF_{eff}}$ of the hypothetical system and the noise figure $G^x \mathrm{NF_{amp}} + 1 - G^{x-1}$ of the actual system, and solve for $\mathrm{NF_{eff}}$. Assuming a 20-dB span loss and mid-span ($x = 0.5$) amplification with a noise figure of $\mathrm{NF_{amp}} = 8$ dB, we obtain $\mathrm{NF_{eff}} = -1.9$ dB. Note that the effective noise figure, being the characteristic of a *hypothetical* amplifier, can well be smaller than 3 dB. As our numerical example shows, the effective noise figure can even be smaller than unity (negative when expressed in dB), even if the noise figure of the amplifier within the span is rather high. This reiterates the noise benefits of distributed amplification.

Expanding one step further, we consider as a DUT a distributed optical amplifier with appreciable DRB on top of ASE. Then, neglecting again all noise-noise beat terms, the output SNR is given by

$$\mathrm{SNR_{out}} = \frac{S^2 G^2 P_s^2}{\sigma^2_{\mathrm{s-ASE}} + \sigma^2_{\mathrm{s-DRB}} + \sigma^2_{\mathrm{shot,out}}} \,, \tag{38}$$

which translates to

$$\mathrm{NF} = \frac{1}{G} \left(\frac{\sigma^2_{\mathrm{s-ASE}}}{G\,\sigma^2_{\mathrm{shot,in}}} + \frac{\sigma^2_{\mathrm{s-DRB}}}{G\,\sigma^2_{\mathrm{shot,in}}} + 1 \right), \tag{39}$$

and after substitution of Eqs. (14), (10), (11), and (9) to

$$\mathrm{NF} = \frac{1}{G} \left(\frac{2\,N_{\mathrm{ASE}}}{h\,f} + \frac{5/9\,P_{\mathrm{DRB}}}{hf\ (B_e^2 + B_s^2/2)^{1/2}} + 1 \right). \tag{40}$$

The factor of $5/9\ P_{\mathrm{DRB}}$ accounts for the fact that only 5/9 of the total DRB power is co-polarized with the signal [64,18], as mentioned above. Note that the relative importance of signal-DRB beat noise to shot noise decreases as either the signal bandwidth or the receiver's electrical bandwidth increases [69,70].

Both N_{ASE} and P_{DRB} refer to quantities evaluated at the amplifier output. Note that the noise figure incorporating DRB now depends on signal power, since P_{DRB} is proportional to the signal power. This implies that the signal power is a required parameter to evaluate the noise figure of a system impaired by DRB.

Delivered OSNR

The quality of a transmission line with respect to ASE generation is characterized by the *delivered OSNR*, $\mathrm{OSNR_{del}}$. To calculate $\mathrm{OSNR_{del}}$, one can first calculate the OSNR at the end of a transmission line, $\mathrm{OSNR_{line}}$, due to the generation of ASE by in-line amplification only. For identical spans, this can be written as [68]

$$\mathrm{OSNR_{line}} = 58 + \mathrm{P_{in}} - \mathrm{NF_{eff}} - \Gamma_{\mathrm{F}} - 10\log \mathrm{N_{amp}} \qquad [\text{ in dB }], \quad (41)$$

where $\mathrm{P_{in}}$ is the signal launch power at the input of each span [dBm], $\mathrm{NF_{eff}}$ is the effective noise figure of the optical amplifiers [dB], Γ_{F} is the span loss [dB], and $\mathrm{N_{amp}}$ is the number of amplifiers that follows each fiber span and, here, is equal to the number of spans, $\mathrm{N_{span}}$.

Assuming that the OSNR at the input of the transmission line, $\mathrm{OSNR_{TX}}$, is of finite value, the delivered OSNR, $\mathrm{OSNR_{del}}$, at the end of a transmission is given by

$$\frac{1}{\mathrm{OSNR_{del}}} = \frac{1}{\mathrm{OSNR_{TX}}} + \frac{1}{\mathrm{OSNR_{line}}} [\text{ linear units }]. \quad (42)$$

2.3. Signal Distortions

This section describes the most important signal distortions affecting optical communication links. Knowledge of the trade-offs between noise and distortions is important to understand system design. For example, although a highly distorted signal with little noise (good OSNR) can yield the same BER as a signal with little distortion but a lot of noise (poor OSNR), system designers will always prefer the latter case. This is because noise *gradually* accumulates in a system over its length, and thus *slowly* deteriorates system performance. On the other hand, most types of signal distortion show a threshold effect, beyond which an *abrupt* decrease in BER occurs. Operating at high signal distortions leaves little margin to a system as any additional impairment from defective components or aging can lead to catastrophic deterioration in system BER.

Dispersion-Induced Signal Distortions

Dispersion-induced signal distortions (e.g., pulse broadening in intensity modulated systems, or phase distortions in phase modulated systems) often limit the performance of digital fiber-optic communications systems. The impact of dispersive pulse broadening on system design depends significantly on the system under consideration: single-span, unamplified access systems (10-100 km), such as coarse wavelength-division multiplexed (CWDM) links, are sufficiently dispersion-tolerant, if the signal distortions due to dispersion are acceptably low for all channels, given the system's power budget. In metropolitan area and regional systems, a large dispersion tolerance for 10-Gbit/s channels may allow the installation of 10-Gbit/s channels on a system built for 2.5-Gbit/s with little or no need for installing DCMs. In terrestrial LH and ULH transport, dispersion tolerance usually measures the ability of a system to accommodate variations in fiber dispersion without having to resort to per-channel fixed or tunable dispersion compensators (TDCs); if unavoidable, one strives to at least minimize the

TDC's required tuning range. Note that even slight uncertainties or variations in fiber dispersion may accumulate to substantial values over system lengths of many hundred kilometers: as discussed in Sec. 3.2, limited characterization accuracies of installed fiber, manufacturing tolerances, imperfect dispersion slope matching (i.e., non-ideal broadband compensation) of DCMs, the availability of a limited set of DCMs with a selection of fixed dispersion values only (*granularity* of DCMs), and appreciable temperature-induced changes in fiber dispersion make dispersion-tolerant transmission attractive. In future transparent optical mesh networks, dispersion tolerance is likely to imply a signal's robustness to propagating over different physical paths with mixed fiber types and changing dispersion maps. Several techniques can be used to achieve dispersion tolerance, including modulation format and modulator technology, optical and electrical equalization, and FEC. We will briefly review these techniques here, which either compete with the use of DCFs or complement it. Understanding these techniques allows us to place the role of DCFs in a broader systems context.

Modulation Formats and Modulator Technology

Access systems predominantly use low-cost, highly integrated transmitter hardware, such as directly modulated lasers or electro-absorption modulators, and are therefore restricted to intensity modulation, in its simplest form non-return-to-zero on/off keying (NRZ-OOK). More sophisticated direct modulation techniques, such as dispersion-supported transmission [71], optical phase modulation [72], and optically filtered or reduced-chirp laser designs [73,74] increase dispersion tolerance at the expense of higher transmitter and/or receiver complexity.

In regional or LH system design, on the other hand, advanced optical modulation formats, typically generated by chirp-free Mach-Zehnder modulators (MZMs) are important to guarantee sufficient dispersion tolerance as well as robustness to fiber nonlinearity and concatenated optical filtering. Table 4 lists the simulation results for linear dispersion tolerance at 1 dB and 2 dB OSNR penalty for the selection of modulation techniques presented in Table 3 [61], attractive for 10-Gb/s and 40-Gb/s regional and long-haul transport systems (see, e.g., [75,61,76] and references therein for an introduction to optical modulation formats). In contrast to the direct modulation techniques used in access systems, all formats listed in Table 3 are generated by chirp-free Mach-Zehnder modulators (MZMs). Return-to-zero (RZ) formats typically (but not exclusively) use two-stage modulator setups, with a first (data) modulator and a second modulator to carve pulses [77]. Typical duty cycles are between 33% and 67%, and are indicated by the percentage numbers in Table 3. Differential quadrature phase shift keying (DQPSK) is either implemented by a cascade of two phase modulators [78] (straight-line or MZM), or by two sub-MZMs nested in a super-MZM [79]. The fact that spectrally narrow formats, in general, yield good dispersion tolerance [80] is reflected by the numbers for Duobinary and DQPSK. However, good dispersion tolerance may come at the expense of reduced back-to-back performance (note the higher required OSNR for Duobinary in Table 3) or higher hardware complexity (DQPSK requires more complex transmitters and receivers [79]). These trade-offs show the importance of assessing the dispersion tolerance of a modulation format with a comprehensive view on all the implications associated with it.

Modulation format	1-dB penalty	2-dB penalty
Units	ps/nm	ps/nm
NRZ-OOK	39	56
Duobinary	182	206
33% duty cycle RZ-OOK	37	49
67% duty cycle CSRZ	37	50
67% duty cycle RZ-DPSK	43	59
50% duty cycle RZ-DQPSK	122	158

Table 4. Dispersion tolerance (OSNR penalty) for different modulation formats at 42.7 Gb/s and at a target BER of 10^{-3}. NRZ: Non return-to-zero, RZ: Return-to-zero, CSRZ: Carrier-suppressed return-to-zero, DPSK: Differential phase shift keying, DQPSK: Differential quadrature phase shift keying

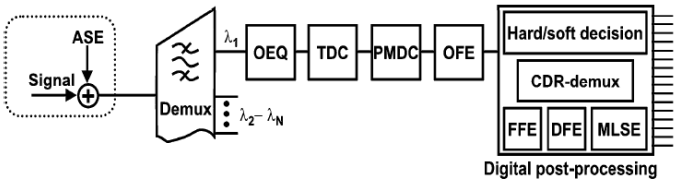

Fig. 11. General layout of an advanced optical receiver [89], using compensators (TDC, PMDC), optical equalizers (OEQ), electrical equalizers, and generic signal processing. OFE: Optical front-end, FFE: Feed-forward equalizer, DFE: Decision feedback equalizer, MLSE: Maximum-likelihood sequence estimator, CDR: Clock and data recovery, ASE: Amplified spontaneous emission.

Equalization to Increase Dispersion Tolerance

In contrast to DCMs and TDCs, which both counteract residual dispersion by passing the optical signal through an element of opposite-sign dispersion (an *inverse filter*) prior to detection, equalizers do not try to undo the physical effect of dispersion. Equalizers rather address the *symptoms* of dispersive pulse broadening on the signal quality by minimizing inter-symbol interference (ISI), which is simultaneously generated by residual dispersion [81–84] and other signal distortions, such as PMD [83–85] limited-bandwidth transmit or receive hardware [86,87], narrow-band in-line optical filtering [88] or fiber nonlinearity. Equalization can be performed in the optical domain and in the electrical domain, and can either substitute or complement impairment-specific compensators (TDC, PMDC), as shown in the advanced optical receiver setup of Fig. 11 [89].

Optical equalization (OEQ), placed before photo-detection, can use the full optical field information rather than only information on the optical intensity [88,90]. Also, if properly designed, OEQ can work *simultaneously* on many WDM channels by placing the OEQ in front of the WDM demultiplexer [88]. This is in contrast to electronic equalization, which always acts on the signals after photo-detection, and therefore is inherently a *per-channel* device. On the other hand, logic processing and bitwise feedback at high data rates is not easily implemented in the optical domain.

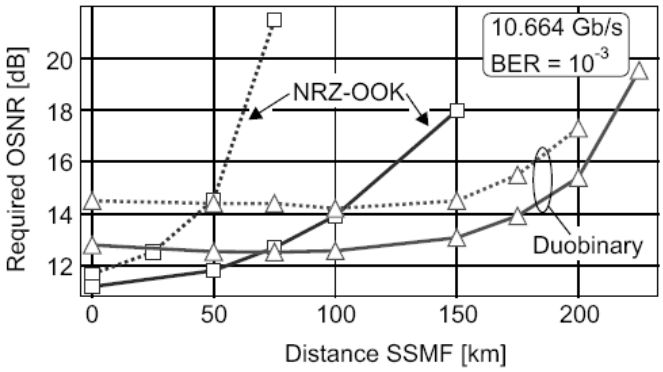

Fig. 12. Required OSNR at BER=10^{-3} vs. SSMF transmission distance at 10.7 Gb/s [61]. Squares: NRZ-OOK. Triangles: Duobinary. Dotted: un-equalized. Solid: using electronic equalization [83].

Studied for over 10 years for lightwave systems [81–86], electronic equalization at 10 Gb/s has recently experienced a boost by progress in high-speed integrated circuits, and has proven a powerful tool to increase dispersion tolerance [91–95]. Equalization techniques range from multi-tap feed-forward and decision feedback structures to sophisticated schemes employing multiple thresholds in conjunction with FEC. Advanced schemes using maximum-likelihood sequence estimation (MLSE) have now also been demonstrated at 10 Gb/s [96].

Figure 12 [61] visualizes the benefit of equalization for chirp-free NRZ-OOK and Duobinary modulation, both generated at 10.7 Gb/s using an x-cut $LiNbO_3$ MZM. The required OSNR, measured at BER=10^{-3} is shown as a function of transmission distance over SSMF at 1550 nm. Using electronic equalization [83], the permissible dispersion for 2 dB OSNR penalty could be shifted from 700 to 1650 ps/nm for NRZ in this experiment. At the same time, the 2-dB penalty point for Duobinary could only be pushed from 3200 to 3490 ps/nm, essentially by improving performance by a dispersion-independent amount. It is evident from this example that the increase in dispersion tolerance can substantially depend on the chosen modulation format and equalization scheme.

Forward Error Correction

Over the past few years, FEC has become an invaluable tool to increase system margins [97], which can be traded for enhanced tolerance to propagation impairments, most notably ASE accumulation. FEC schemes are characterized by their bit rate overhead and their correction curve, which is typically specified for uncorrelated (non-bursty) detection errors and translates the *raw channel* BER at the FEC input to a *corrected* (or decoded) BER at the FEC output (cf. inset to Fig. 13).

Alternatively, an FEC scheme may be specified by its coding gain, which is the gain in required OSNR for achieving the same target BER with FEC as for an uncoded system [97]. However, when assessing the benefits of FEC in a particular system

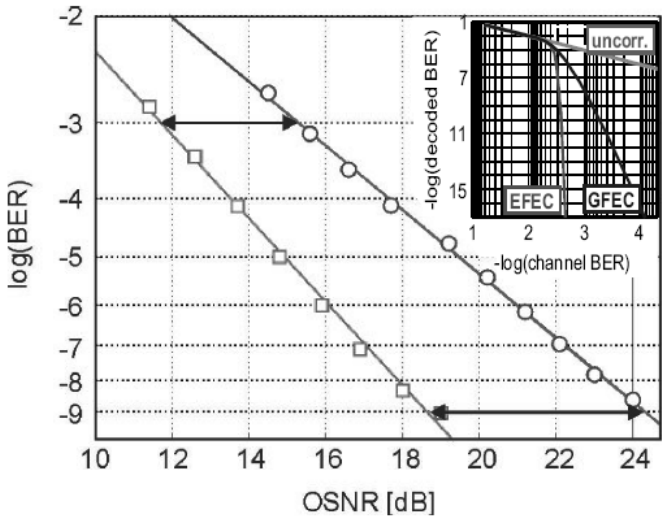

Fig. 13. BER vs. OSNR for NRZ-OOK at 10.7 Gb/s. Squares: back-to-back; circles: after 60 km of SSMF; arrows: BER-dependent dispersion penalties. - Inset: Correction curves for generic FEC (GFEC) and enhanced FEC (EFEC).

scenario, coding gains alone are insufficient: firstly, the FEC overhead implies a higher data rate, which changes the impact of certain propagation impairments. For example, the tolerance to dispersion shrinks with the square of the bit rate, which implies a 14% reduction in dispersion tolerance for a typical FEC overhead of 7% and reduces the coding gain. Secondly, many impairments (including dispersion) lead to higher penalties at good BER than at poor BER (cf. double-headed arrow in Fig. 13), or even to error floors, which together with the steep correction curve of FECs results in enhanced coding gains in the presence of impairments. Thirdly, the occurrence of burst errors can degrade FEC characteristics for certain kinds of impairments [98].

Fiber Nonlinearity

Transport systems spanning more than a few hundred kilometers of transmission fiber are likely to induce nonlinear distortions on the optical signal. The most important nonlinear phenomenon that results in signal distortion is the instantaneous Kerr effect [99], which occurs as a result of the very high optical intensities inside the core of single-mode optical fibers, typically exceeding 1 MW/cm^2. Such high intensities lead to the fiber's refractive index becoming proportional to the signal intensity.

Kerr nonlinearity can be decomposed into a host of nonlinear interactions that are referred to as self-phase modulation (SPM) [99], cross-phase modulation (XPM) [99], four-wave mixing (FWM) [99], intra-channel cross-phase modulation (IXPM) [100] and intra-channel four-wave mixing (IFWM) [100,101].

Cumulative Nonlinear Phase

The distortions imprinted on a signal by nonlinear effects depend, in general, on both the transmission line parameters and the operating conditions. The line parameters affecting nonlinear transmission include the fiber nonlinear coefficient, the fiber length, the fiber dispersion and the dispersion map [102], as discussed in more detail in Sec. 3.2. The operating conditions impacting nonlinear transmission are the signal launch power into each optical fiber span, the signal power evolution along the fiber length (e.g. discrete versus distributed amplification), the bit rate, the channel spacing and the modulation format.

Accurately evaluating the effects of fiber nonlinearity on the signal involves solving the *Generalized Nonlinear Schrödinger Equation* (GNSE) [99] that describes the evolution of the optical field along the transmission line. Solving the GNSE with high accuracy can be done numerically using the split-step algorithm [99], but is computationally intensive. However, it is possible for some systems to *approximate* the effects of fiber nonlinearity analytically. In transmission lines where propagation is limited by SPM, XPM or IXPM (after optimization of the dispersion map), one can approximate that the distortions induced on the signal by fiber nonlinearity is determined by the cumulative nonlinear phase shift given by

$$\phi(L) = \int_0^L \gamma(z)\,\mathrm{P}(z)\,dz\ , \tag{43}$$

where $\mathrm{P}(z)$ is the evolution of the average signal power along a fiber of length L having a nonlinear coefficient $\gamma(z)$ [99]. The nonlinear coefficient $\gamma(z)$ is given by

$$\gamma(z) = \frac{\mathrm{n}_2\,\omega_0}{\mathrm{c}\,\mathrm{A}_{\mathrm{eff}}}\ , \tag{44}$$

where n_2 is the nonlinear refractive index coefficient, an intrinsic material property of the fiber, ω_0 is the angular frequency at the signal wavelength, c the speed of light in vacuum and $\mathrm{A}_{\mathrm{eff}}$) the fiber effective mode area [99]. Equation (43) is useful to compare, for instance, the relative impact of fiber nonlinearity on two transmission lines having different signal power evolutions at a fixed bit rate, modulation format and fiber dispersion. For example, we can compare a transmission line consisting of passive fiber spans with a line containing distributed (Raman) amplification by using the ratio of nonlinear phases,

$$\mathrm{R}_{\mathrm{NL}} \equiv \frac{\phi_{\mathrm{DRA}}(L)}{\phi_{\mathrm{Pas}}(L)}, \tag{45}$$

where $\phi_{\mathrm{DRA}}(L)$ and $\phi_{\mathrm{Pas}}(L)$ are the integrated nonlinear phase for a DRA and a passive fiber, respectively. Assuming constant γ and fixed signal input power to the fiber, the nonlinear phase ratio factor R_{NL} can be written as

$$\mathrm{R}_{\mathrm{NL}} = \frac{\alpha_{\mathrm{s}}}{1-\exp(-\alpha_s\,L)} \int_0^L G(0,z)\,dz, \tag{46}$$

which can be interpreted as the ratio of *path-averaged signal powers* in the DRA as compared to the passive fiber. Raman pumping of fibers provides gain to the signal, which increases the path-averaged signal power, and thus results in an effective increase

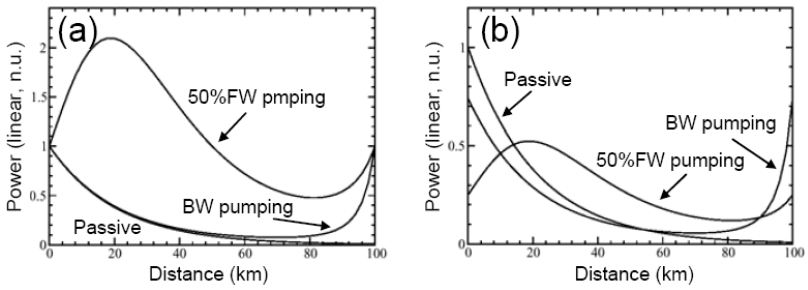

Fig. 14. Signal power evolution along a fiber span at a) fixed signal launch power and b) constant cumulative nonlinear phase. Three configurations are shown: passive fiber and DRAs with full backward (BW) and 50% forward (FW) pumping. Both DRAs are pumped at transparency (0 dB net gain).

in nonlinear signal distortion. This is illustrated in Fig. 14a, showing the signal power evolution within a passive optical fiber as well as within two different DRAs, one using backward Raman pumping only, and the other using 50% backward and forward Raman pumping. Both pumping configurations are operated at transparency (i.e. producing identical output and input power levels). As seen in the figure, using forward pumping rapidly increases the signal power, as it amplifies the signal at the *input* end of the fiber where the signal power is highest. In contrast, a large backward Raman gain is necessary to bring the signal at the fiber output end to a level comparable to the level at the fiber input end. As a result, only a small increase in nonlinearity occurs with backward Raman pumping relative to a passive fiber. For the two Raman pumping scenarios of Fig. 14a, one can make the cumulative nonlinear phase equal by decreasing the signal power by the factor $\mathrm{R_{NL}}$ at the input of the span. This is illustrated in Fig. 14b where the launch powers have been reduced to achieve equal cumulative nonlinear phases.

Figure 15 shows how the nonlinear phase increases with increasing Raman pumping in a DRA for different levels of forward and backward Raman pumping. Because backward Raman pumping mainly increases the low signal power levels towards the end of the transmission span, it features the lowest increase in nonlinear phase. Thus, backward Raman pumping is very efficient to provide distributed signal gain with minimum impact on fiber nonlinearity. However, large backward Raman gain leads to excessive DRB generation that limits transmission [102]. As a result, backward Raman pump powers should not exceed certain levels; optimized Raman pumping configuration therefore include some amount of forward pumping to minimize the effect of DRB while still providing large Raman gain [103,63]. A typical ratio of forward to total Raman pump powers to optimize transmission is around 30%. Specialized fiber designs can also be developed to minimize the impact of nonlinearity and DRB in DRAs [104,105].

Dispersion Tolerance and Fiber Nonlinearity

Signal distortions due to fiber nonlinearity can affect the signal in many ways. Two important effects of fiber nonlinearity are a change in the value of NRD at which

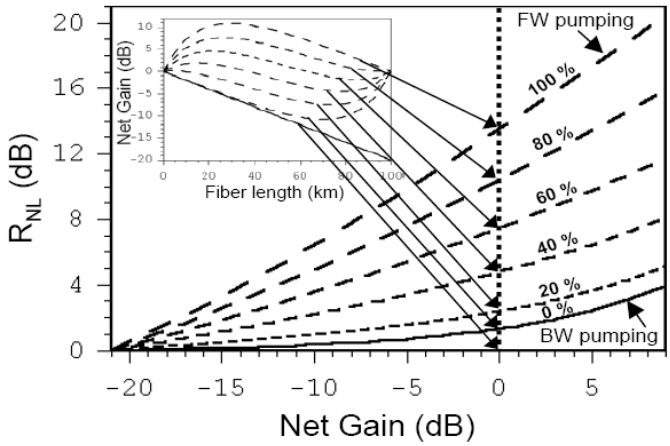

Fig. 15. Increase in nonlinear phase ratio, $\mathrm{R_{NL}}$, in a DRA as a function of the net Raman gain for various percentage values of forward pump power to total Raman pump power. 0% forward pumping corresponds to backward pumping only. The DRA is 100 km, and the signal and pump losses are α_s = 0.21 dB/km and α_p = 0.26 dB/km, respectively. The inset shows the signal power evolution within the fiber when pumping to transparency (0 dB net Raman gain).

detection is optimum, and a reduction in dispersion tolerance. As a consequence, the dispersion tolerance in the nonlinear regime can be substantially different from the linear dispersion tolerance values listed in Table 4.

Figure 16 shows simulation results of the required OSNR for Duobinary, CSRZ, and NRZ-OOK modulation at 42.7 Gb/s and BER=10^{-3} as a function of NRD in the linear regime (dashed) and after 3,200 km of single-channel propagation (solid) over TrueWave® fiber (4.5 ps/nm dispersion, 55 μm^2 effective area). Each 100-km span was followed by discrete optical amplification (see Fig. 1a). A SPDM with a pre-compensation of -500 ps/nm and an RDPS of 25 ps/nm was used. The per-span launch power was chosen to generate a 1.5-dB OSNR penalty due to fiber nonlinearity at the optimum NRD, as compared to the back-to-back performance (zero NRD and linear propagation). As evident from Fig. 16, the 2-dB dispersion tolerance windows are reduced to 50%, 60%, and 80% of their widths in the linear regime for Duobinary, NRZ, and CSRZ, respectively, and the shift in optimal NRD is different for each modulation format. Note that the effect of fiber nonlinearity on the dispersion tolerance of various modulation formats can also be observed at much *shorter* transmission distances, for example if the signal launch power has to be increased to compensate for higher span losses or more amplification noise, or if the system is composed of a large number of shorter but lossier transmission spans (e.g., 32 highly lossy spans of 20 km each), which may occur in metropolitan area networks.

In addition to the tolerance to NRD, the tolerance to temperature-induced dispersion variations of the transmission fiber, as well as to the granularity of DCMs (pre-compensation, in-line compensation, post-compensation) has to be considered to assess a format's dispersion tolerance, as discussed in more detail in [106].

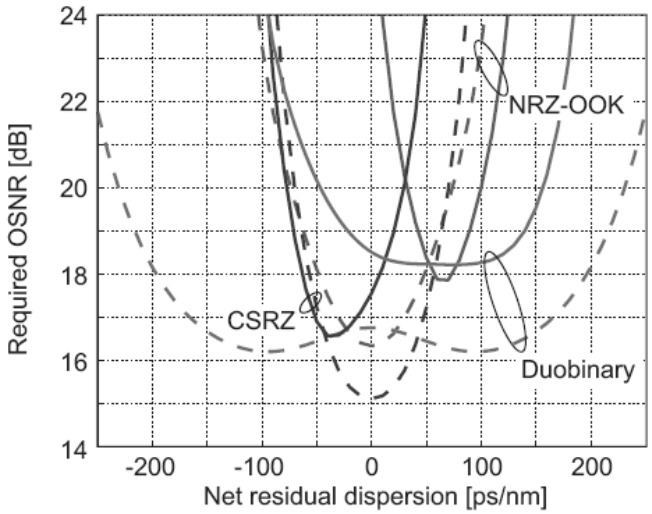

Fig. 16. Dispersion tolerance of various modulation formats without (dashed) and with (solid) fiber nonlinearity. The bit rate is 42.7 Gb/s.

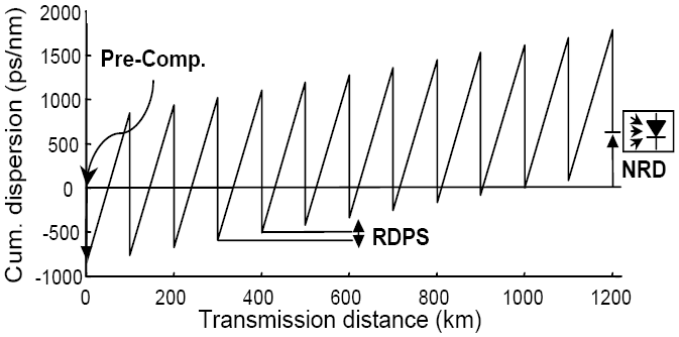

Fig. 17. The three parameters defining a singly-periodic dispersion map (SPDM): Pre-compensation, residual dispersion per span (RDPS) and net residual dispersion (NRD).

Dispersion Mapping

As mentioned in Sec. 1.2, SPDMs are the simplest to implement and facilitate the writing of engineering rules for system deployment. Figure 17 shows the three parameters that define a SPDM: pre-compensation, RDPS and NRD. Varying these three map parameters leads to all possible dispersion maps that are singly periodic.

The effects of dispersion mapping on transmission can be seen in Fig. 18 that shows transmission of a NRZ signal in the absence of nonlinearity (Fig. 18a) and

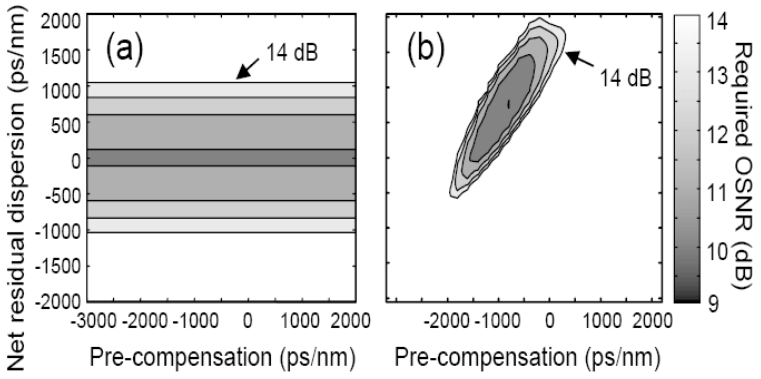

Fig. 18. Required OSNR at 10^{-3} BER as a function of pre-compensation and NRD: a) in the absence of fiber nonlinearity; b) after nonlinear transmission (parameters in main text). The outermost contour indicates 14 dB of required OSNR and decreasing by step of 1 dB going inwards. The bit rate is 10.7 Gb/s.

after nonlinear transmission (Fig. 18b) over 15 spans of 80 km of SSMF at 3.67 mW launch power per channel. The WDM channel spacing is 50 GHz, and the back-to-back required OSNR is 10.9 dB. SSMF parameters are D = 17 ps/(nm km) and S = 0.055 ps/(nm^{2}km). The fiber's nonlinear coefficient is $\gamma = 1.3 \quad (\mathrm{W\,km})^{-1}$. The DCF is assumed to have the same RDS as the transmission fiber, and nonlinearity in the DCF is neglected.

Figure 18 demonstrates how critical dispersion mapping is to minimize signal distortions. Deviations of a few hundred ps/(nm km) in pre-compensation or in NRD can lead to a significant OSNR penalty.

Polarization-Mode Dispersion

PMD and System Outage

The transversal index profile of real optical fibers deviates from ideal circular symmetry, which can be due to manufacturing imperfections or due to bending stress when the fiber is cabled and deployed in the field. As a consequence, the fiber becomes slightly birefringent, i.e., different polarizations of light travel at different speeds within the fiber. The two polarization eigenstates are referred to as the *principal states of polarization* (PSP), and the difference in group velocity between them is called *differential group delay* (DGD). The impact of the DGD on digital communication systems manifests itself in dispersive pulse broadening, called *polarization-mode dispersion* (PMD). If the DGD is constant over wavelength, only *first-order* PMD is present, while we need to include *higher-order* PMD if the DGD changes with wavelength (see, e.g., [107] for a detailed overview on the broad topic of PMD).

Figure 19 shows simulations of the OSNR penalty for NRZ, CSRZ, and 33% duty cycle RZ signals for typical beat-noise limited receiver parameters, and for first-order

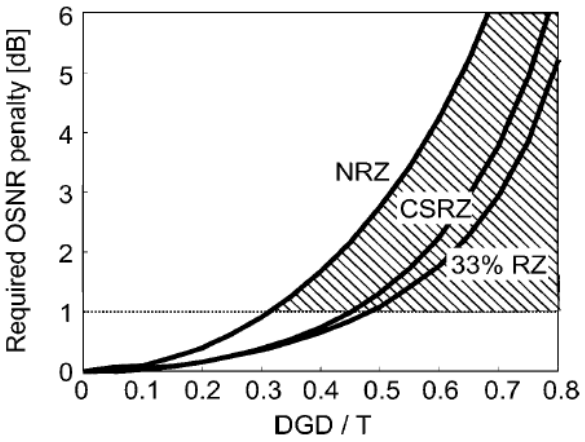

Fig. 19. OSNR penalty versus DGD, normalized to the bit duration T, for first-order PMD and various OOK modulation formats.

PMD with the signal split equally between the fiber's PSPs. It can clearly be seen that RZ formats are generally more robust to first-order PMD than NRZ formats [108]. The 1-dB OSNR penalty occurs at a DGD of around 30% of the bit duration for NRZ systems. This suggests that signal distortions due to PMD could be fully accounted for by allocating a 1-dB margin in the system's OSNR budget, provided the fiber PMD does not exceed 30% of the bit duration. However, this simple link budgeting approach, which can be successfully applied to most types of signal distortion, fails for PMD, since fiber PMD is a fundamentally random process: neither the amount of DGD nor the fiber's PSPs are deterministic, but may fluctuate randomly over time, obeying Maxwellian statistics; the probability density function (PDF) of the DGD is given by

$$\mathrm{PDF}[\mathrm{DGD}] = \frac{8}{\pi^2 \langle \mathrm{DGD} \rangle} \left(\frac{2\mathrm{DGD}}{\langle \mathrm{DGD} \rangle} \right)^2 \exp\left[- \left(\frac{2\mathrm{DGD}}{\langle \mathrm{DGD} \rangle} \right)^2 / \pi \right] \quad (\mathrm{DGD} > 0) \,, \tag{47}$$

with mean $\langle \mathrm{DGD} \rangle$.

It is important to understand that the tail of the Maxwellian PDF is unbounded, which implies that arbitrarily high values of DGD may be encountered with some low, but finite probability. This fact can pose severe problems on system design, since any OSNR margin that is allocated to accommodate penalties due to PMD in a system's link budget may be occasionally exceeded, leading to infrequent (but fundamentally unavoidable) instances of *system outage*. If a 1-dB OSNR margin is assigned, as shown in Fig. 19, the outage probability for a system using NRZ modulation can be obtained by calculating the Maxwellian probability that the DGD of a fiber with some given mean DGD exceeds 30% of the bit duration (hatched area in Fig. 19). Thus, the effect of PMD drags system specifications from a purely deterministic approach to probabilistic characterizations.

Specifying the most appropriate value for system outage is a matter of trading system complexity (and cost) against system reliability and a method for PMD specification is not completely defined among network operators; outage probability targets ranging between 10^{-3} to 10^{-7} are mentioned in this context.

Specification of Fiber PMD

For long fibers typically encountered in communication systems, it can be shown that the mean fiber DGD is proportional to the square-root of the fiber length [107]. Therefore, fiber PMD is specified by the *PMD coefficient*, given in ps/$\sqrt{\text{km}}$. Multiplying this value by the square-root of the fiber length yields the mean fiber DGD. While older fiber, installed in the 1980s, may have PMD coefficients as high as 0.8 ps/$\sqrt{\text{km}}$, the PMD coefficients of modern transmission fiber are well below 0.1 ps/$\sqrt{\text{km}}$.

To illustrate the impact of fiber PMD on system performance, consider a beat-noise limited NRZ system with an allocated margin for PMD of 1 dB, leading to system outage whenever the instantaneous DGD exceeds 30% of the bit duration (cf. Fig. 19). Assume a system outage specification of 4×10^{-5}. Integrating the Maxwellian PDF, Eq. (47), we identify this outage probability as the probability that the instantaneous DGD exceeds three times its mean value, i.e. $P[\text{DGD} > 3\langle\text{DGD}\rangle] = 4 \times 10^{-5}$. Therefore, the mean fiber PMD has to be lower than 10% of the bit duration to let the system stay within the outage specifications. At 10 Gb/s operating over old fiber (0.8 ps/$\sqrt{\text{km}}$), this limits the transmission distance only to some 160 km. Using new fiber (0.04 ps/$\sqrt{\text{km}}$), PMD could be tolerated for system lengths up to 4000 km, even for a 40 Gb/s system. Even longer system reach can be achieved by going to RZ formats.

3. Impact of DCF on Transmission

As mentioned in previous sections, dispersion compensation is necessary in systems operating at 10 Gb/s and above to limit the accumulation of dispersion and the resulting inter-symbol interference through pulse broadening. In addition, careful dispersion mapping is also used to minimize the impact of fiber nonlinearity. The presence of dispersion compensation in a transmission line also impacts transmission in many other ways. In the case of DCFs, the main impact on transmission are, additional generation of noise (i.e., ASE and DRB), signal distortions from fiber nonlinearity within the DCF, a possible increase in PMD, and signal distortions from a mismatch in dispersion between the practically achieved and the targeted dispersion maps. In this section, we will describe the general framework and the basic tools for evaluating the impact of DCFs on each of these aspects.

The parameters of the optical fibers that are used in this section are summarized in Table 5.

3.1. Noise

Noise generation along a transmission line takes mainly two forms, ASE and DRB (see Sec. 2.2). Inserting DCFs in a line system can increase both sources of noise through the additional amplification required by DCF loss as well as through Rayleigh scattering within the DCF, the latter increasing when the DCF is Raman pumped.

Property	Units	NZDF	SSMF	DCF
$\mathrm{A_{eff}}$	$\mu\mathrm{m}^2$	52.8	78.9	17.0
α_s	dB/km	0.2	0.2	0.5
α_p	dB/km	0.25	0.25	0.6
$\mathrm{C_r}(\lambda_\mathrm{s}, \lambda_\mathrm{p})$	1/(W km)	0.691	0.470	2.41
r	1/km	9.64×10^{-5}	6.63×10^{-5}	3.70×10^{-4}
n_2	m^2/W	2.5×10^{-20}	2.5×10^{-20}	2.5×10^{-20}

Table 5. Parameters of the optical fibers considered in this section. $\mathrm{A_{eff}}$ and r are evaluated at the signal wavelength $\lambda_s = 1550$ nm while $\mathrm{C_r}(\lambda_\mathrm{s}, \lambda_\mathrm{p})$ is the Raman gain efficiency for a signal at a given $\lambda_s = 1550$ nm for a pump located at $\lambda_p = 1450$ nm.

Optical Signal-to-Noise Ratio

As described in Sec. 2.2, the accumulation of ASE generated by optical amplification in the transmission line degrades the delivered OSNR, $\mathrm{OSNR_{del}}$, at the receiver. The insertion of dispersion compensation in the line introduces additional loss that requires additional amplification, and thus leads to additional ASE generation. It is important to note that, at large net gain G, the OSNR degradation from a single optical amplifier is virtually independent of the gain value [see Eqs. (18) and (19) noting that $P_s = G\,\mathrm{P_{in}^A}$, where $\mathrm{P_{in}^A}$ is the input power to an amplifier]. In contrast to the gain G (for large values of G), $\mathrm{P_{in}^A}$ has a direct impact on the OSNR at the output of an amplifier. The impact that a specific optical amplifier has on the delivered OSNR in a transmission line thus depends mainly on the input power of this amplifier relative to the input powers of the other amplifiers present in the line. As a result, the location of the DCFs in a line, either localized or diffused, greatly impacts $\mathrm{OSNR_{del}}$ as it determines the signal power evolution in each span. Such signal power evolution is represented schematically in Fig. 20 for a span using discrete optical amplification in the absence of dispersion compensation (Fig. 20a), with localized dispersion compensation (Fig. 20b) and with diffused dispersion compensation (Fig. 20c).

In transmission lines using localized dispersion compensation (Fig. 20b), the reduction in $\mathrm{OSNR_{del}}$ relative to a line without localized dispersion compensation (Fig. 20a) originates from the additional ASE generated by the second stage of amplification of the dual-stage amplifier that contains the dispersion-compensating element. As mentioned previously, the importance of the contribution of the second amplification stage relative to the first stage on the OSNR degradation depends on their relative signal input power (for similar noise figures of both stages). For instance, when the input power to the second amplification stage is identical to the input power of the first stage, the dual-stage amplifier degrades $\mathrm{OSNR_{del}}$ nearly twice as much as a single-stage amplifier with the same noise figure. The impact on $\mathrm{OSNR_{del}}$ of a dual-stage amplifier can also be viewed in terms of noise figure. The dual-stage amplifier is then considered as a single amplifier with an effective noise figure that is the weighted sum of the individual stages' noise figures by combining the expression for the noise figure of a single-stage optical amplifier, Eq. (33), with the noise figure concatenation rule, Eq. (35),

$$\mathrm{NF_{loc}} = \mathrm{NF_1} + \frac{\mathrm{NF_2} - \mathrm{T_{DCF}}}{G_1 \mathrm{T_{DCF}}}, \qquad [\text{ linear units }], \tag{48}$$

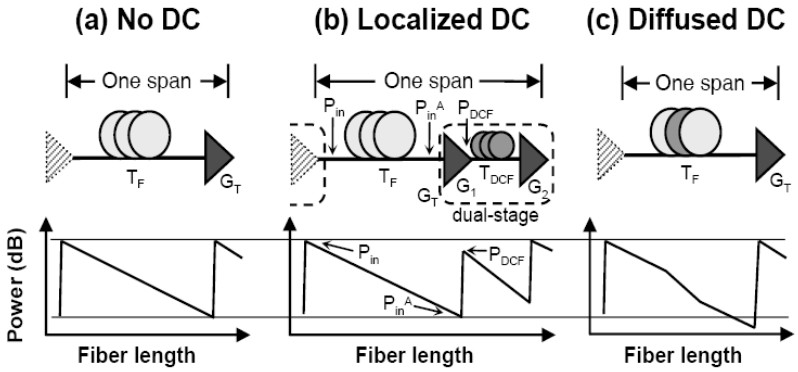

Fig. 20. Evolution of the signal power (in dB) over one span in a system a) without dispersion compensation, b) with localized dispersion compensation, and c) with diffused dispersion compensation.

where NF_1 and NF_2 are the noise figure of the first and second amplification stages of a dual-stage amplifiers, respectively. The noise figure can also be expressed explicitly in terms of spontaneous emission factors,

$$\mathrm{NF}_{\mathrm{loc}} = 2\,\mathrm{n}_{\mathrm{sp},1}\left(1-\frac{1}{G_1}\right)+\frac{2\,\mathrm{n}_{\mathrm{sp},2}}{G_1\,\mathrm{T}_{\mathrm{DCF}}}-\frac{2\,\mathrm{n}_{\mathrm{sp},2}-1}{G_T}, \qquad [\text{ linear units }], \quad (49)$$

where $\mathrm{n}_{\mathrm{sp},1}$ and $\mathrm{n}_{\mathrm{sp},2}$ are the spontaneous emission factors of the first and second amplification stages, respectively, and G_1 and G_T ($= G_1\mathrm{T}_{\mathrm{DCF}}G_2$) are the net gains of the first amplification stage and of the entire dual-stage amplifier, respectively. (The insertion loss of the DCF, expressed in dB, is $\mathit{\Gamma}_{\mathrm{DCF}} = -10\log\mathrm{T}_{\mathrm{DCF}}$.) In a transmission line exceeding a few spans, the total gain G_T of the dual-stage amplifier is set to exactly compensate the fiber span loss, so that the launch power into each transmission span is equal. Note that the gain G_1 can also be expressed as the ratio of powers $\mathrm{P}_{\mathrm{in}}^{\mathrm{A}}/\mathrm{P}_{\mathrm{DCF}}$ where $\mathrm{P}_{\mathrm{in}}^{\mathrm{A}}$ and $\mathrm{P}_{\mathrm{DCF}}$ are the signal powers at the input of the first amplification stage and at the input of the DCF, respectively. $\mathrm{P}_{\mathrm{in}}^{\mathrm{A}}$ and $\mathrm{P}_{\mathrm{DCF}}$ are typically monitored in transmission systems.

Following Eqs. (41) and (42), and assuming a noise-free transmitter (i.e. infinite $\mathrm{OSNR}_{\mathrm{TX}}$) as well as identical spontaneous emission factors for both amplification stages (i.e., $\mathrm{n}_{\mathrm{sp},1} = \mathrm{n}_{\mathrm{sp},2} \equiv \mathrm{n}_{\mathrm{sp}}$), the delivered OSNR for localized dispersion compensation, $\mathrm{OSNR}_{\mathrm{del}}^{\mathrm{loc}}$ can be written as

$$\mathrm{OSNR}_{\mathrm{del}}^{\mathrm{loc}} = 58 + \mathrm{P}_{\mathrm{in}} - 10\,\log\left[\mathrm{NF}+\frac{2\,\mathrm{n}_{\mathrm{sp}}}{G_1}\left(\frac{1}{\mathrm{T}_{\mathrm{DCF}}}-1\right)\right] - \mathit{\Gamma}_{\mathrm{F}} - 10\log\mathrm{N}_{\mathrm{amp}} \qquad [\text{ in dB }], \quad (50)$$

where NF (linear units) is the noise figure of a single-stage amplifier of gain G_T (compensating for the fiber span loss $\mathit{\Gamma}_{\mathrm{F}}$ (in dB)) and spontaneous emission factor n_{sp}.

Using Eq. (50), one can easily see that the degradation in delivered OSNR, $\mathrm{OSNR}_{\mathrm{deg}}$, due to the presence of the DCF in the dual-stage amplifier is given by

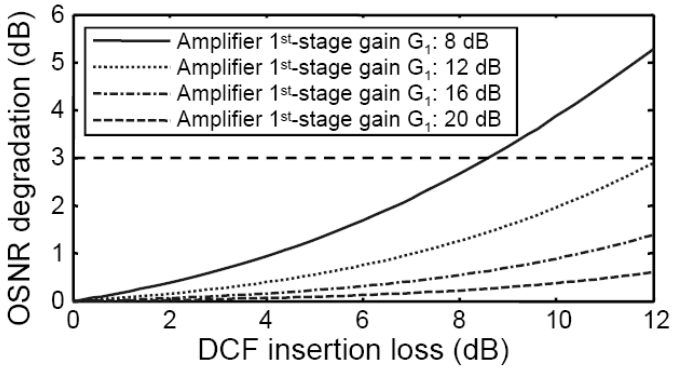

Fig. 21. Degradation in delivered OSNR caused by inserting localized dispersion compensation in a transmission line as a function of the DCF insertion loss. The DCF is assumed to sit in a dual-stage amplifier (Fig. 20b) and the delivered OSNR is compared the a line without DCF (Fig. 20a). The fiber span loss, $\Gamma_{\rm F}$, is assumed to be 20 dB.

$$\mathrm{OSNR}_{\rm deg}^{\rm loc} = 10\,\log\left[\mathrm{NF} + \frac{2\,\mathrm{n_{sp}}}{G_1}\,\left(\frac{1}{\mathrm{T_{DCF}}} - 1\right)\right] - 10\,\log \mathrm{NF} \qquad [\text{ in dB }], \tag{51}$$

where the last term of Eq. (51) is obtained by noting that the absence of DCF is equivalent to having $\mathrm{T_{DCF}} = 1$.

Figure 21 shows the OSNR degradation, $\mathrm{OSNR}_{\rm deg}^{\rm loc}$, for a span loss $\Gamma_{\rm F}$ of 20 dB and a spontaneous emission factor, $\mathrm{n_{sp}} = 2$ (noise figure at high gain of 6 dB). Note that when the gain of the first amplification stage equals the insertion loss of the DCF, the input power to the two amplification stages are identical. This leads to nearly a doubling of the ASE level (at identical noise figures) and thus an OSNR reduction close to 3 dB as expected (see dashed horizontal line in Fig. 21). The same figure also suggests that one can minimize the OSNR degradation by having a large gain for the first stage of amplification. However, as we will see in Sec. 3.2, nonlinear effects within the DCF may start to contribute significantly to the overall nonlinearity of transmission, thereby offsetting the advantages gained in delivered ONSR. Typical maximum DCF insertion loss for 100-km of SSMF is 10 dB and can decrease to as low as 3 dB for NZDF family fibers because of their low dispersion values.

For diffuse dispersion compensation such as shown in Fig. 20c, the DCF is part of the transmission fiber itself. Since DCFs generally have higher loss than state-of-the-art transmission fibers, the insertion of DCFs in the fiber span generally results in higher fiber span losses, as depicted in the signal power evolution of Fig. 20c. Consequently, a lower signal power enters the amplifier following the fiber span, resulting in a degradation of the delivered OSNR.

The delivered OSNR, $\mathrm{OSNR}_{\rm del}^{\rm dif}$, of a passive diffused dispersion compensation differs from the passive fiber delivered OSNR, $\mathrm{OSNR}_{\rm del}$ in two ways: An increase in fiber loss $\Gamma_{\rm F}$ and a very slight increase in effective noise figure, $\mathrm{NF_{eff}}$ due to the extra gain G_T necessary to compensate the extra loss. Neglecting the small difference in $\mathrm{NF_{eff}}$ and using Eq.(41), one can easily show that the delivered OSNR for diffused

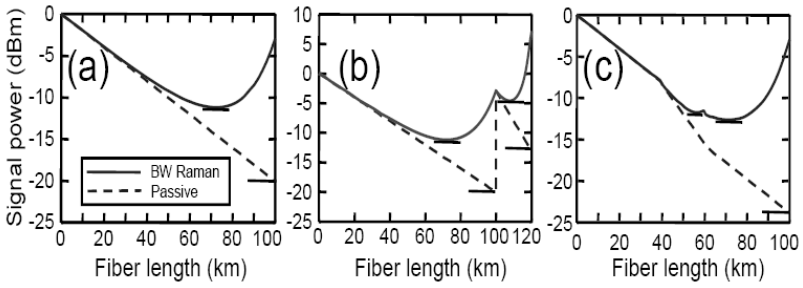

Fig. 22. Signal power evolution in passive and in backward Raman-pumped fibers: a) over NZDF, b) over SSMF compensated by a DCF and c) over a DMF. The fiber span length L, input power $\mathrm{P_{in}}$, and DRA net gain are 100 km, 0 dBm, and -3 dB, respectively, for all three scenarios. Short horizontal lines indicate the location of lowest power for all fiber segments.

dispersion compensation can be written as,

$$\mathrm{OSNR_{del}^{dif}} = \mathrm{OSNR_{del}} \; + \; 10 \; \log \left[\frac{\exp(-\alpha_{\mathrm{F}} \; \mathrm{L_{DCF}})}{\exp(-\alpha_{\mathrm{DCF}} \; \mathrm{L_{DCF}})} \right] \quad [\text{ in dB }], \qquad (52)$$

where α_{F} is the loss coefficient [dB/km] of the fiber that the DCF replaces in the DMF and $\exp(-\alpha_{DCF}\mathrm{L_{DCF}})$ is the DCF insertion loss $\mathrm{T_{DCF}}$ introduced previously. The last term of Eq. (52) can be rewritten as,

$$\mathrm{OSNR_{deg}^{dif}} = 10 \; \log(e) \; (\alpha_{\mathrm{DCF}} - \alpha_F) \; \mathrm{L_{DCF}} \qquad [\text{ in dB }]. \qquad (53)$$

which is the difference [in dB] between the insertion loss of the DCF and the insertion loss of the transmission fiber of the same length it replaces. Consequently, every additional 'dB' of loss to the DMF due to the presence of the DCF results in a 'dB' of delivered OSNR degradation. Note that typical DMFs are nearly 100% dispersion compensated so that the condition $\mathrm{L_{DCF}} \approx (\mathrm{L_{DCF}} - \mathrm{L}) \, \mathrm{D_F}/\mathrm{D_{DCF}}$ approximately holds.

The above considerations are valid for transmission lines using *discrete amplification* (e.g., discrete erbium or discrete Raman amplification, Figs. 1a and 1b). However, for hybrid or all-Raman systems (Figs. 1c and 1d), establishing simple analytic expressions to calculate the OSNR degradation due to the presence of localized dispersion compensation turns out to be challenging [109,110]. For such systems, an accurate evaluation of $\mathrm{OSNR_{deg}}$ can be obtained by numerically solving the equations of Sec. 2.2.

Despite the large variety of possible Raman pumping configurations, one can develop an understanding of the OSNR degradation resulting from the insertion of localized dispersion compensation based on physical considerations of ASE generation and power evolution (Fig. 22). Assuming that the noise figure remains constant, the ASE generated by an amplifier is independent of the input signal power. The maximum impact of ASE generation on OSNR degradation in such amplifier occurs near the location of lowest signal power within the amplifier [62]. The minimum signal powers in segments of passive fibers and DRAs are indicated in Fig. 22, for the three scenarios

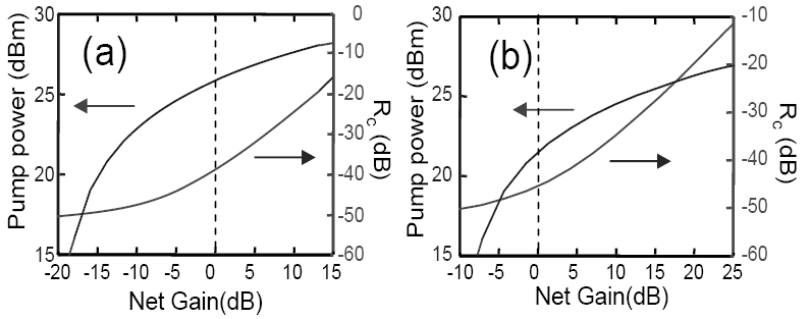

Fig. 23. Generation of DRB in a) a transmission fiber, SSMF, and b) a DCF for backward pumping. Fiber parameters are given in Table 5. The vertical dash line indicates when the amplifier is transparent.

depicted in Fig. 20. As shown in Fig 22, the minimum signal power in a DRA increases significantly relative to a passive fiber, reducing the OSNR degradation from this fiber section. Consequently, in a hybrid system (Fig. 1c), the minimum signal power in a span may occur at the end of the localized DCF (see Fig. 22b), increasing the impact of DCF loss on the delivered OSNR. In an all-Raman system (Fig. 1d) on the other hand, the relative impact of the presence of the DCF in the system is lowered relative to a hybrid system as the minimum power of a Raman-pumped DCF can be much higher than a passive DCF because the DCF is Raman pumped (see Fig. 22b). Even though the picture developed above on OSNR degradation is qualitative, it is a helpful guideline to estimate the relative contributions of each fiber segment in a transmission line without having to resort to elaborate calculations.

The use of Raman amplification helps reducing the impact of ASE generation but can also enhance other impairments. We will see in the next two sections (Secs. 3.1 and 3.2) that the net Raman gain possible in fiber spans and in DCFs is limited by the generation of DRB and by signal distortions from fiber Kerr nonlinearity.

Double Rayleigh Backscatter

As discussed in Sec. 2.2, the generation of DRB in hybrid systems becomes particularly important because the fiber span becomes a DRA. Similarly, generation of DRB in DCF becomes important only when the DCF itself is Raman-pumped. This situation occurs in systems using discrete Raman amplification (Fig. 1b) and in all-Raman systems (Fig. 1d).

The impact of DRB on a signal is best described by the crosstalk ratio, $\mathrm{R_c}$ (see Sec. 2.2). Figure 23 shows how $\mathrm{R_c}$ grows with the net Raman gain for a transmission fiber (Fig. 23a) and a DCF (Fig. 23b) for backward Raman pumping. The Raman pump power required to achieve such net gain is also presented for reference. In the absence of Raman pumping, the crosstalk ratios for both fibers, SSMF and DCF, are comparable, at a value around -50 dB. As the net Raman gain increases, the crosstalk ratios increase in such a way that, at transparency (0 dB of net gain, dashed vertical

line), $\mathrm{R_c}$ for SSMF is higher than $\mathrm{R_c}$ for the DCF by about 7 dB. At 10 dB of net Raman gain, the difference has grown to 11 dB. This indicates that signal degradation from DRB in DCFs occurs at higher values of net gain than for SSMF. Knowing that the generation of DRB in DRAs forces to operate a few dBs below transparency [111,103], Fig. 23 indicates that DCF can operate as a DRA with positive net gain with only a small increase in $\mathrm{R_c}$. This property of DCF relative to DRB has been used to design all-Raman systems with DCFs used as Raman amplifiers with positive net gain.

3.2. Signal Distortions

As discussed in Sec. 2.3, in addition to the generation of noise, propagation over transmission lines also introduces deterministic signal distortions. In this section, we discuss how the insertion of DCFs in a line contributes to deterministic signal distortions.

Dispersion Compensation

It is well known that dispersion compensation has been introduced in transmission lines to control the accumulation of dispersion in order to provide optimum transmission. However, achieving the target dispersion values and dispersion map can be a difficult task. The challenges associated with generating a target dispersion value at a given wavelength include the dispersion accuracy of the DCFs, the commercial availability of a finite set of DCFs with discrete dispersion values, and temperature-induced fluctuations of dispersion.

Dispersion Accuracy

The dispersion characteristics of an optical fiber depend on many fiber parameters such as material concentration and the physical fiber parameters [112]. Any variations in the fiber parameters translate into changes in fiber dispersion. Variations in dispersion of individual fibers in a transmission line can lead to significant dispersion walk-off from the target dispersion values along the line. As a result, both the NRD at the receiver as well the dispersion map can be affected.

Assuming a random distribution of fiber dispersion around a nominal value, the variance of the dispersion in a transmission line evolves as

$$\sigma^2_{\mathrm{line}} = \sum_{i=1}^{N_{\mathrm{span}}} \sigma^2_{\mathrm{F,i}} + \sum_{i=1}^{N_{\mathrm{DCF}}} \sigma^2_{\mathrm{DCF,i}} \ , \tag{54}$$

where $\sigma_{\mathrm{F,i}}$ and $\sigma_{\mathrm{DCF,i}}$ are the standard deviations of dispersion of the i^{th} fiber segment around the mean dispersion value for the transmission fibers and DCF, respectively. Equation (54) indicates that, even though inserting DCFs in a line may be necessary to limit the dispersion, it also increases the uncertainty of the dispersion value at detection. This equation can then provide an estimate of the magnitude of dispersion deviations in transmission lines. Such deviations need to be compared to dispersion tolerances of the modulation format and receiver design used in the system.

Finally, we want to mention that some fibers have their local dispersion values accurately measured after fabrication. Through a selection process, fibers with large

deviations from the nominal dispersion value are not made available under the fiber type denomination. Such a selection process is particularly efficient in reducing large deviations of cumulative dispersion in a transmission line that may result from the inadvertent concatenation of a large number of fibers having either large positive or negative dispersion deviations from the nominal dispersion value.

Dispersion Granularity

Practical and commercially attractive deployment of fiber-optic communication systems requires the use of a finite set of dispersion compensation modules, resulting in a *granularity* in the dispersion compensation values. Such a granularity results in deterministic deviations in the prescribed dispersion map of installed systems relative to the optimum possible dispersion map. As an example, if one allows six different dispersion values for DCMs to compensate up to 120 km of SSMF (2,040 ps/nm), one can choose to have a DCM starting at -340 ps/nm of cumulative dispersion up to $-2{,}040$ ps/nm by steps of -340 ps/nm. Equipped with such DCMs, deviations from a target dispersion value at each DCF location in a point-to-point system can reach ± 170 ps/nm, i.e., $\pm$ half the magnitude of the dispersion granularity. On the other hand, in mesh networks, individual channels can be directed in multiple directions and deviations from a target map can increase as channels can go through paths dominated by positive or negative dispersion deviations. A monitoring of the maximum deviations over all possible paths may need to be done at the design stage of mesh networks to prevent large dispersion deviations.

Even though a reduced granularity is generally desirable to better achieve the dispersion target values, a larger set of DCFs modules become required, which potentially increases system cost. This cost increase may offset the advantages that accurate dispersion mapping brings to system design. Therefore, the best choice of DCF granularity depends on the system design and on the distance of interest.

Dispersion Fluctuations

Temperature fluctuations of optical fibers can lead to changes in dispersion [113–117], which may occur on at least two time scales: a few *hours*, typically showing diurnal periodicity, or a few *months*, showing seasonal periodicity [117,118].

The dependence of dispersion variation on temperature has been measured extensively and is on the order of $\pm 2 \times 10^{-3}$ ps/nm/km/°C for most fiber types [116]. For large diurnal variations in temperature on the order of $25°$C, aerial fibers of most fiber types will experience dispersion variations of many tens of ps/nm after several hundreds of kilometers, exceeding the 40-Gb/s dispersion tolerance (see Table 3 and Fig. 16). Since the dispersion tolerance of any modulation format can shrink considerably (up to a factor of $\sim$10 times) after nonlinear transmission (see for instance Figs. 18 and 17 for 10 Gb/s), the impact of temperature-dependent dispersion fluctuations is more severe for systems operating in the nonlinear transmission regime. Such dispersion variations with temperature, along with the dispersion uncertainty of transmission fiber and the granularity of DCFs may result in significant BER degradations [117].

Channelized and Tunable Dispersion

To address dispersion variations with temperature and uncertainties in dispersion from various sources, *tunability* in dispersion compensation is desirable. Such tunability

can be provided by different technologies (see Sec. 4 for a review). Most of these technologies operate over a limited bandwidth around a single channel central frequency or over a comb of channels if the device has a periodic frequency response. In both cases, discontinuities in dispersion occur between the channel frequencies. Dispersion compensation exhibiting such discontinuities in frequency is referred to as *channelized dispersion compensation*. Channelized dispersion compensators with non-periodic frequency response, such as fiber Bragg gratings (FBGs) [119], can offer independent dispersion tunability on a per-channel basis, a feature that may become desirable in networks incorporating multiple OADMs, where channels with different propagation histories share common physical paths and may be dropped at the same OADM site. On the other hand, for WDM systems having a large number of channels, many FBGs become necessary with a potential increase in system cost. This can be partially circumvented using broadband tunable dispersion compensation based on devices having periodic responses, where the dispersion of all WDM channels can be simultaneously tuned. For such tunable dispersion compensators, a single device can in principle be used for all channels, potentially reducing cost in high-capacity WDM systems. It is worth mentioning that, for all devices exhibiting channelized dispersion compensation, fixed or tunable, cascadability may become an important issue, especially in systems operating at very high spectral efficiency (> 0.4 bit/s/Hz). This aspect will be discussed further in Sec. 4.

Fiber Nonlinearity

Along with noise generation, fiber nonlinearity is one of the two main effects limiting transmission in optical fibers. The impact of DCF on nonlinear transmission is twofold. First, a DCF impacts nonlinear transmission through control of the dispersion map (see Sec. 2.3). For this purpose, the accuracy of the dispersion compensation parameters is critical to achieve the desired dispersion map. Second, for sufficiently high launch power into the DCF, the presence of a DCF increases the total fiber nonlinearity present in the transmission line by adding its own nonlinear contribution.

Dispersion Mapping

As described in Sec. 2.3, dispersion mapping is a key technique to reduce signal distortions from fiber nonlinearity. Figure 24 shows the result of a proper numerical exploration of SPDMs in a form of a matrix of plots, each one similar to the plot shown in Fig. 18b. From the upper to the lower row, the RDPS is increasing from zero to 100 ps/nm by steps of 25 ps/nm. Each column represents a transmission distance (measured by the length of the transmission fiber) from 400 to 1600 km by steps of 400 km. Note that in the calculations of Fig. 24, the nonlinearity in the DCF has been neglected (see Fig. 26 for the effect of nonlinearity in the DCF). The system parameters are the same as Fig. 18: 10-Gb/s NRZ signals on a 50-GHz grid at a launch power per channel P_{in} of 3.67 mW. At lower powers, the areas of each plot enlarge to eventually become like Fig. 18a at sufficiently low power ("linear regime"). At higher powers, the areas shrink to eventually disappear when the required OSNR exceeds 14 dB. Arrays of plots similar to Fig. 24 need to be recalculated for different systems types to determine their optimum dispersion maps. It is generally required to recalculate the 'good performance' regions of the array of plots at higher and lower powers to

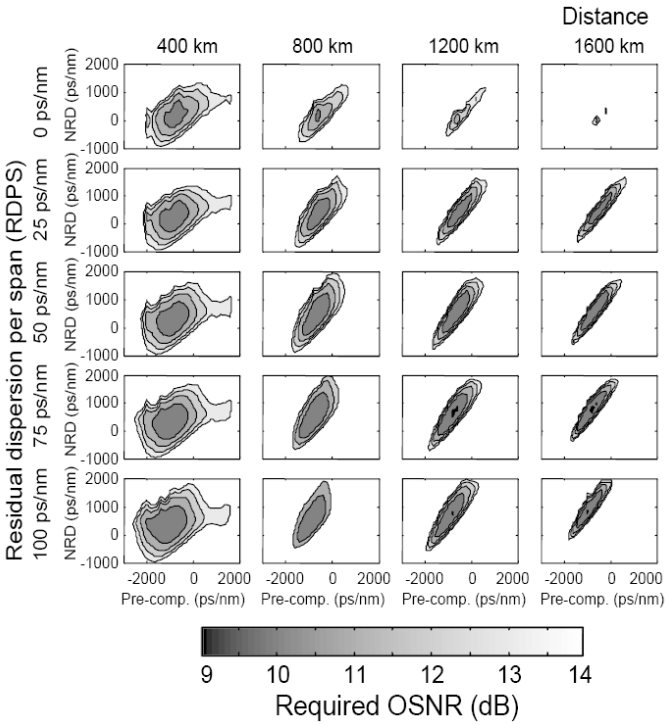

Fig. 24. Dispersion mapping for various RDPS and transmission distances for SPDMs (see Fig. 17). As seen in the figure, the required OSNR depends critically on the dispersion map parameters. The system parameters are identical to those of Fig. 18 except that the RDPS and the transmission distance are varied here.

establish the maximum power for the optimum dispersion map and the performance for the low power channels, respectively.

From Fig. 24, one can clearly see the variations in system performance occurring by changes in RDPS, and how these variations depend on the transmission distance. Even though a SPDM with full dispersion compensation per span may appear attractive due to its simplicity, Fig. 24 shows dramatic signal degradations from nonlinear transmission at distances beyond a few hundred kilometers. Such degradations originate from XPM between 10-Gb/s channels in WDM system [120]. The best ULH nonlinear transmission for the parameters of Fig. 24 occurs for an RDPS above 25 ps/nm. One should note, however, that signal degradations from XPM at zero RDPS can be mitigated by periodically introducing additional time delays between the WDM channels by using, for instance, a channelized dispersion compensator [121–124]. Such an approach has the advantage of providing a simple rule of full dispersion compensation per span but has the drawback of limited cascadability at high spectral efficiency (0.4 bit/s/Hz and above) for the channelized elements generally required to generate such relative time delays.

Transmission systems operating a 40 Gb/s also benefit greatly from dispersion mapping. An important difference to 10-Gb/s systems is that most 40-Gb/s systems operate in the pseudo-linear regime of transmission [102] where the dominant nonlinearities are single-channel nonlinear effects: IXPM and IFWM. For such high-speed systems, dispersion mapping on a single channel is generally sufficient to establish the optimum dispersion map that provides optimum transmission even for a WDM configuration.

Nonlinear Phase

The second impact of DCF on nonlinear transmission is an increase in the total nonlinearity of the transmission line due to the presence of the DCF. In the localized dispersion compensation scheme (Fig. 2a) the signal power at the input of the DCF can be controlled in a dual-stage amplifier configuration (Fig. 1a). Reducing the input signal power to the DCF, $\mathrm{P_{DCF}}$, reduces the impact of fiber nonlinearity in the DCF, but at the expense of an OSNR degradation, as described in Sec. 3.1. If one approximates the effect of fiber nonlinearity by the integrated nonlinear phase ϕ (see Sec. 2.3), the ratio of nonlinearity in the DCF to the nonlinearity in the transmission fiber is given by

$$\mathrm{R_{DCF}} \equiv \frac{\phi_{\mathrm{DCF}}}{\phi_{\mathrm{F}}} = \frac{\int_0^{\mathrm{L_{DCF}}} \mathrm{P_{DCF}}(z)\,\gamma_{\mathrm{DCF}}(z)\,dz}{\int_0^{\mathrm{L_F}} \mathrm{P_F}(z)\,\gamma_{\mathrm{F}}(z)\,dz}, \tag{55}$$

where $\gamma(z)$ is the nonlinear coefficient defined in Eq. (44) of Sec. 2.3.

For systems using localized dispersion compensation and passive fibers (Fig. 2a), the ratio $\mathrm{R_{DCF}}$ can be written as

$$\mathrm{R_{DCF}} = \frac{\gamma_{\mathrm{DCF}}}{\gamma_{\mathrm{F}}}\ \frac{\alpha_{\mathrm{F}}}{\alpha_{\mathrm{DCF}}}\ \frac{[1-\exp(-\alpha_{\mathrm{DCF}}\,\mathrm{L_{DCF}})]}{[1-\exp(-\alpha_{\mathrm{F}}\,\mathrm{L_F})]}, \tag{56}$$

where we assumed that γ and α are independent of distance. For fibers that are Raman pumped, $\mathrm{R_{DCF}}$ can be evaluated by integrating explicitly Eq. (55) or in some cases using approximate solutions [110].

Figure 25 shows the integrated nonlinear phase for a SSMF transmission fiber and a DCF for an identical input power of 0 dBm (fiber parameters in Table 5). As seen on the figure, even without Raman pumping, the nonlinear phase in the DCF can exceed the nonlinear phase in the transmission fiber at identical signal launch powers. However, because the insertion loss of DCFs is generally much smaller than the loss of fiber spans, the launch power into the DCF, $\mathrm{P_{DCF}}$, can be set below the input power to the fiber span, $\mathrm{P_{in}}$, which minimizes the degradation of the delivered OSNR (see Sec. 3.1). The nonlinear phase in the DCF decreasing linearly with the launch power, a reduction of the launch power to the DCF by a few dBs generally lowers the nonlinear phase in the DCF below the nonlinear phase of the transmission span.

To illustrate the impact of nonlinearity in the DCF, Fig. 26 shows required OSNR contour plots for different signal powers launch into the DCF. The parameters are the same as in Fig. 24, with RDPS = 100 ps/nm and at 1200 km [12]. The number in the lower corner of each contour plot is $10\log(\mathrm{P_{DCF}}/\mathrm{P_{in}})$, the power in the DCF relative to the input power to the span, expressed in dB. Nonlinearity in the DCF starts to

[12] The slight difference between the low-power plots of Fig. 26 and the corresponding plot of Fig. 24 comes from small differences in dispersion slopes of the DCF used for both figures.

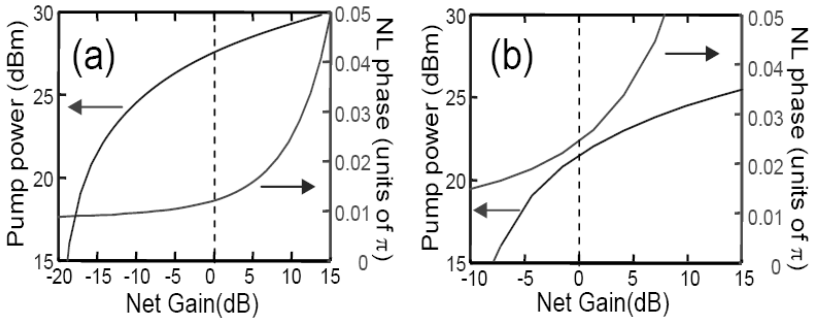

Fig. 25. Integrated nonlinear phase for a) a transmission fiber, SSMF and b) a DCF for identical input signal powers of 0 dBm. As seen in the figure, the nonlinear phase in the DCF can exceed the nonlinear phase in the transmission fiber if input power levels are comparable. The vertical dash line indicates when the amplifier is transparent.

significantly impact nonlinear transmission in the system at around -4 dB of relative power or $\mathrm{P_{DCF}} = 1.46$ mW. This corresponds to a nonlinear phase in the DCF, ϕ_{DCF}, of 67.2% of the nonlinear phase in the transmission fiber, ϕ_{F}.

For systems using *diffused dispersion compensation* and Raman amplification, the increase in nonlinear phase in the DCF generally depends on the location of the DCF in the DMF as well as the Raman pumping scheme. One should note however, that, even though DCFs can be located far from the fiber span input and output ends where Raman pumps are located, the small effective areas of DCFs make them simultaneously more efficient to produce Raman gain with low pump powers [18] and to generate more nonlinear phase [see Eqs. (43) and (44)] at identical signal powers. As a result, detailed analyses need to be performed for each fiber design to determine the importance of the nonlinearity in the DCF present in a DMF [31].

Polarization Mode Dispersion

Polarization-mode dispersion of fibers can cause significant impairments in transmission, especially at 40 Gb/s and above [107]. This section describes how inserting DCF in a line affects its PMD value.

If a system is comprised of N sections of fiber (transmission fiber and DCF), each section with PMD coefficient x_i and length l_i, the total PMD coefficient (in ps/$\sqrt{\mathrm{km}}$) of the line is given by

$$x_{\mathrm{line}} = \sqrt{\frac{\sum_{i=1}^{N} x_i^2 l_i}{\sum_{i=1}^{N} l_i}} \,. \tag{57}$$

Assuming a system composed of N_{span} spans of transmission fiber of length L and N_{DCF} DCFs of length L_{DCF}, we find for the system's PMD coefficient

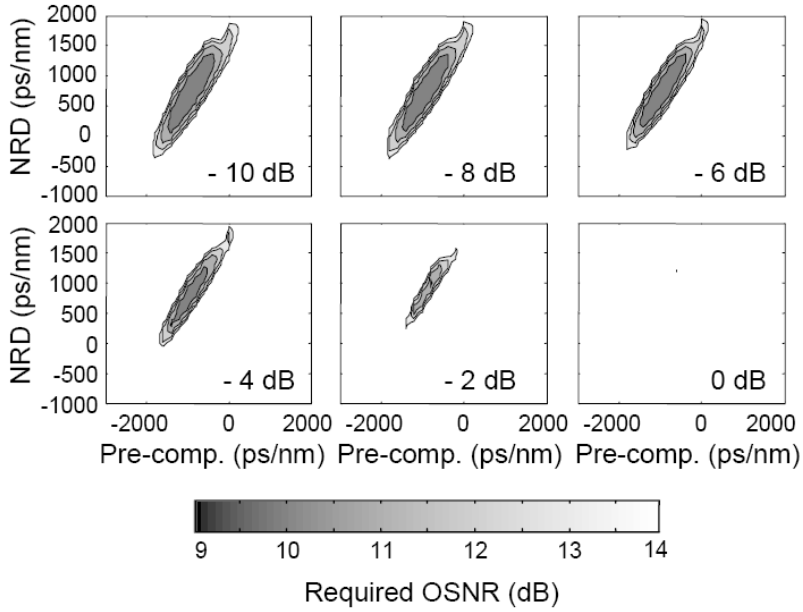

Fig. 26. Effect of the nonlinearity in DCF on transmission. The system parameters are the same as in Fig. 24 with RDPS = 100 ps/nm and a distance of 1200 km. The numbers in the lower corners indicate the power in the DCF relative to the fiber span (see main text). As the power in the DCF increases, nonlinear distortions from the DCF reduces the area of low required OSNR.

$$x_{\text{line}} = \sqrt{\frac{N_{\text{span}}\, x_{\text{span}}^2\, L_{\text{span}} + N_{\text{DCF}}\, x_{\text{DCF}}^2\, L_{\text{DCF}}}{L_{\text{line}}}}\ , \tag{58}$$

where $L_{\text{line}} = N_{\text{span}} L_{\text{span}} + N_{\text{DCF}} L_{\text{DCF}}$ is the total fiber length in the system.

Equations (57) and (57) for calculating the PMD coefficient of a transmission line assumes that the PMD coefficients of the individual fiber spans are known precisely. However, PMD coefficients of commercial fiber depend randomly on stress imposed on the fiber during manufacturing and cabling, which lets nominally identical fiber cables have statistically different PMD coefficients. In an actual transmission line, many fiber cables are concatenated, and the probability that *all* cable sections simultaneously exhibit high PMD coefficients is low. Therefore, it is convenient to specify the PMD of fiber cables using the *probability* $P_Q(M)$ that the PMD coefficient of a transmission line ('*link*') composed of M cable sections exceeds a certain value. This value is called the *link design value* PMD_Q, and is given in conjunction with the number of cable section M and the probability $P_Q(M)$ according to [125],

$$P[x_{\text{line}} > \text{PMD}_Q] = P_Q(M)\ . \tag{59}$$

Therefore, the PMD coefficient of an individually purchased fiber cable may well exceed PMD_Q, but the concatenation of at least M such cables in a transmission line will not, at least not with appreciable probability. Typically, fiber manufacturers specify $M = 20$ and $P_Q(20) = 10^{-4}$.

3.3. DCF Design Issues: The Figure of Merit (FOM)

As we have seen, the insertion of a DCF in a transmission line has an impact on both the delivered OSNR (Sec. 3.1) and on fiber nonlinearity (Sec. 3.2). The design of a DCF should take into account both phenomena to minimize the impact on system performance.

The figure of merit (FOM) [45,46] defined in Eq. (1) is often used to compare different DCF designs [126] for localized dispersion compensation. A high value of FOM indicates that a DCF can offer a large value of dispersion compensation with relatively low insertion loss. However, since Eq. (1) only takes into account OSNR aspects, it often happens that DCFs with identical FOM but different fiber designs have a different system impact, depending on how much additional degradation from *fiber nonlinearity* they impose on transmission (see Fig. 26). For this reason a FOM parameter that includes the effect of fiber nonlinearity has been introduced [45,46]. Assuming passive fibers, the 'nonlinear' FOM is given by

$$\mathrm{FOM_{NL}} = \frac{A_{\mathrm{eff}}^{\mathrm{DCF}}}{A_{\mathrm{eff}}^{\mathrm{F}}} \frac{\alpha_{\mathrm{DCF}}}{\alpha_{\mathrm{F}}} \frac{(T_{\mathrm{F}}-1)^2}{T_{\mathrm{F}}} \frac{T_{\mathrm{DCF}}}{(T_{\mathrm{DCF}}-1)^2}. \tag{60}$$

Neglecting shot noise, one can show that Eq. (51) on the OSNR degradation for localized dispersion, $\mathrm{OSNR}_{\mathrm{deg}}^{\mathrm{loc}}$, can be put in the form,

$$\mathrm{OSNR}_{\mathrm{deg}}^{\mathrm{loc}} = T_{\mathrm{F}} \frac{(G_1-1)G_2 T_{\mathrm{DCF}} + (G_2-1)}{1-T_{\mathrm{F}}} \qquad [\text{ linear units }], \tag{61}$$

where G_1 and G_2 are the gains of the two stages of a dual-stage amplifier. By defining the ratio $\eta \equiv \phi_{\mathrm{NL}}^{\mathrm{DCF}}/\phi_{\mathrm{NL}}^{\mathrm{F}}$ [see Eq. (43) for the definition of nonlinear phase] and using Eq. (60) for a two-stage amplifier with identical spontaneous emission factors ($\mathrm{n_{sp}}$), one can show that [45,46],

$$\mathrm{OSNR}_{\mathrm{deg}}^{\mathrm{loc}} = 1 + \frac{1}{\eta \mathrm{FOM_{NL}}} \qquad [\text{ linear units }]. \tag{62}$$

At constant nonlinearity, the signal power in a system with DCF needs to be reduced by a factor (1 + η) to insure constant nonlinear phase ϕ_{NL}. The ratio of OSNR without and with DCF *at constant nonlinearity* can be expressed as,

$$\mathrm{OSNR}_{\mathrm{deg}}^{\mathrm{loc}}(\eta) = (1+\eta)\left(1 + \frac{1}{\eta \mathrm{FOM_{NL}}}\right) \qquad [\text{ linear units }]. \tag{63}$$

Figure 27 shows the degradation of delivered OSNR for different values of gain G_1 of the first-stage of a dual-stage amplifier for different DCF loss coefficient values. There is an optimum gain G_1 that minimizes the impact of the DCF on delivered OSNR. At low values of G_1, the first stage provides insufficient gain so that the power at the output of the DCF is very low, creating OSNR degradation through amplification by the second stage. At high gain values, the additional nonlinearity generated in the DCF exceeds the benefits in delivered OSNR brought by a large value of G_1. Notice that higher DCF loss coefficients produce larger reduction in delivered OSNR and shift the optimum value of G_1 upwards. A similar approach to the one described in this section can be taken to study systems using Raman amplification and generating DRB.

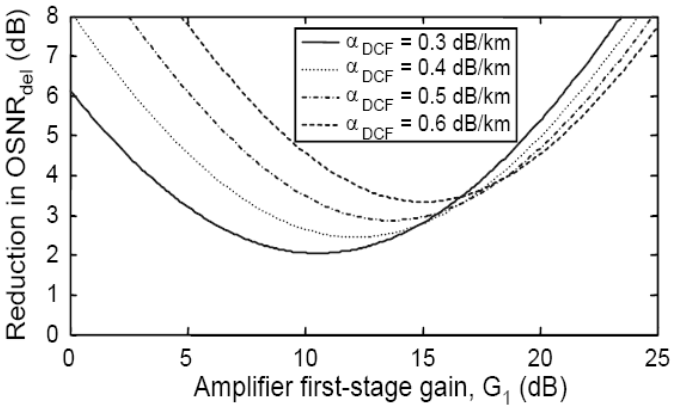

Fig. 27. Reduction in delivered OSNR due to the presence of DCF in a transmission line as a function of the first-stage gain G_1 of a dual-stage amplifier. Curves for different DCF loss coefficients α_{DCF} are shown. The total nonlinearity (transmission fiber plus DCF) is kept constant. A different optimal gain exists for each value of DCF loss.

4. Alternatives to DCF-Based Dispersion Compensation

As discussed in Sec. 1, the per-channel bit rate upgrade from 2.5 to 10 Gb/s in optical communication systems required the implementation of dispersion compensation in order to transmit information beyond a few tens to a few hundred kilometers. For virtually all such systems, dispersion compensation is provided by DCF-based DCMs. However, depending on the application, dispersion compensation can also be implemented by dispersion compensation technologies that are *not* based on DCF.

For systems operating at 10 Gb/s per channel, non-tunable (i.e., fixed) values of dispersion compensation are typically used, because, in 10-Gb/s systems, fixed dispersion compensation is generally sufficiently accurate to achieve the target NRD and near optimum system performance. For such systems, both fiber and non-fiber DCMs can be used for pre-, in-line, and post-compensation. At 40 Gb/s per channel , a given modulation format has a 16-fold reduction in dispersion tolerance relative to 10-Gb/s transmission. As mentioned in Sec. 3.2, 40-Gb/s systems impose stringent dispersion requirements that often necessitate TDC at the receiver to accommodate net residual dispersion variations, especially those produced by temperature fluctuations in optical fibers [113–117].

Systems needing TDC require some form of performance monitoring to provide feedback to adjust the degree of compensation. At the turn of the millennium, state-of-the-art optical transmission systems started to incorporate FEC which provides a convenient feedback on the BER that can be used to control parameters of the TDC. Demonstrations of TDC implementations include per-channel dispersion tuning using Fiber Bragg Gratings (FBGs) [127] in 40-Gb/s systems as well as fixed broadband or tunable broadband dispersion compensation based on Gires-Tournois Etalons (GTEs) [128]. At the time of writing, GTEs and broadband FBGs are commercially available for 2.5 and 10-Gb/s systems (both for fixed and tunable dispersion compensation

applications), whereas FBGs are available for tunable dispersion compensation on a per-channel basis or for a group-of-channels at 40 Gb/s [127].

Besides dispersion tunability, advantages of non-DCF devices over DCFs include total immunity to Kerr nonlinearities (see Sec. 2.3), a smaller form factor, cost, and the possibility of engineering arbitrary dispersion profiles. A high FOM and small form factor make non-DCF devices attractive candidates for use in dispersion compensation in OADMs.

In this section we will review the challenges and perspectives of various dispersion compensation technologies, and discuss the trade-offs in different contexts of metropolitan, LH and ULH transmission systems.

4.1. Challenges for Future DCF Designs

Current systems requiring dispersion compensation mostly use DCF. In systems employing either discrete EDFA (Fig. 1a) or hybrid amplification (EDFA and Raman amplification, see Fig. 1c), it is particularly important to achieve a high FOM (see Sec. 1.3). Using high-FOM DCMs is particularly efficient in reducing the degradation of the delivered OSNR from the presence of dispersion compensation in the line (see Sec. 3.1). For instance, in the case where the DCF is inserted within a dual-stage EDFA, the lower DCF loss (or larger transmittivity $\mathrm{T_{DCF}}$) of a high-FOM DCF (i.e. larger $\mathrm{T_{DCF}}$) leads to less degradation in delivered OSNR [see Eq. (51)].

For systems using discrete Raman (Fig. 1b) or all-Raman (Fig. 1d), additional challenges in DCF design arise. These stem from the need for DCMs to simultaneously provide Raman gain and broadband dispersion compensation [129] with low generation of DRB. In particular, ULH systems require precise control of the RDPS in order to mitigate fiber nonlinearity (see Fig. 24). The DCF design challenge in this case is to achieve an adequate level of Raman gain from the DCM, with low DRB and low PMD while simultaneously providing broadband dispersion compensation across the entire WDM band.

The introduction of 40-Gb/s-based transmission into optical networks will most likely bring scenarios of mixed data rates (10 Gb/s and 40 Gb/s) with different modulation formats present on the same transmission line [130]. Furthermore, state-of-the-art ULH terrestrial systems will incorporate OADMs to optically route transmitted signals [131,132]. These OADMs should be able to handle mixed data rate traffic with different dispersion compensation requirements. Such mixed data rate applications may require large TDC dynamic ranges at OADM sites, especially when the system dispersion compensation is provided by a SPDM which lets dispersion continuously accumulate along the line. One way to alleviate the required TDC dynamic range is to use a DPDM (see Sec. 1.2) [42–44]. In DPDM, the dispersion accumulation is 'reset' periodically to a low value, thereby reducing the excursion of dispersion seen at the OADM sites.

4.2. Non DCF-Based Dispersion Compensation

In recent years, alternatives to DCF-based dispersion compensation have emerged, and some technologies matured sufficiently to become commercially available. Among the most important technologies are devices based on FBGs [127,128,133] and on GTEs [134–136].

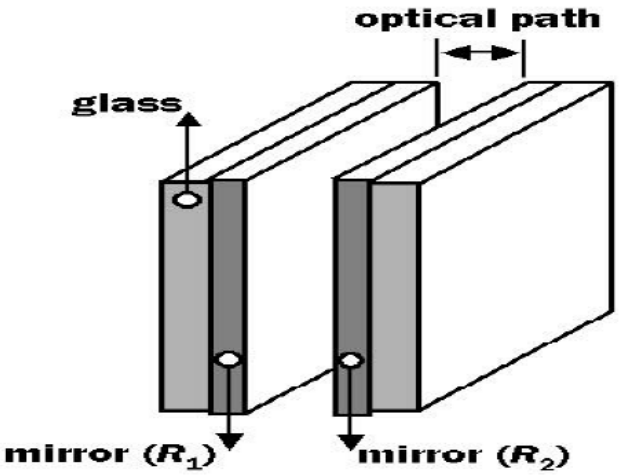

Fig. 28. Fabry-Perot (R_1 and $\mathrm{R}_2 < 1$) and Gires-Tournois etalons ($\mathrm{R}_1 < 1$, $\mathrm{R}_2 = 1$).

Technologies employed for 40-Gb/s TDC (and higher bit rates) are typically based on FBG. FBGs, being fiber-based devices, are fully compatible with optical fibers in the sense that they do not incur any extra fiber-to-device-to-fiber insertion losses, have low PMD, and are generally low cost. Drawbacks of FBGs include a Group Delay Ripple (GDR) of, typically, $\pm$10-20 ps peak-to-peak, and a limited dispersion tuning range of approximately 400 ps/nm. With the advent of ULH systems, this limited tuning range can become an important factor limiting the reach of 40-Gb/s systems.

In 10-Gb/s applications, in addition to FBG-based TDCs, there are also devices based on GTEs. GTE-based technologies have recently started to make way into 10-Gb/s applications as an alternative to DCF-based DCMs due to their large tuning range, small form factor, low cost, and, in some cases, better FOM; in particular, at the time of writing, DCMs based on GTEs are commercially available for high-capacity 10-Gb/s WDM dispersion-compensation applications. Interestingly, in addition to dispersion compensation, GTEs can also be used to build interleavers when placed within the arms of a Michelson Interferometers [137].

A GTE is represented schematically in Fig. 28. Etalons are cavities formed by two reflecting interfaces, with reflectivity coefficients R_1 and R_2 respectively, separated by a fixed gap that provides an optical path difference. If both interfaces are imperfect reflectors (i.e. R_1 and $\mathrm{R}_2 < 1$) the device is called a Fabry-Perot Etalon (FPE), first introduced in 1899. If one of the surfaces is a perfect reflector the device is called a Gires-Tournois Etalon, first introduced in the mid 1960s.

The optical path length can be adjusted to produce reflection resonances coincident with the ITU grid by setting the channel spacing $\delta\nu$ according to

$$\delta\nu = \frac{c}{2\,n\,\mathrm{d}}, \tag{64}$$

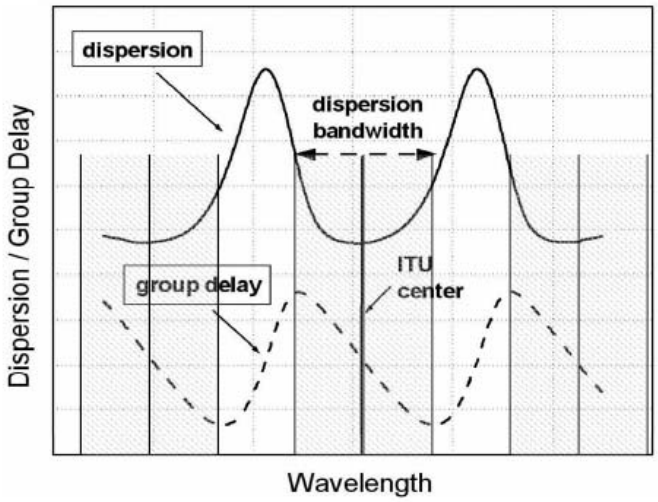

Fig. 29. Dispersion and group delay characteristics of a GTE dispersion compensator.

where c is the speed of light in vacuum, n is the refractive index of the etalon medium, and d is the distance between reflecting surfaces. $\delta\nu$ is called the Free Spectral Range (FSR) of the etalon and can be set to 100 or 50 GHz, for instance. In connection with the reflection resonances, there is a periodic optical delay response that can be used to compensate the dispersion of the transmission fiber simultaneously for all transmitted WDM channels. Typical optical delay and dispersion characteristics of a GTE device are shown in Fig. 29.

GTEs belong to a broad category of filters called *all-pass filters* (APFs); these filters are characterized by a constant amplitude response and a frequency-dependent phase response. For a cascade of N GTEs there is a relation between the dispersion, D, and the half-width dispersion bandwidth Δ, given by [138]

$$D \cong \frac{N}{\mathrm{FSR}^2\,\Delta^2}. \tag{65}$$

Current GTE-based DCMs for 10-Gb/s applications typically have a dispersion bandwidth of 25 GHz centered around an ITU frequency. As seen in Fig. 29, GTEs are providing channelized dispersion compensation that can pose cascadability issues at high spectral efficiency (see end of Sec. 3.2). Note that since the number of GTEs scales linearly with *D*, compensating the dispersion of SSMFs requires, typically, four times more GTEs than to compensate the dispersion of NZDF, thus having higher insertion loss of the device for SSMF than for NZDF. We can also estimate the number of GTEs needed to achieve a desired level of dispersion compensation for 40-Gb/s applications. At such bit rate, GTE-based DCMs will require a dispersion bandwidth of, typically, 80 GHz with an FSR = 100 GHz. According to Eq. (65), the number of GTEs needed to compensate the dispersion of a given fiber type is approximately 40 times larger than that for 10-Gb/s applications. This will seriously impact both the

insertion loss and the form factor of a potential GTE-based DCM for use in 40-Gb/s transmission.

There are a number of non-DCF-based dispersion devices, other than FBGs and GTEs, that at the time of writing are not yet commercially available but represent promising technologies. These include devices based on Ring Resonators (RR) [139,140], cascaded Mach-Zehnder Interferometers (MZI) [88], Waveguide-Grating Routers (WGR) [87], all of which can be built on planar waveguides, High-Order Mode (HOM) fibers [141], and Virtually-Imaged Phased Arrays (VIPA) [142]. Schematics of some of these devices are shown in Fig. 30. RRs, MZIs, WGRs, and VIPAs offer channelized and tunable dispersion compensation for 10 and 40-Gb/s applications; HOM-based DCMs offer broadband non-channelized tunable dispersion compensation when combined with 2×2 mode-converting switches (see Fig. 30). Finally, Photonic Crystal Fibers (PCFs) made from a single material and with a regular array of empty holes running along the length of the cladding may provide very large negative dispersion values in excess -2000 ps/nm km [143,144].

4.3. System Applications and Impact on Non-DCF Dispersion Compensation

Table 6 summarizes current applications and some relevant characteristics of various dispersion compensation technologies currently available to the system designer.

Tunable dispersion compensation is generally used as post-compensation before a receiver to compensate for dispersion fluctuations and uncertainties, especially in 40-Gb/s systems [145] where the tolerable residual dispersion is only on the order of a few tens of ps/nm (see Sec. 2.3). One should point out that in some 10-Gb/s systems, designed such that different dispersion compensation values are required for different network configurations, tunable dispersion compensation can find applications. In such systems, tunability in DCMs can be used to generate arbitrary values of pre-, in-line, and post- dispersion compensation, resulting in a reduction in the DCM inventory.

FBG-based devices have the highest FOM due to an insertion loss that does not depend on the amount of dispersion, unlike GTE-based devices where higher dispersion values are obtained by concatenating more GTEs, thus increasing the device loss. Both FBG and GTE-based devices exhibit channelized dispersion compensation. FBG-based dispersion compensation devices are currently available for single-channel and broadband 10-Gb/s applications [133], and for single-channel and group-of-channels 40-Gb/s applications. Devices for 40-Gb/s transmission typically exhibit an 80-GHz dispersion bandwidth and a channel spacing of 200 GHz. For tunable devices, the dynamic tuning range is currently 400 ps/nm and, in order to compensate for both signs of residual dispersion, higher insertion-loss setups including a circulator and two FBGs are required [127].

DCMs based on GTEs are currently available for 10-Gb/s WDM applications with dispersion passbands of typically 25 GHz and a channel spacing of 50 GHz (parameters also found in their FBG counterparts).

The main disadvantages of FBG and GTE DCMs originate from their channelized dispersion compensation. The existence of dispersion passbands may lead to limitations in spectral efficiency (due to dispersion discontinuities between channels). For this reason channelized dispersion compensators are generally limited to systems with spectral efficiencies up to 0.2 bit/s/Hz. A potential disadvantage of non-DCF based

DC technology	Current application	Systems types	Tunable range	Chan-nelized	Broad-band	FOM
Units			ps/nm			ps/(nm dB)
DCF	Pre-comp., in-line comp., post-comp.	Metro, Regional, LH and ULH	Not tunable	No	Yes	160-420
FBG	post-comp.	40 Gb/s: Regional, LH and ULH	400	Yes	No	< 500
GTE	Pre-comp., in-line comp., post-comp.	2.5 and 10 Gb/s: Metro ?, Regional ? and LH ?	2800	Yes	Yes	80-200

Table 6. Typical properties and system applications of several commercial dispersion compensation technologies. DC: Dispersion compensation.

dispersion compensation is its inability to provide Raman gain, a desirable feature especially in ULH all-Raman systems [146].

Long fiber links require DCMs for pre-, in-line, and post-compensation to mitigate nonlinear effects (Sec. 3.2). In this context, the question of whether there will be deleterious effects due to cascading effects in long haul applications arises. Two experiments have been recently reported addressing this problem. In one experiment [136] at 0.2 bit/s/Hz, 40×10 Gb/s NRZ C-Band channels were transmitted over 3200 km of SSMF in a loop configuration. GTEs provided in-line dispersion compensation every 80 km, inserted between the stages of a dual-stage EDFA [136]. In this experiment, GTEs were shown to perform as well as their fiber-based counterparts and no additional penalty was observed due to group-delay and/or insertion loss ripple. In another experiment [147] also at 0.2 bit/s/Hz, 80×10 Gb/s 50% RZ L-band channels were transmitted over 1200 km of NZDF (12×100 km in a loop configuration). An average system margin and a transmission penalty of 4.5 dB and less than 2 dB, respectively, were measured. In this experiment, the additional penalty due to the wavelength drift of the transmitters was also measured. It was found that a drift of ± 2.5 GHz (consistent with commonly found system specifications) led to less than 0.5 dB additional penalty. Note that when evaluating penalties due to the wavelength drift at the transmitter, all filters are misaligned relative to the laser which represents a stringent test. In straight-line systems each filter will have slightly different center frequencies relative to the ITU grid providing some degree of averaging of the concatenated filtering effect.

Both experiments point to the feasibility of employing GTE-based devices, not only for pre- and post-dispersion compensation, but also for in-line dispersion compensation, for LH and ULH high-capacity optical communication systems at moderate to low spectral efficiency (0.2 bit/s/Hz and below).

4.4. Perspective of Non-DCF Compensators

The advent of 40-Gb/s transmission has ushered in the use of tunable dispersion compensation, mostly provided by FBG-based devices. Technologies based on FBGs and

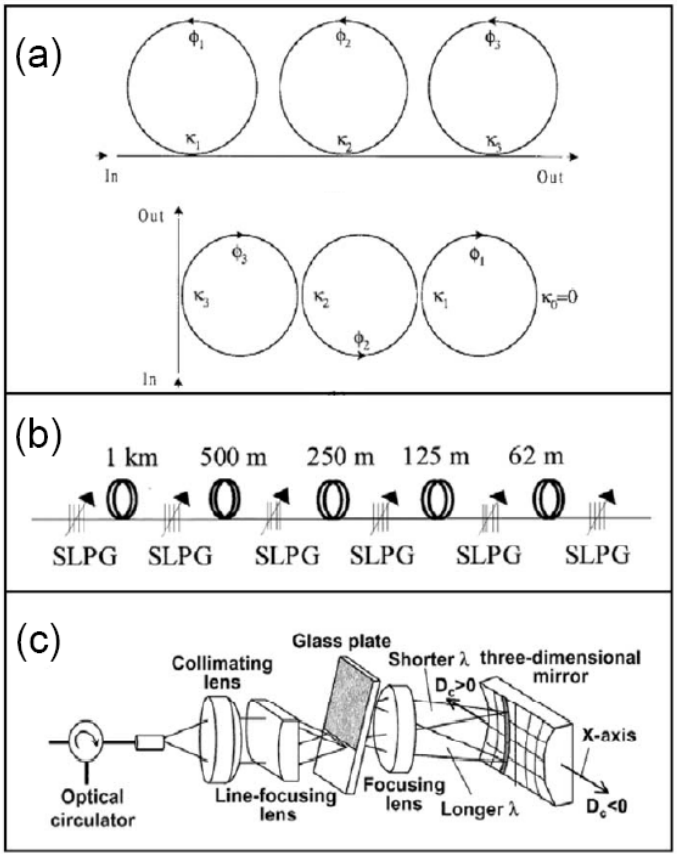

Fig. 30. Non-fiber dispersion compensation technologies: a) ring resonators (RR), b) higher-order mode (HOM) fiber, and c) virtually imaged phased arrays (VIPA). The upper graph in a) is a ring cascade while the lower graph is a ring lattice. κ and ϕ are the power coupling ratio and relative phase delay, respectively. SLFG: Switchable Long-period Fiber Gratings. D_c is the dispersion parameter value. Graphs (a) to (c) are from [140–142], respectively.

GTEs are currently available for tunable as well as fixed dispersion compensation applications. Low loss FBG-based DCMs find applications in both 10-Gb/s and 40-Gb/s single- and multi-channel dispersion compensation, whereas GTE-based devices are becoming attractive candidates for multi-channel pre-, in-line, and post-dispersion compensation in LH 10-Gb/s systems at moderate or low spectral efficiencies (i.e., 0.2 bit/s/Hz or lower).

Non-DCF dispersion compensation devices have generally the advantage of a small footprint, immunity to Kerr nonlinearities, the ability of engineering arbitrary dispersion profiles, and low cost. A small footprint and a high FOM make non-DCF DCMs especially attractive for use in dispersion compensation at OADM sites. Disadvantages of non-DCF DCMs are their channelized nature and, potentially, group-

delay and insertion-loss ripple. Recent high-capacity WDM experiments have been performed to evaluate transmission impairments due to GTE-based DCMs for long-haul and ultra-long-haul 10-Gb/s systems. These experiments showed no degradation attributable to group-delay and/or insertion-loss ripple, cascading effects of dispersion bandwidths, and wavelength drift of transmitters, thus pointing at the feasibility of employing such devices to provide dispersion compensation at 10 Gb/s as required along the signal path.

At the time of writing, there is a number of not yet commercially-available but very promising dispersion-compensation technologies such as Ring Resonators, cascaded Mach-Zehnder Interferometers, Waveguide-Grating Routers , High-Order Mode Fibers, Virtually Imaged Phased Arrays, and Photonic Crystal Fibers, all of which will add to the tools system designers have at their disposal to address the various dispersion-compensation needs arising in next-generation high-speed optical communication systems.

5. Summary

The insertion of dispersion compensation in fiber-optic communication systems has allowed high-speed optical signals, at 10 Gb/s per channel and above, to be transmitted over hundreds and thousands of kilometers without electrical regeneration. Signal propagation over such large distances becomes challenging as many physical phenomena enter into play.

In the first part of this paper, we introduced the tools and models required to assess the performance of an optical transmission system. This included the modeling and performance assessment of optical receivers, the calculations of the accumulation of amplified spontaneous emission generated by EDFA and Raman amplifiers, and the evaluation of double Rayleigh backscatter in Raman amplifiers. It also included phenomena that generally lead to signal distortions such as the accumulation of dispersion, fiber Kerr nonlinearity and polarization-mode dispersion. We also described how the judicious placement of dispersion compensation in a transmission line (i.e., dispersion mapping), can significantly reduce the effects of fiber nonlinearity. A brief description of technologies that can be used to mitigate various impairments has also been presented. Such technologies include forward error correction, advanced modulation formats and optical and electrical equalizations.

The second part of this paper has been devoted to describe the tools necessary to assess the impact of the presence of dispersion-compensating fiber in transmission lines that include erbium-doped amplifiers and Raman amplification. It was shown, for instance, that the impact of dispersion-compensating fiber on the delivered optical signal-to-noise ratio greatly depends on the fiber type of the transmission fiber and whether or not Raman amplification is used in the transmission line. The system impact of Raman pumping dispersion-compensating fibers to compensate their intrinsic loss and to provide some net gain has also been presented. It was shown that the positive net gain of Raman-pumped dispersion-compensating fiber is limited by the generation of double Rayleigh backscatter that becomes excessive at large values of positive gain. The impact of dispersion compensating fiber on signal distortions has also been evaluated. It was shown that one should carefully choose the signal power launched into the dispersion-compensating fiber to prevent fiber nonlinearity in that fiber to become

comparable to the nonlinearity in the transmission fiber. It was also shown, by way of example, what dispersion map parameters are optimum for a wavelength-division multiplexed system operating at 10 Gb/s per channel. The effect of polarization-mode dispersion within the dispersion-compensating fiber has also been described.

Finally, a review of alternative technologies to dispersion-compensating fibers was presented in the last section of this chapter. A description of the trade-offs between various commercial technologies as well as a discussion of novel dispersion-compensation technologies was given at various stages.

Acknowledgments

We would like to thank Andy Chraplyvy, Jake Bromage, Greg Raybon, Sethumadhavan Chandrasekhar, Aref Chowdhury, Dan Fishman, Paul Claisse, Bob Jopson, Lars Grüner-Nielsen, Lynn Nelson, Anjali Agarwal, Christopher Doerr, Dan Marom and Christi Madsen for contributing to this chapter through numerous discussions, advice and reading of the manuscript.

Acronyms

Acronym	Signification
APF	All-pass filter
ASE	Amplified spontaneous emission
BER	Bit-error rate
BW	Backward
CDR	Clock and data recovery
CSRZ	Carrier-suppressed return-to-zero
CW	Continuous wave
CWDM	Coarse wavelength-division multiplexing
DC	Dispersion compensation
DCF	Dispersion-compensating fiber
DCM	Dispersion-compensating module
DFE	Distributed feedback equalizer
DGD	Differential group delay
DMC	Dispersion-managed cable
DMF	Dispersion-managed fiber
DRA	Distributed Raman amplifier
DRB	Distributed Rayleigh scattering
DSF	Dispersion-shifted fiber
DUT	Device under test
DPDM	Doubly periodic dispersion map
DPSK	Differential phase-shift keying
DQPSK	Differential quaternary phase-shift keying

Acronym	Signification
EDFA	Erbium-doped fiber amplifier
EF	Electrical filter
EFEC	Enhanced forward error correction
FBG	Fiber Bragg grating
FEC	Forward error correction
FFE	Feed-forward equalizer
FOM	Figure of merit
FPE	Fabry-Perot Etalon
FSR	Free spectral range
FW	Forward
FWHM	Full width at half maximum
FWM	Four-wave mixing
GDR	Group delay ripple
GFEC	Generic forward error correction
GTE	Gires-Tournois Etalon
GNSE	Generalized nonlinear Schrödinger equation
HOM	Higher-order mode
IFWM	Intra-channel four-wave mixing
ISI	Inter-symbol interference
ITU	International telecommunication union
IXPM	Intra-channel cross-phase modulation
LH	Long-haul
MLSE	Maximum-likelihood sequence estimator
MPI	Multiple-path interference
MZI	Mach-Zehnder interferometer
MZM	Mach-Zehnder modulator
NL	Nonlinear or nonlinearity
NRD	Net residual dispersion
NRZ	Non-return to zero
NZDF	Non-zero dispersion-shifted fiber
OADM	Optical add-drop multiplexer
OEQ	Optical equalization
OF	Optical filter
OFE	Optical front-end
OOK	On-off keying
OSNR	Optical signal-to-noise ratio
OXC	Optical cross connect
PCF	Photonic crystal fiber
PD	Photodiode
PDL	Polarization-dependent loss
PMD	Polarization-mode dispersion
PMDC	Polarization-mode dispersion compensation
PSP	Principal states of polarization

Acronym	Signification
RB	Rayleigh backscatter
RR	Ring resonator
RDPS	Residual dispersion per span
RZ	Return-to-zero
RDS	Relative dispersion slope
SLFG	Switchable long-period fiber gratings
SNR	Signal-to-noise ratio
SONET	Synchronous Optical NETwork
SPDM	Singly-periodic dispersion map
SPM	Self-phase modulation
SSMF	Standard single-mode fiber
TDC	Tunable Dispersion Compensators
TF	Transmission fiber
TWRS	Truewave® reduced slope
ULH	Ultra-long haul
VIPA	Virtually-imaged phase array
WDM	Wavelength-division multiplexing
WGR	Waveguide-grating router
XPM	Cross-phase modulation

References

1. E. Desurvire, *Erbium-doped Fiber Amplifiers: Principles and Applications* (John Wiley & Sons, 1994).

2. P.S. Henry, R.A. Linke, and A.H. Gnauck, *Introduction to Lightwave Systems, in Optical Fiber Telecommunications II*, edited by Stewart E. Miller and I. P. Kaminov (Academic Press, 1988), Chapter 21, pp. 781–831.

3. F.P. Kapron, D.B. Keck and R.D. Maurer, "Radiation losses in glass optical waveguides," Appl. Phys. Lett. **17**, 423–425 (1970).

4. D. Marcuse, A.R. Chraplyvy, and R.W. Tkach, "Effect of fiber nonlinearity on longdistance transmission," J. Lightwave Technol. **9**, 121–128 (1991).

5. D. Marcuse, "Single-channel operation in very long nonlinear fibers with optical amplifiers at zero dispersion," J. Lightwave Technol. **9**, 356–361 (1991).

6. C. Lin, H. Kogelnik, and L.G. Cohen, "Optical-pulse equalization of low-dispersion transmission in single-mode fibers in the 1.3–1.7-μm spectral region," Opt. Lett. **5**, 476–478 (1980).

7. F. Ouellette, "Dispersion cancellation using linearly chirped Bragg grating filters in optical waveguides," Opt. Lett. **12**, 847–849 (1987).

8. L.J. Cimini, L.J. Greenstein, and A.A.M. Saleh, "Optical Equalization to Combat the Effects of Laser Chirp and Fiber Dispersion," J. Lightwave Technol. **8**, 649–659 (1990).

9. K. Iwashita and N. Takachio, "Chromatic dispersion compensation in coherent optical communications", J. Lightwave Technol. **8**, 367–375 (1990).

10. A.R. Chraplyvy, A.H. Gnauck, R.W. Tkach, and R.M. Derosier, "8 × 10 Gb/s transmission through 280-km of dispersion-managed fiber," IEEE Photon. Technol. Lett. **5**, 1233–1235 (1993).

11. C. Kurtzke, "Suppression of fiber nonlinearities by appropriate dispersion management," IEEE Photon. Technol. Lett. **5**, 1250–1253 (1993).

12. A.H. Gnauck, R.M. Jopson, P.P. Iannone, and R.M. Derosier, "Transmission of two wavelength-multiplexed 10 Gbit/s channels over 560 km of dispersive fibre," Electron. Lett. **30**, 727–728 (1994).

13. A. Naka, and S. Saito, "Transmission distance of in-line amplifier systems with groupvelocity- dispersion compensation," J. Lightwave Technol. **13**, 862–867 (1995).

14. M. Suzuki, I. Morita, N. Edagawa, S. Yamamoto, H. Taga, and S. Akiba, "Reduction of Gordon-Haus timing jitter by periodic dispersion compensation in soliton transmission," Electron. Lett. **31**, 2027–2029 (1995).

15. R.A. Jensen, R.E. Tench, D.G. Duff, C.R. Davidson, C.D. Chen, O. Mizuhara, T.V. Nguyen, L.D. Tzeng, and P.D. Yeates, "Field Measurements of 10 Gb/s Line Rate Transmission on the Columbus-2B Submarine Lightwave System," IEEE Photon. Technol. Lett. **7**, 1366–1368 (1995).

16. J.C. Feggeler, D.G. Duff, N.S. Bergano, C.C. Chen, Y.C. Chen, C.R. Davidson, D.G. Ehrenberg, S.J. Evangelides, G.A. Ferguson, F.L. Heismann, G.M. Homsey, H.D. Kidorf, T.M. Kissell, A.E. Meixner, R. Menges, J.L. Miller Jr., O. Mizuhara, T.V. Nguyen, B.M. Nyman, Y.K. Park, W.W. Patterson, and G.F. Valvo, "10 Gb/s WDM Transmission Measurements on an Installed Optical Amplifier Undersea Cable System," Electron. Lett. **31**, 1676–1678 (1995).

17. A.R. Chraplyvy and R.W. Tkach, "Terabit/Second Transmission Experiments," IEEE J. Quantum Electron. **34**, 2103–2108 (1998).

18. J. Bromage, P.J. Winzer, and R.-J. Essiambre, *Multiple-path interference and its impact on system design*, in Raman Amplifiers and Oscillators in Telecommunications, edited by M. N. Islam (Springer Verlag, 2003).

19. P.B. Hansen, G. Jacobovitz-Veselka, L. Grüner-Nielsen, and A.J. Stentz, "Raman amplification for loss compensation in dispersion compensating fibre modules," Electron. Lett. **34**, 1136–1137 (1998).

20. P.B. Hansen, L. Eskildsen, A.J. Stentz, T.A. Strasser, J. Judkins, J.J. DeMarco, R. Pedrazzani, and D.J. DiGiovanni, "Rayleigh Scattering Limitations in Distributed Raman Pre-Amplifiers," IEEE Photon. Technol. Lett. **10**, 159–161 (1998).

21. A. Altuncu, L. Noel, W.A. Pender, A.S. Siddiqui, T. Widdowson, A.D. Ellis, M.A. Newhouse, A.J. Antos, G. Kar, and P.W. Chu, "40 Gbit/s error free transmission over a 68-km distributed erbium-doped fibre amplifier," Electron. Lett. **32**, 233–234 (1996).

22. L.F. Mollenauer, R.H. Stolen, and M.N. Islam, "Experimental demonstration of soliton propagation in long fibers: Loss compensated by Raman gain," Opt. Lett. **10**, 229–231 (1985).

23. L.F. Mollenauer and K. Smith, "Demonstration of soliton transmission over more than 4000 km in fiber with loss periodically compensated by Raman gain," Opt. Lett. **13**, 675–677 (1988).

24. M.N. Islam (Ed.), *Raman Amplifiers for Telecommunications 1: Physical Principles and Raman Amplifiers for Telecommunications 2: Sub-Systems and Systems*, Springer Series in Optical Sciences (Springer-Verlag, 2003).

25. H.J. Thiele, L. Molle, T. Eggert, F. Raub, and R. Freund, "S-band Erbium-Doped Fibre Amplifiers for 40 Gb/s WDM Transmission," Proc. of the European Conference on Optical Communications (ECOC'04), paper Tu1.5.7 (2004).

26. R. Ohhira, Y. Yano, A. Noda, Y. Suzuki, C. Kurioka, M. Tachigori, S. Moribayashi, K. Fukuchi, T. Ono, and T. Suzuki, "40 Gbit/s $\times$ 8-ch NRZ WDM transmission experiment over 80 km $\times$ 5-span using distributed Raman amplification in RDF," Proc. of the European Conference on Optical Communications (ECOC'99), pp. 176–177 (1999).

27. T. Okuno, T. Tsuzaki, and M. Nishimura, "Novel lossless optical transmission line with distributed Raman amplification," Proc. of the European Conference on Optical Communications (ECOC'00), Vol. 2, pp. 7576 (2000).

28. I. Morita, K. Tanaka, N. Edagawa, and M. Suzuki, "40 Gbit/s $\times$ 16 WDM transmission over 2000 km using dispersion managed low-nonlinear fiber span," Proc. of the European Conference on Optical Communications (ECOC'00), Vol. 4, pp. 2526 (2000).

29. H.S. Chung, H. Kim, S.E. Jin, E.S. Son, D.W. Kim, K.M. Lee, H.Y. Park, and Y.C. Chung, "320-Gb/s WDM Transmission with 50-GHz Channel Spacing Over 564 km of Short-Period Dispersion-Managed Fiber (Perfect Cable)," IEEE Photon. Technol. Lett. **12**, 1397–1399 (2000).

30. T. Yamamoto, E. Yoshida, K. R. Tamura, K. Yonenaga, and M. Nakazawa, "640-Gbit/s Optical TDMTransmission Over 92 km Through a Dispersion-Managed Fiber Consisting of Single-Mode Fiber and Reverse Dispersion Fiber," IEEE Photon. Technol. Lett. **12**, 353–355 (2000).

31. S.N. Knudsen, M.O. Pedersen, and L. Grüner-Nielsen, "Optimisation of dispersion compensating fibres for cabled long-haul applications," Electron. Lett. **36**, 2067–2068 (2000).

32. S.N. Knudsen, B. Zhu, L. E. Nelson, M.O. Pedersen, D.W. Peckham, and S. Stulz, "420 Gbit/s (4210 Gbit/s) WDM transmission over 4000 km of UltraWave fibre with 100 km dispersion-managed spans and distributed Raman amplification," Electron. Lett. **37**, 965–967 (2001).

33. B. Zhu, S.N. Knudsen, L.E. Nelson, D.W. Peckham, M.O. Pedersen, and S. Stulz, "800 Gbit/s (80 × 10.664 Gbit/s) WDM transmission over 5200 km of fibre employing 100km dispersion Managed spans," Electron. Lett. **37**, 1467–1469 (2001).

34. R. Hainberger, T. Hoshida, T. Terahara, and H. Onaka, "Comparison of Span Configurations of Raman-Amplified Dispersion-Managed Fibers," IEEE Photon. Technol. Lett. **14**, 471–473 (2002).

35. C. Rasmussen, T. Fjelde, J. Bennike, F. Liu, S. Dey, B. Mikkelsen, P. Mamyshev, P. Serbe, P. van der Wagt, Y. Akasaka, D. Harris, D. Gapontsev, V. Ivshin, and P. Reeves- Hall, "DWDM 40G Transmission Over Trans-Pacific Distance (10 000 km) Using CSRZDPSK, Enhanced FEC, and All-Raman-Amplified 100-km UltraWave Fiber Spans," J. Lightwave Technol. **22**, 203–207 (2004).

36. T. Tsuritani, K. Ishida, A. Agata, K. Shimomura, I. Morita, T. Tokura, H. Taga, T. Mizuochi, N. Edagawa, and S. Akiba, "70-GHz-Spaced 40 42.7 Gb/s Transpacific Transmission Over 9400 km Using Prefiltered CSRZ-DPSK Signals, All-Raman Repeaters, and Symmetrically Dispersion-Managed Fiber Spans," J. Lightwave Technol. **22**, 215–223 (2004).

37. D.F. Grosz, A. Agarwal, A.P. Küng, S. Banerjee, D.N. Maywar, and T.H. Wood, "Performance of a ULH Single Wide-Band All-Raman DWDM Transmission System Over Dispersion-Managed Spans," IEEE Photon. Technol. Lett. **16**, 1197–1199 (2004).

38. M.M.E. Said, J. Sitch, and M.I. Elmasry, "An electrically pre-equalized 10-Gb/s duobinary transmission system," J. Lightwave Technol. **23**, 388–400 (2005).

39. D. McGhan, C. Laperle, A. Savchenko, C. Li, G. Mak, and M. O'Sullivan, "5120 km RZ-DPSK transmission over G.652 fiber at 10 Gb/s with no optical dispersion compensation," Proc. of the Optical Fiber Communication (OFC'05), paper PDP27 (2005).

40. R.-J. Essiambre and P.J. Winzer, "Fibre Nonlinearities in Electronically Pre- Distorted Transmission," Proc. of the European Conference on Optical Communication (ECOC'05), invited paper Tu3.2.2 (2005).

41. P.J. Winzer and R.-J. Essiambre, "Electronic pre-distortion for advanced modulation formats," Proc. of the European Conference on Optical Communication (ECOC'05), paper Tu4.2.2 (2005).

42. H. Sugahara, "Analysis of power jitter induced by interchannel interactions in dispersion-managed optical soliton transmission systems," IEEE Photon. Technol. Lett. **13**, 963–965 (2001).

43. S. Banerjee, A. Agarwal, D.F. Grosz, A.P. Küng, and D.N. Maywar, "Doubly periodic Dispersion Maps for 10 Gb/s and 40 Gb/s Ultra-Long-Haul Transmission," Electron. Lett. **40**, 1287–1288 (2004).

44. C. Xie, "A doubly periodic dispersion map for ultralong-haul 10- and 40-Gb/s hybrid DWDM optical mesh networks," IEEE Photon. Technol. Lett. **17**, 1091–1093 (2005).

45. F. Forghieri, R.W. Tkach, A.R. Chraplyvy, and A.M. Vengsarkar, "Dispersion Compensating Fiber: Is There Merit in the Figure of Merit?" Proc. of the Optical Fiber Communications Conference (OFC'96), paper ThM5 (1996).

46. F. Forghieri, R.W. Tkach, and A.R. Chraplyvy, "Dispersion Compensating Fiber: Is There Merit in the Figure of Merit?" IEEE Photon. Technol. Lett. **9**, 970–972 (1997).

47. P. Sillard, B. Dany, A. Bertaina, L. Curinckx, C. Bastide, O. Courtois, J.-C. Antona, and S. Bigo, "Simple criterion of quality to evaluate DCM impact on WDM system performance," Proc. of the Optical Fiber Communications Conference (OFC'04), paper FA3 (2004).

48. N.S. Bergano, *Undersea communication systems*, in Optical Fiber Telecommunications IV B, edited by I. Kaminow and T. Li (Academic Press, 2002).

49. S.D. Personick, "Receiver design for digital fiber optic communication systems, I," Bell. Syst. Technol. J. **52**, 843–874 (1973).

50. G. Einarsson, *Principles of Lightwave Communications* (John Wiley & Sons, 1996).

51. G. P. Agrawal, *Fiber-optic communication systems* (John Wiley & Sons, 3rd edition, 2002).

52. L. Kazovsky, S. Benedetto, and A. Willner, *Optical Fiber Communication Systems* (Artech House, Inc., 1996).

53. P.J. Winzer, "Receiver noise modeling in the presence of optical amplification," Proc. of the Optical Amplifiers and their Applications (OAA'01), OTuE16 (2001); P.J. Winzer, Performance estimation of receivers corrupted by optical noise, in OSA Trends in Optics and Photonics (TOPS), vol. 60, (N. Jolley, J.D. Minelly, and Y. Nakano, eds.), pp 268–273, (2001).

54. P.J. Winzer, S. Chandrasekhar, and H. Kim, "Impact of filtering on RZ-DPSK reception," IEEE Photon. Technol. Lett. **15**, 840–842 (2003).

55. R.D. Gitlin, J. F. Hayes, and S. B. Weinstein, Data Communications Principles, Plenum Press (1992).

56. P.J. Winzer and A. Kalmar, "Sensitivity Enhancement of Optical Receivers by Impulsive Coding," J. Lightwave Technol. **17**, 171–177 (1999).

57. P.J.Winzer, R.-J. Essiambre, and J. Bromage, "Combined Impact of Double-Rayleigh Backscatter and Amplified Spontaneous Emission on Receiver Noise," Proc. of the Optical Fiber Communications Conference (OFC'02), Paper ThGG87, pp. 734–735 (2002).

58. N.A. Olsson, "Lightwave Systems with Optical Amplifiers," J. Lightwave Technol. **7**, 1071–1082 (1989).

59. P. Wan and J. Conradi, "Impact of Double Rayleigh Backscatter Noise on Digital and Analog Fiber Systems," J. Lightwave Technol. **14**, 288–297 (1996).

60. B.E.A. Saleh and M.C. Teich, *Fundamentals of Photonics* (John Wiley & Sons, Inc., 1991).

61. P.J. Winzer, R.-J. Essiambre, and S. Chandrasekhar, "Dispersion-tolerant optical communication systems," Proc. of the European Conference on Optical Communications (ECOC'04), paper We2.4.1 (2004).

62. R.G. Smith, "Optical Power Handling Capacity of Low Loss Optical Fibers as Determined by Stimulated Raman and Brillouin Scattering," Appl. Opt. **11**, 2489–2494 (1972).

63. M. Nissov, K. Rottwitt, H.D. Kidorf, and M.X. Ma, "Rayleigh Crosstalk in Long Cascades of Distributed Unsaturated Raman Amplifiers," Electron. Lett. **35**, 997–998 (1999).

64. M. Oskar van Deventer, "Polarization Properties of Rayleigh Backscattering in Single- Mode Fibers," J. Lightwave Technol. **11**, 1895–1899 (1993).

65. H.A. Haus, *Electromagnetic noise and quantum optical measurements* (Springer Verlag, 2000).

66. E. Desurvire, D. Bayart, B. Desthieux, and S. Bigo, *Erbium-Doped Fiber Amplifiers, Device and System Developments* (John Wiley & Sons, 2002).

67. R.I. Laming, M.N. Zervas, and D.N. Payne, "Erbium-doped fiber amplifier with 54 dB gain and 3.1 dB noise figure," IEEE Photon. Technol. Lett. **4**, 1345–1347 (1992).

68. P.C. Becker, N.A. Olsson, and J.R. Simpson, *Erbium-Doped Fiber Amplifiers Fundamentals and Technology* (Academic Press, San Diego, 1999).

69. A. Yariv, H. Blauvelt, and S.-W. Wu, "A Reduction of Interferometric Phase-to-Intensity Conversion Noise in Fiber Links by Large Index Phase Modulation of the Optical Beam," J. Lightwave Technol. **10**, 978–981 (1992).

70. K. Shimizu, T. Horiguchi, and Y. Koyamada, "Charateristics and Reduction of Coherent Fading Noise in Rayleigh Backscattering Measurement for Optical Fibers and Components," J. Lightwave Technol. **10**, 982–987 (1992).

71. B. Wedding, "New method for optical transmission beyond dispersion limit," Electron. Lett. **28**, 1298–1300 (1992).

72. R.S. Vodhanel, A.F. Elrefaie, M.Z. Iqbal, R.E. Wagner, J.L. Gimlett, and S. Tsuji, "Performance of directly modulated DFB lasers in 10-Gb/s ASK, FSK, and DPSK lightwave systems," J. Lightwave Technol. **8**, 1379–1386 (1990).

73. F.N. Timofeev, P. Bayvel, V. Mikhailov, O.A. Lavrova, R. Wyatt, R. Kashyap, M. Robertson, and J.E. Midwinter, "2.5 Gbit/s directly-modulated fibre grating laser for WDM networks," Electron. Lett. **33**, 1406–1407 (1997)

74. L. Nelson, I. Woods, and J. K. White, "Transmission over 560 km at 2.5 Gb/s using a directly modulated buried heterostructure gain-coupled DFB semiconductor laser," Proc. of the Optical Fiber Communication Conference (OFC'02), pp. 422–423 (2002).

75. P.J.Winzer and R.-J. Essiambre, "Advanced optical modulation formats," Proc. of the European Conference on Optical Communications (ECOC'03), paper Th2.6.1, pp. 1002–1003 (2003).

76. P.J. Winzer and R.-J. Essiambre, "System trade-offs for different optical modulation formats," Proc. of the Optical Amplifiers and Their Applications (OAA"04), OTuC4 (2004).

77. P.J. Winzer, C. Dorrer, R.-J. Essiambre, and I. Kang, "Chirped return-to-zero modulation by imbalanced pulse carver driving signals," IEEE Photon. Technol. Lett. **16**, 1379–1381 (2004).

78. H. Kim and R.-J. Essiambre, "Transmission of 8×20 Gb/s DQPSK signals over 310-km SMF with 0.8-b/s/Hz spectral efficiency," IEEE Photon. Technol. Lett. **15**, 769–771 (2003).

79. R. Griffin, R. Johnstone, R. Walker, S. Wadsworth, A. Carter, and M. Wale, "Integrated DQPSK transmitter for dispersion-tolerant and dispersion-managed DWDM transmission," Proc. of the Optical Fiber Communications Conference (OFC'03), pp. 770–771 (2003).

80. S. Walklin and J. Conradi, "On the relationship between chromatic dispersion and transmitter filter response in duobinary optical communication systems," IEEE Photon. Technol. Lett. **9**, 1005–1007 (1997); [comments by D. Penninckx: IEEE Photon. Technol. Lett. **10**, 902 (1998).]

81. J.H. Winters and R.D. Gitlin, "Electrical signal processing techniques in long-haul fiber-optic systems", IEEE Trans. Commun. **38**, 1439–1453 (1990).

82. F. Buchali, H. Bulow, and W. Kuebart, "Adaptive decision feedback equalizer for 10 Gbit/s dispersion mitigation," Proc. of the European Conference on Optical Communications (ECOC'00), vol.2, pp. 101–102 (2001).

83. D. Castagnozzi, "Digital signal processing and electronic equalization (EE) of ISI," Proc. of the Optical Fiber Communications Conference (OFC'04), paper WM6 (2004).

84. H.F. Haunstein, K. Sticht, A. Dittrich, M. Lorang, W. Sauer-Greff, and R. Urbansky, "Implementation of near optimum electrical equalization at 10 Gbit/s," Proc. of the European Conference on Optical Communications (ECOC'00), vol.3, pp. 223–224 (2000).

85. F. Buchali and H. Bulow, "Adaptive PMD compensation by electrical and optical techniques," J. Lightwave Technol. **22**, 1116–1126 (2004).

86. G.S. Kanter, A.K. Samal, O. Coskun, and A. Gandhi,"Electronic equalization for enabling communications at OC-192 rates using OC-48 components," Optics Express **11**, 2019–2029 (2003).

87. C.R. Doerr, A.H. Gnauck, L.W. Stulz, and D.M. Gill, "Using an optical equalizer to transmit a 43-Gb/s signal with an 8-GHz bandwidth modulator," IEEE Photon. Technol. Lett. **15**, 1624–1626 (2003).

88. C.R. Doerr, S. Chandrasekhar, P.J. Winzer, A.R. Chraplyvy, A.H. Gnauck, L.W. Stulz, R. Pafchek, and E. Burrows, "Simple multichannel optical equalizer mitigating intersymbol interference for 40-Gb/s nonreturn-to-zero signals," J. Lightwave Technol. **22**, 249–256 (2004).

89. P.J. Winzer and R.-J. Essiambre, "Receivers for advanced optical modulation formats," Proc. of the 16th annual meeting of IEEE/LEOS (LEOS"03), paper ThA1 (2003).

90. A.J. Weiss, "On the performance of electrical equalization in optical fiber transmission systems," IEEE Photon. Technol. Lett. **15**, 1225–1227 (2003).

91. S.L. Woodward, S.-Y. Huang, M.D. Feuer, and M. Boroditsky, "Demonstration of an electronic dispersion compensator in a 100-km 10-Gb/s ring network," IEEE Photon. Technol. Lett. **15**, 867–869 (2003).

92. M.D. Feuer, S.-Y. Huang, S.L. Woodward, O. Coskun, and M. Boroditsky, "Electronic dispersion compensation for a 10-Gb/s link using a directly modulated laser," IEEE Photon. Technol. Lett. **15**, 1788–1790 (2003).

93. P.J. Winzer, F. Fidler, M.J. Matthews, L.E. Nelson, S. Chandrasekhar, L.L. Buhl, M. Winter, and D. Castagnozzi, "Electronic equalization and FEC enable bidirectional CWDM capacities of 9.6 Tb/s-km," Proc. of the Optical Fiber Communications Conference (OFC'04), paper PDP7 (2004).

94. C.R.S. Fludger, J.E.A. Whiteaway, and P.J. Anslow, "Electronic Equalisation for Low Cost 10 Gbit/s Directly Modulated Systems," Proc. of the Optical Fiber Communications Conference (OFC'04), paper WM7 (2004).

95. M. Cavallari, C.R.S. Fludger, and P.J. Anslow, "Electronic Signal Processing for Differential Phase Modulation Formats," Proc. of the Optical Fiber Communications Conference (OFC'04), paper TuG2 (2004).

96. A. Faerbert, S. Langenbach, N. Stojanovic, C. Dorschky, T. Kupfer, C. Schulien, J.P. Elbers, H. Wernz, H. Griesser, and C. Glingener, "Performance of a 10.7 Gb/s receiver with digital equalizer using maximum likelihood sequence estimation," Proc. of the European Conference on Optical Communication (ECOC'04), paper Th4.1.5 (2004).

97. T. Mizuochi, K. Kubo, H. Yoshida, H. Fujita, H. Tagami, M. Akita, and K. Motoshima, "Next generation FEC for optical transmission systems," Proc. of the Optical Fiber Communications Conference (OFC'03), paper ThN1 (2003).

98. S. Chandrasekhar and L. L. Buhl, "Performance of forward error correction coding in the presence of in-band crosstalk," Proc. of the Optical Fiber Communications Conference (OFC'02), paper WP1 (2002).

99. G.P. Agrawal, *Nonlinear Fiber Optics, 3rd Edition* (Academic Press, San Diego, 2001).

100. R.-J. Essiambre, B. Mikkelsen, and G. Raybon, "Intra-channel cross-phase modulation and four-wave mixing in high-speed TDM systems," Electron. Lett. **35**, 1576–1578 (1999).

101. P.V. Mamyshev and N.A. Mamysheva, "Pulse-overlapped dispersion-managed data transmission and intra-channel four-wave mixing," Opt. Lett. **24**, 1454–1456 (1999).

102. R.-J. Essiambre, G. Raybon, and B. Mikkelsen, *Pseudo-linear transmission of highspeed TDM signals: 40 and 160 Gb/s*, in Optical Fiber Telecommunications IV B, edited by I. Kaminov and T. Li, pp. 232–304 (Academic Press, 2002).

103. R.-J. Essiambre, P. Winzer, J. Bromage, and C.H. Kim , "Design of Bidirectionally Pumped Fiber Amplifiers Generating Double Rayleigh Backscattering," IEEE Photon. Technol. Lett. **14**, 914–916 (2002).

104. C. Fukai, K. Nakajima, J. Zhou, K. Tajima, K. Kurokawa, and I. Sankawa, "A Study of the Optimum Fiber Design for a Distributed Raman Amplification Transmission System, " IEEE Photon. Technol. Lett. **15**, 1642–1644 (2003).

105. H.S. Seo, Y.G. Choi, and K.H. Kim, "Design of Transmission Optical Fiber With a High Raman Gain, Large Effective Area, Low Nonlinearity, and Low Double Rayleigh Backscattering," IEEE Photon. Technol. Lett. **16**, 72–74 (2004).

106. P. Pecci, S. Lanne, Y. Frignac, J-C. Antona, G. Charlet and S. Bigo, "Tolerance to dispersion compensation parameters of six modulation formats in systems operating at 43Gbit/s," Proc. of the European Conference on Optical Communications (ECOC'03), paper We3.5.5 (2003).

107. H. Kogelnik, L.E. Nelson, and R.M. Jopson, *Polarization-mode dispersion*, in Optical Fiber Telecommunications IV B, edited by I. Kaminow and T. Li (Academic Press, 2002).

108. P.J. Winzer, H. Kogelnik, C.-H. Kim, H. Kim, R.M. Jopson, L.E. Nelson, and K. Ramanan, "Receiver Impact on first-order PMD Outage," IEEE Photon. Technol. Lett. **15**, 1482–1484 (2003).

109. S.R. Chinn, "Analysis of counter-pumped small-signal fibre Raman amplifiers," Electron. Lett. **33**, 607–608 (1997).

110. A. Kobyakov, M. Vasilyev, S. Tsuda, G. Giudice, and S. Ten, "Analytical model for Raman noise figure in dispersion-managed fibers," IEEE Photon. Technol. Lett. **15**, 30–32 (2003).

111. A. Carena, V. Curri, and P. Poggiolini, "On the Optimization of Hybrid Raman/ Erbium-Doped Fiber Amplifiers," IEEE Photon. Technol. Lett. **13**, 1170– 1172 (2001).

112. E.M. Dianov, "Advances in Raman fibers," J. Lightwave Technol. **20**, 1457–1462 (2002).

113. W. Hatton and M. Nishimura, "Temperature dependence of chromatic dispersion in single mode fibers," J. Lightwave Technol. **4**, 1552–1555 (1986).

114. K.S. Kim and M.E. Lines, "Temperature dependence of chromatic dispersion in dispersion-shifted fibers: Experiment and analysis," Appl. Phys. Lett. **73**, 2069–2074 (1993).

115. K. Yonenaga, A.Hirano, S. Kuwahara, Y. Miyamoto, H. Toba, K. Sato, and H. Miyazawa, "Temperature-independent 80 Gbit/s OTDM transmission experiment using zero-dispersion-flattened transmission line," Electron. Lett. **36**, 343–345 (2000).

116. M.J. Hamp, J. Wright, M. Hubbard, and B. Brimacombe, "Investigation into the temperature dependence of chromatic dispersion in optical fiber," IEEE Photon. Technol. Lett. **14**, 1524–1526 (2002).

117. H.C. Ji, J.H. Lee, and Y.C. Chung, "Evaluation on system outage probability due to temperature variation and statistically distributed chromatic dispersion of optical fiber," J. Lightwave Technol. **22**, 1893–1898 (2004).

118. A. Walter, G.S. Schaefer, "Chromatic dispersion variations in ultra-long-haul transmission systems arising from seasonal soil temperature variations," Proc. of the Optical Fiber Communication Conference (OFC'02), paper WU4, 332–333 (2002).

119. R. Kashyap, *Fiber Bragg Gratings* (Harcourt Brace & Company, 1999).

120. L.E. Nelson, R.M. Jopson, A.H. Gnauck, and A.R. Chraplyvy, "Resonances in cross-phase modulation impairment in wavelength-division-multiplexed lightwave transmission," IEEE Photon. Technol. Lett. **11**, 907–909 (1999).

121. G. Bellotti and S. Bigo, "Cross-phase modulation suppressor for multispan dispersionmanaged WDM transmissions," IEEE Photon. Technol. Lett. **12**, 726–728 (2000).

122. M.H. Eiselt, "Does spectrally periodic dispersion compensation reduce nonlinear effects?," Proc. of the European Conference on Optical Communications (ECOC'99), paper TuC1.2 (1999).

123. G. Bellotti, S. Bigo, P.-Y. Cortes, S. Gauchard, and S. LaRochelle, "10/spl times/10 Gb/s cross-phase modulation suppressor for multispan transmissions using WDM narrow-band fiber Bragg gratings," IEEE Photon. Technol. Lett. **12**, 1403–1405 (2000).

124. M.H. Eiselt, C.B. Clausen, and R.W. Tkach, "Performance Characterization of Components With Group Delay Fluctuations," IEEE Photon. Technol. Lett. **15**, 1076–1078 (2003).

125. International Standard IEC 60794-3, Part 3: "Optical fiber cables," September 2001, Appendix A.

126. L. Grüner-Nielsen, S.N. Knudsen, B. Edvold, T. Veng, D. Magnussen, C.C. Larsen, and H. Damsgaard, "Dispersion Compensating Fibres," Opt. Fiber Technol. **6**, 164–180 (2000).

127. Y. Painchaud, M. Lapointe, and M. Guy, "Slope-matched tunable dispersion compensation over the full C-band based on fiber Bragg gratings," Proc. of the European Conference on Optical Communication (ECOC'04), paper We3.3.4 (2004).

128. L.M. Lunardi, D.J. Moss, S. Chandrasekhar, L.L. Buhl, M. Lamont, S. McLaughlin, G. Randall, P. Colbourne, S. Kiran, and C.A. Hulse, "Tunable Dispersion Compensation at 40-Gb/s Using a Multicavity Etalon All-Pass Filter With NRZ, RZ, and CS-RZ Modulation," J. Lightwave Technol. **20**, 2136–2144 (2002).

129. D.N. Maywar, S. Banerjee, A. Agarwal, D.F. Grosz, M. Movassaghi, A.P. Küng, and T.H. Wood, "Impact of relaxed dispersion map and gain ripple on ultra-wideband 10-Gb/s transmission," Electron. Lett. **39**, 1266–1267 (2003).

130. A. Agarwal, S. Banerjee, D.F. Grosz, A.P. Küng, D.N. Maywar, T.H. Wood, "Ultralong- haul transmission of 40 Gb/s RZ-DPSK in a 10/40G hybrid system over 2500 km of NZ-DSF," IEEE Photon. Technol. Lett. **15**, 1779–1781 (2003).

131. M. Vasilyev, I. Tomkos, J.-K. Rhee, M. Mehendale, B.S. Hallock, B.K. Szalabofka, M. Williams, S. Tsuda, M. Sharma, "Broadcast and Select OADM in 80 $\times$ 10.7 Gb/s ultra-longhaul network", J. Lightwave Technol. **15**, 332–334 (2003).

132. D.F. Grosz, A. Agarwal, S. Banerjee, D.N. Maywar, and A.P. Küng, "All-Raman Ultralong-Haul Single-Wideband DWDM Transmission Systems With OADM Capability," J. Lightwave Technol. **22**, 423–432 (2004).

133. M. Morin, M. Poulin, A. Mailloux, F. Trepanier, and Y. Painchaud, "Full C-Band slope-matched dispersion compensation based on a phase sampled Bragg grating," Proc. of the Optical Fiber Communication Conference (OFC'04), paper WK1 (2004).

134. X. Shu, K. Sugden, P. Rhead, J. Mitchell, I. Felmeri, G. Lloyd, K. Byron, Z. Huang, I. Khrushchev, and I. Bennion, "Tunable Dispersion Compensator Based on Distributed Gires-Tournois Etalons," IEEE Photon. Technol. Lett. **15**, 1111–1113 (2003).

135. S. Doucet, R. Slavk, and S. LaRochelle, "Tunable Dispersion and Dispersion Slope Compensator Using Novel Gires-Tournois Bragg Grating Coupled-Cavities," IEEE Photon. Technol. Lett. **16**, 2529–2531 (2004).

136. D. Yang, C. Lin, W. Chen, and G. Barbarossa, "Fiber Dispersion and Dispersion Slope Compensation in a 4-Channel 10-Gb/s 3200-km Transmission Experiment Using Cascaded Single-Cavity Gires-Tournois Etalons," IEEE Photon. Technol. Lett. **16**, 299–301 (2004).

137. C.-H. Hsieh, R. Wang, Z.J. Wen, I. McMichael, P. Yeh, C.-W. Lee, and W.-H. Chen, "Flat-Top Interleavers Using Two Gires-Tournois Etalons as Phase-Dispersive Mirrors in a Michelson Interferometer," IEEE Photon. Technol. Lett. **15**, 242–244 (2003).

138. G. Lenz and C.K. Madsen, "General Optical All-Pass Filter Structures for Dispersion Control in WDM Systems," J. Lightwave Technol. **17**, 1248–1254 (1999).

139. C.K. Madsen and G. Lenz, "Optical All-Pass Filters for Phase Response Design with Applications for Dispersion Compensation," IEEE Photon. Technol. Lett. **10**, 994– 996 (2003)

140. C.K. Madsen, E.J. Laskowski, J. Bailey, M.A. Capuzzo, S. Chandrasekhar, L.T. Gomez, A. Griffin, P. Oswald, and L.W. Stulz, "The Application of Integrated Ring Resonators to Dynamic Dispersion Compensation," Proc. of the Optical Fiber Communication Conference (OFC'02), Paper TuJ2, pp. 29–30 (2002).

141. S. Ramachandran, S. Ghalmi, S. Chandrasekhar, I. Ryazansky, M.F. Yan, F.V. Dimarcello, W.A. Reed, and P. Wisk, "Tunable Dispersion Compensators Utilizing Higher Order Mode Fibers," IEEE Photon. Technol. Lett. **15**, 727–729 (2003).

142. H. Ooi, K. Nakamura, Y. Akiyama, T. Takahara, T. Terahara, Y. Kawahata, H. Isono, and G. Ishikawa, "40-Gb/s WDM Transmission With Virtually Imaged Phased Array (VIPA) Variable Dispersion Compensators," J. Lightwave Technol. **20**, 2196–2203 (2002).

143. T.A. Birks, D. Mogilevtsev, J.C. Knight, and P. St.J. Russell, "Dispersion Compensation Using Single-Material Fibers," IEEE Photon. Technol. Lett. **11**, 674–676 (1999).

144. Y. Ni, L. Zhang, L. An, J. Peng, and C. Fan, "Dual-Core Photonic Crystal Fiber for Dispersion Compensation," IEEE Photon. Technol. Lett. **16**, 1516–1518 (2004).

145. M. Yagi, S. Satomi, S. Tanaka, S. Ryu, and S. Asano, "Field Trial of Automatic Chromatic Dispersion Compensation for 40-Gb/s-Based Wavelength Path Protection," IEEE Photon. Technol. Lett. **17**, 229–231 (2005).

146. D.F. Grosz, A. Küng, D.N. Maywar, L. Altman, M. Movassaghi, H.C. Lin, D.A. Fishman, and T.H. Wood, "Demonstration of All-Raman Ultra-Wide-Band Transmission of 1.28 Tb/s (128 $\times$ 10 Gb/s) over 4000 km of NZ-DSF with Large BER Margins," Proc. of the European Conference on Optical Communication (ECOC'01), Paper PD B.1.3, pp. 72–73 (2001).

147. D.F. Grosz, D.N. Maywar, A.P. Küng, A. Agarwal, and S. Banerjee, "Performance of Non-Fiber Based Dispersion Compensation for Long-haul 10.7 Gb/s DWDM Transmission," Electron. Lett. **40**, 825–827 (2004).